



## P-model v1.0: An optimality-based light use efficiency model for simulating ecosystem gross primary production

Benjamin D. Stocker<sup>1,2</sup>, Han Wang<sup>3</sup>, Nicholas G. Smith<sup>4</sup>, Sandy P. Harrison<sup>5</sup>, Trevor F. Keenan<sup>6,7</sup>, David Sandoval<sup>8</sup>, Tyler Davis<sup>8,9</sup>, and I. Colin Prentice<sup>8</sup>

<sup>1</sup>CREAF, Campus UAB, 08193 Bellaterra, Catalonia, Spain

<sup>2</sup>Earth System Science, Stanford University, Stanford, 94305-4216, California, USA

<sup>3</sup>Department of Earth System Science, Tsinghua University, Haidian, Beijing, 100084, China

<sup>4</sup>Department of Biological Sciences, Texas Tech University, Box 43131 Lubbock, TX 79409, USA

<sup>5</sup>Geography and Environmental Science, Reading University, Reading, RG6 6 AH, UK

<sup>6</sup>Earth and Environmental Sciences Area, Lawrence Berkeley National Lab, Berkeley, CA 94709, USA

<sup>7</sup>Department of Environmental Science, Policy and Management, UC Berkeley, Berkeley, CA 94720, USA

<sup>8</sup>AXA Chair of Biosphere and Climate Impacts, Department of Life Sciences, Imperial College London, Silwood Park Campus, Ascot, Berkshire, SL5 7PY, UK

<sup>9</sup>Center for Geospatial Analysis, The College of William & Mary, Williamsburg, VA, 23185, USA.

**Correspondence:** B. D. Stocker (b.stocker@creaf.uab.cat)

**Abstract.** Terrestrial photosynthesis is the basis for vegetation growth and drives the land carbon cycle. Accurately simulating gross primary production (GPP, ecosystem-level apparent photosynthesis) is key for satellite monitoring and Earth System Model predictions under climate change. While robust models exist for describing leaf-level photosynthesis, predictions diverge due to uncertain photosynthetic traits and parameters which vary on multiple spatial and temporal scales. Here, we describe and evaluate a gross primary production (GPP, photosynthesis per unit ground area) model, the P-model, that combines the Farquhar-von Caemmerer-Berry model for  $C_3$  photosynthesis with an optimality principle for the carbon assimilation-transpiration trade-off, and predicts a multi-day average light use efficiency (LUE) for any climate and  $C_3$  vegetation type. The model is forced here with satellite data for the fraction of absorbed photosynthetically active radiation and site-specific meteorological data and is evaluated against GPP estimates from a globally distributed network of ecosystem flux measurements. Although the P-model requires relatively few inputs and prescribed parameters, the  $R^2$  for predicted versus observed GPP based on the full model setup is 0.75 (8-day mean, 131 sites) – better than some state-of-the-art satellite data-driven light use efficiency models. The  $R^2$  is reduced to 0.69 when not accounting for the reduction in quantum yield at low temperatures and effects of low soil moisture on LUE. The  $R^2$  for the P-model-predicted LUE is 0.37 (means by site) and 0.53 (means by vegetation type). The P-model provides a simple but powerful method for predicting – rather than prescribing – light use efficiency and simulating terrestrial photosynthesis across a wide range of conditions. The model is available as an R package (*rpmodel*).



## 1 Introduction

Realistic, reliable and robust estimates of terrestrial photosynthesis are required to understand variations in the carbon cycle, monitor forest and cropland productivity, and predict impacts of global environmental change on ecosystem function (Prentice et al., 2015). Understanding how photosynthetic rates depend on temperature, humidity, solar radiation, CO<sub>2</sub> and soil moisture is at the core of this challenge. Process-based Dynamic Vegetation Models (DVMs) and Earth System Models (ESMs) in use today almost always use some form of the Farquhar-von Caemmerer-Berry (FvCB) model for C<sub>3</sub> photosynthesis (Farquhar et al., 1980; von Caemmerer and Farquhar, 1981), in combination with stomatal conductance ( $g_s$ ) models (Ball et al., 1987; Leuning, 1995; Medlyn et al., 2011), that couple water and carbon fluxes at the leaf surface.

The FvCB model describes the instantaneous saturating relationship between leaf-internal CO<sub>2</sub> concentrations ( $c_i$ ) and assimilation ( $A$ ), and how this relationship depends on absorbed photosynthetically active radiation (APAR). It simulates  $A$  as the minimum of a light-limited and a Rubisco-limited assimilation rate,  $A_J$  and  $A_C$  respectively:

$$A = \min(A_J, A_C) \quad (1)$$

Although the FvCB model is standard for leaf-scale photosynthesis, and its environmental responses at time scales of minutes to hours, DVMs and ESMs using FvCB produce divergent results for ecosystem-level fluxes and their response to environment at longer time scales (Rogers et al., 2017). This is due to assumptions that have to be made about photosynthetic parameters that are not predicted by the FvCB model: stomatal conductance ( $g_s$ ) and the maximum rates of Rubisco carboxylation ( $V_{\text{cmax}}$ ) and electron transport ( $J_{\text{max}}$ ) for ribulose-1,5-bisphosphate (RuBP) regeneration, which together determine the relationship between  $c_i$  and  $A$ . Common approaches for determining the values of  $V_{\text{cmax}}$  and  $J_{\text{max}}$  in DVMs and ESMs are to prescribe fixed values per plant functional type (PFT) and attempt to simulate the distribution of PFTs in space, or to use empirical relationships between leaf N and  $V_{\text{cmax}}$  and simulate leaf N internally or prescribe it per PFT (Smith and Dukes, 2013; Rogers, 2014).

While the FvCB model describes a non-linear relationship between instantaneous assimilation and absorbed light, ecosystem production, integrated over weeks to months, scales proportionally with absorbed photosynthetically active radiation (APAR) (Monteith, 1972; Medlyn, 1998). This observation underlies the general light use efficiency (LUE) model which describes ecosystem-level photosynthesis (gross primary production, GPP) as the product of APAR and LUE:

$$\text{GPP} = \text{PAR} \cdot \text{fAPAR} \cdot \text{LUE} , \quad (2)$$

where PAR is the incident photosynthetically active radiation and fAPAR is the fraction of PAR that is absorbed by green tissue. The LUE model is the basis for observation-driven GPP models that use fAPAR and PAR based on remote sensing data and combine this with different approaches for simulating LUE (Running et al., 2004; Zhang et al., 2017; Field et al., 1995), and for some forest growth models (Landsberg and Waring, 1997). Other remote sensing data-based models (Jiang and Ryu, 2016) apply the FvCB model in combination with vegetation cover and type data and prescribed  $V_{\text{cmax}}$  for a set of PFTs.

Here, we describe a model, referred to as the *P-model*, that unifies the FvCB and LUE models following the theory developed by Prentice et al. (2014) and Wang et al. (2017a). The model assumes an optimality principle that balances the C cost (per



unit of assimilation) of maintaining transpiration and carboxylation ( $V_{\text{cmax}}$ ) capacities. It thus predicts how the ratio of leaf-internal to ambient  $\text{CO}_2$  ( $c_i : c_a = \chi$ ) acclimates to the environment, given temperature ( $T$ ), water vapour pressure deficit ( $D$ ), atmospheric pressure ( $p$ ) and ambient  $\text{CO}_2$  concentration ( $c_a$ ) (Prentice et al., 2014). The P-model also assumes that the photosynthetic machinery tends to coordinate  $V_{\text{cmax}}$  and  $J_{\text{max}}$  in order to operate close to the intersection of the light-limited and Rubisco-limited assimilation rates (*Coordination Hypothesis*, Chen et al. (1993); Maire et al. (2012)) under mean daytime environmental conditions. By further assuming equality in the marginal cost and benefit of  $J_{\text{max}}$ , daily-to-monthly average assimilation rates can then be described as fractions of absorbed PAR, i.e. as a LUE model (Eq. 2) (Wang et al., 2017a).

Thus, the P-model embodies an optimality-based theory for predicting the acclimation of leaf-level photosynthesis to its environment and for simulating LUE. In combination with prescribed PAR and remotely sensed fAPAR, it estimates GPP across diverse environmental conditions (Wang et al., 2017a). Its prediction for acclimating photosynthetic parameters reduces the number of prescribed (and temporally fixed) values and avoids the distinction of model parameterisation by vegetation types or biomes (apart from a distinction between the  $\text{C}_3$  and  $\text{C}_4$  photosynthetic pathways). The P-model has a further advantage over other data-driven GPP models ((Running et al., 2004; Zhang et al., 2017), and empirically upscaled GPP estimates (Jung et al., 2011) in that it accounts for the influence of changing  $\text{CO}_2$ , and that it uses first principles (rather than imposed functions) to represent effects of  $T$ ,  $D$  and  $p$  (Sect. 2). The theory underlying the P-model regarding the water-carbon tradeoff has been described by Prentice et al. (2014) and applied by Keenan et al. (2017) to simulate how changes in primary production have driven the terrestrial C sink over past decades; and by Smith et al. (2019) to explain variations in observed  $V_{\text{cmax}}$ . Wang et al. (2017a) complemented the theory by including effects of limited electron transport capacity ( $J_{\text{max}}$ ) and predicted variations in observed  $\chi$  across environmental gradients.

The purpose of this paper is to summarise the theory underlying the P-model and to provide a complete description and reference for its implementation, along with open access model code, available as an R package (*rmodel*, <https://stineb.github.io/rmodel/>). The paper also provides a comprehensive evaluation of GPP and LUE simulated by the P-model, using data from ecosystem flux measurements (FLUXNET 2015 Tier 1 dataset). The evaluation focuses on different components of variability (spatial, annual, seasonal, daily anomalies) (Secs. 4.6 - 4.1). We evaluate three P-model setups (Tab 1). We further address uncertainties associated with the fAPAR forcing (Sect. 4.4) and the uncertainties in the evaluation data by using GPP data derived from different flux decomposition methods (Sect. 4.5). The use of continuous GPP measurements, rather than experimentally disturbed measurements, makes it challenging to assess modelled GPP under extreme environmental conditions. We therefore make a further evaluation of simulated GPP during the course of soil moisture drought events (*fLUE droughts*, Sect. 4.3).

## 2 Theory

The theory underlying the P-model has been described by Wang et al. (2017a) and the derivation of equations is given therein. It is presented here again for completeness.



## 2.1 Balancing carbon and water costs

The P-model centres around a prediction for the optimal ratio of leaf-internal to ambient CO<sub>2</sub> concentration  $c_i : c_a$  (termed  $\chi$ )  
 85 that balances the costs associated with maintaining the transpiration stream and the cost of maintaining a given carboxylation  
 capacity. The optimal balance is achieved when the two marginal costs are equal:

$$a \frac{\partial(E/A)}{\partial\chi} = -b \frac{\partial(V_{\text{cmax}}/A)}{\partial\chi} . \quad (3)$$

Here,  $a$  and  $b$  are the respective unit costs.  $b$  is assumed to be constant, and  $a$  to scale linearly with the temperature-dependent  
 viscosity of water  $\eta(T)$ , calculated following Huber et al. (2009). Below, we introduce  $\beta = b/a'$ , with  $a = \eta^* a'$  and  $\eta^* =$   
 90  $\eta(T)/\eta(25^\circ\text{C})$ . The optimal  $\chi$  solves the above equation. We use Fick's law (Fick, 1855) to express transpiration and assimilation  
 as a function of stomatal conductance  $g_s$ :

$$E = 1.6g_s D \quad (4)$$

and

$$A = g_s c_a (1 - \chi) , \quad (5)$$

95 and use the Rubisco-limited assimilation rate from the FvCB model:

$$A = A_C = V_{\text{cmax}} m_C , \quad (6)$$

with

$$m_C = \frac{c_i - \Gamma^*}{c_i + K} , \quad (7)$$

where  $c_i$  is given by  $c_a \chi$ .  $K$  is the effective Michaelis-Menten coefficient for Rubisco-limited assimilation (Sect. B3), and  $\Gamma^*$   
 100 is the photorespiratory compensation point in the absence of dark respiration (Sect. B1). The optimal  $\chi$  can be derived as

$$\chi = \frac{\Gamma^*}{c_a} + \left(1 - \frac{\Gamma^*}{c_a}\right) \frac{\xi}{\xi + \sqrt{D}} , \quad (8)$$

with

$$\xi = \sqrt{\frac{\beta(K + \Gamma^*)}{1.6\eta^*}} . \quad (9)$$

(See Appendix E1 for intermediate steps.) Because both terms in Eq. 3 are divided by  $A$ , the solution is independent of whether  
 105 the Rubisco-limited rate  $A_C$  or the light-limited rate  $A_J$  (see below) are followed. With this prediction for  $\chi$ , we can use the  
*Coordination Hypothesis* (Chen et al., 1993; Haxeltine and Prentice, 1996; Maire et al., 2012) and the light-limited assimilation  
 rate from the FvCB model to write

$$A_J = \varphi_0 I_{\text{abs}} m , \quad (10)$$



with

$$110 \quad m = \frac{c_i - \Gamma^*}{c_i + 2\Gamma^*}. \quad (11)$$

This equation has the form of a LUE model (Eq. 2) in that  $A_J$  scales linearly with  $I_{\text{abs}}$ . Using Eqs. 9 and 8,  $m$  can be expressed directly as

$$m = \frac{c_a - \Gamma^*}{c_a + 2\Gamma^* + 3\Gamma^* \sqrt{\frac{1.6\eta^* D}{\beta(K + \Gamma^*)}}}. \quad (12)$$

The unit cost ratio  $\beta$  has been estimated by Wang et al. (2017a) based on global leaf  $\delta^{13}\text{C}$  data and a simplified version of the  
 115 P-model (assuming  $\Gamma^* = 0$  and neglecting the  $J_{\text{max}}$  limitation). Here, we re-estimated  $\beta$  based on the full version of the model using the same global leaf  $\delta^{13}\text{C}$  dataset. This is more strictly consistent with the model formulation implemented here. The value for  $\beta$  used here is 146.0 (unitless). Eq. 12 provides the basis for predicting  $\text{CO}_2$  assimilation rates in the form of a LUE model (Eq. 2) where LUE is a function of  $T$  and  $p$  (both affecting  $\Gamma^*$ ,  $K$ , and  $\eta^*$ ; see Secs. B1 and B3),  $D$ , and  $c_a$ .

The prediction of optimal  $\chi$  has a number of corollaries (see Appendix C). An estimate for stomatal conductance ( $g_s$ ) and  
 120 the intrinsic water use efficiency ( $\text{iWUE} = A/g_s$ ) directly follow from the optimal water-carbon balance (Eq. 3). By assuming  $A_J = A_C$ , we can further derive  $V_{\text{cmax}}$ , as well as dark respiration ( $R_d$ ), which is a function of  $V_{\text{cmax}}$  (see Secs. C3 and C4).

## 2.2 Introducing $J_{\text{max}}$ limitation

Eq. 10 assumes that the light response of  $A$  is linear up to the coordination point. In reality, rates saturate towards high light  
 125 levels because the electron transport rate  $J$ , necessary for the regeneration of ribulose-1,5,- bisphosphate (RuBP) tends towards a maximum  $J_{\text{max}}$ . To account for this effect, Eq. 10 can be modified, following the formulation by Smith (1937), using a non-rectangular hyperbola relationship between  $A_J$  and  $I_{\text{abs}}$  to allow for the effect of finite  $J_{\text{max}}$ :

$$A_J = \varphi_0 I_{\text{abs}} m \frac{1}{\underbrace{\sqrt{1 + \left(\frac{4\varphi_0 I_{\text{abs}}}{J_{\text{max}}}\right)^2}}_L} \quad (13)$$

In this equation  $A_J$  is no longer linear with respect to  $I_{\text{abs}}$  and thus does not have the form of a LUE model. However,  $J_{\text{max}}$  is  
 130 assumed here to acclimate on longer time scales to  $I_{\text{abs}}$ , so that the marginal gain in assimilation  $A$  per unit change in  $J_{\text{max}}$  is equal to the unit cost ( $c$ ) of maintaining  $J_{\text{max}}$ .

$$\frac{\partial A}{\partial J_{\text{max}}} = c \quad (14)$$

The unit cost  $c$  is assumed to include the maintenance of light-harvesting complexes and various proteins involved in the  
 electron transport chain. The cost of maintaining a given  $J_{\text{max}}$  is thus assumed to scale linearly with  $J_{\text{max}}$  and that this pro-  
 135 portionality is constant ( $c$  is constant). By taking the derivative of Eq. 13 with respect to  $J_{\text{max}}$  and re-arranging terms (see Appendix E2 for intermediate steps), we obtain the  $J_{\text{max}}$  limitation factor  $L$  in Eq. 13 as:

$$L = \sqrt{1 - \left(\frac{c^*}{m}\right)^{2/3}}, \quad (15)$$



with  $c^* = 4c$ . Note that  $L$  is independent of  $I_{\text{abs}}$ . Hence,  $A_J$  is again a linear function of absorbed light. The cost factor  $c^*$  is estimated from published values of  $J_{\text{max}}:V_{\text{cmax}} = 1.88$  at  $25^\circ\text{C}$ . (Kattge and Knorr, 2007) and  $\chi = 0.8$  (Lloyd and Farquhar, 1994) at  $c^* = 0.41$  (Wang et al., 2017a). The revised LUE model thus becomes

$$140 \quad A = \varphi_0 I_{\text{abs}} m', \quad (16)$$

with

$$m' = m \sqrt{1 - \left(\frac{c^*}{m}\right)^{2/3}}. \quad (17)$$

Wang et al (2017a) showed that this formulation of  $J_{\text{max}}$  costs leads to a realistic dependence of the  $J_{\text{max}}:V_{\text{cmax}}$  ratio on growth temperature.

145 As shown by Smith et al. (2019), an alternative approach can be used to introduce the effects of  $J_{\text{max}}$  limitation, replacing Eq. 13 by the more widely used one-parameter family of saturation curves following Farquhar and Wong (1984). This alternative is described in Appendix E3 and implemented as an optional method in the R package *rpmode*.

### 3 Methods

#### 3.1 The light use efficiency model

150  $A$  is commonly expressed in  $\text{mol m}^{-2} \text{s}^{-1}$ . For further model description and evaluation, we refer to ecosystem-scale quantities in mass units of assimilated C and model GPP ( $\text{g C m}^{-2} \text{d}^{-1}$ ) following Eq. 2 with

$$\text{fAPAR} \cdot \text{PPFD} \hat{=} I_{\text{abs}} \quad (18)$$

$$\text{LUE} \hat{=} \varphi_0(T) \beta(\theta) m' M_C \quad (19)$$

155 Here,  $M_C$  is the molar mass of carbon ( $12.0107 \text{ g mol}^{-1}$ ) to convert from molar units to mass units, and PPFD is the photosynthetic photon flux density per square metre, integrated over a day ( $\text{mol m}^{-2} \text{d}^{-1}$ ). fAPAR is unitless and integrates across the canopy, i.e., from fluxes per unit leaf area to fluxes per unit ground area. LUE is in units of  $\text{g C mol}^{-1}$ . The intrinsic quantum yield parameter  $\varphi_0$  is modelled as temperature-dependent, and an additional (unitless) empirical soil moisture stress factor ( $\beta(\theta)$ ) is included for modelling LUE.

##### 3.1.1 Temperature dependence of the intrinsic quantum yield of photosynthesis

160 The temperature dependence of the intrinsic quantum yield ( $\varphi_0(T)$ ,  $\text{mol mol}^{-1}$ ) is modelled following the temperature dependence of the maximum quantum yield of photosystem II in light-adapted leaves, determined by Bernacchi et al. (2003) as

$$\varphi_0(T) = \frac{a_L b_L}{4} (0.352 + 0.022 T - 0.00034 T^2) \quad (20)$$



where  $a_L$  is the leaf absorptance, and  $b_L$  is the fraction of absorbed light that reaches photosystem II. The factor  $1/4$  is introduced here as the equation given by Bernacchi et al. (2003) applies to electron transport rather than C assimilation. Here,  $(a_L b_L / 4)$  is treated as a single calibratable parameter (see Section 3.3) and is henceforth referred to as  $\widehat{c}_L \equiv a_L b_L / 4$ . (All calibratable parameters are thereafter indicated by a hat over the symbol.) This temperature dependence was not accounted for in earlier P-model publications (Keenan et al., 2017; Wang et al., 2017a). To test the effect of this temperature dependence on simulated GPP, we conducted alternative simulations, where a constant  $\widehat{\varphi}_0$  was calibrated instead (Sect. 3.2). Note, that  $\varphi_0$  includes the factor  $a_L$  for incomplete leaf absorptance, which is commonly quantified separately from the quantum yield efficiency. In other vegetation models,  $a_L$  is commonly ascribed a value of 0.72-0.88 (Rogers et al., 2017). Values of  $\varphi_0$  used here are accordingly lower than values for the intrinsic quantum yield reported from experimental studies (Long et al., 1993; Singaas et al., 2001). Furthermore, within-canopy reflection and reabsorption mean that leaf-level absorptance is not equivalent to canopy-level absorptance, thus  $\varphi_0$  should be regarded as canopy-scale *effective* value of intrinsic quantum yield. It is treated here as a calibratable parameter, which may vary according to the fAPAR forcing data set used.

### 3.1.2 Soil moisture stress

$\beta(\theta)$  is an empirical soil moisture stress function. We use results by Stocker et al. (2018) to fit this function based on two general patterns. First, the functional form of  $\beta(\theta)$  is approximated by a quadratic expression that approaches 1 for soil moisture above a certain threshold  $\theta^*$  and held constant at 1 for soil moisture values above this threshold. Here  $\theta$  is the plant-available soil water, expressed as a fraction of field capacity, and  $\theta^*$  is set to 0.6. The general form is:

$$\beta = \begin{cases} q(\theta - \theta^*)^2 + 1, & \theta \leq \theta^* \\ 1, & \theta > \theta^* \end{cases} \quad (21)$$

Second, the sensitivity of  $\beta(\theta)$  to extreme soil dryness ( $\theta \rightarrow 0$ ) is related to the mean aridity, quantified as the mean annual ratio of actual over potential evapotranspiration (AET/PET) (Stocker et al., 2018). The decline in  $\beta(\theta)$  with drying soils is steep in dry climates and less steep in less dry climates. In equation 21, the sensitivity parameter  $q$  is defined by the maximum  $\beta$  reduction at low soil moisture  $\beta_0 \equiv \beta(\theta = \theta_0)$ , leading to  $q = (\beta_0 - 1) / (\theta^* - \theta_0)^2$ . Note that  $q$  has a negative value.  $\beta_0$  is modelled as a linear function of the mean aridity, :

$$\beta_0 = \widehat{a}_\theta + \widehat{b}_\theta (\text{AET/PET}) \quad (22)$$

$\widehat{a}_\theta$  and  $\widehat{b}_\theta$  are treated as calibratable parameters.

Soil moisture ( $\theta$ ), AET, and PET are simulated using the SPLASH model (Davis et al., 2017), which treats soil water storage as a single bucket and calculates potential evapotranspiration based on Priestley and Taylor (1972). We also account for a variable water holding capacity calculated based on soil texture and depth data from SoilGrids (Hengl et al., 2014). A detailed description of the applied empirical functions for calculating plant-available water holding capacity from texture data is given in Appendix D.



### 3.2 Simulation protocol

195 We conducted multiple simulations (Tab. 1) to investigate the dependence of model performance on alternative model setups (variable/fixed soil moisture and temperature effects), alternative choices of forcing data (fAPAR), and alternative observational target data for calibration (GPP based on different flux decompositions). Parameters ( $\widehat{c}_L$ ,  $\widehat{a}_\theta$ , and  $\widehat{b}_\theta$ ) were calibrated and evaluated against the appropriate observational data for each set of simulations separately.

The setup ORG is the P-model in its original form, as described in Wang et al. (2017a). It uses a fixed quantum efficiency of photosynthesis ( $\widehat{\varphi}_0$  is calibrated, instead of  $\widehat{c}_L$ ), and does not account for soil moisture stress ( $\beta(\theta) = 1$ ). Here, the model is forced with fAPAR data based on MODIS FPAR (MCD15A3H), splines of 4-daily values to daily values (see Section 3.4.1), and is calibrated against GPP data from FLUXNET 2015 based on the nighttime partitioning method (NT) (see Section 3.5.2). The simulation set BRC (Bernacchi) is identical to ORG except that  $\widehat{\varphi}_0$  is allowed to vary with temperature following Bernacchi et al. (2003) and Eq. 20, and  $\widehat{c}_L$  is calibrated. The full P-model setup (FULL) includes the soil moisture stress function described above, and  $\widehat{c}_L$ ,  $\widehat{a}_\theta$ , and  $\widehat{b}_\theta$  are calibrated simultaneously.

All additional simulations account for both temperature and soil moisture effects. The simulation set FULL\_FPARitp also uses MODIS FPAR data for fAPAR, but applies a linear interpolation to get daily values to evaluate the impact of using smoothed values from the splined data set. The simulation set FULL\_EVI uses MODIS EVI (MOD13Q1), splined to daily from 8-daily data, to assess to which the degree to which model performance depends on the fAPAR forcing data. See Section 3.4.1 for more information.

All simulations were calibrated against GPP data, calculated using the nighttime flux decomposition method (Reichstein et al., 2005). Additional simulation sets FULL\_DT, FULL\_NTsub, and FULL\_Ty were used to investigate the dependence of model performance on the choice of observational data used for calibration. We used GPP data based on the nighttime decomposition method (Reichstein et al., 2005) for FULL\_NTsub, the daytime decomposition method (Lasslop et al., 2010) for FULL\_DT, and an alternative decomposition method from Wang et al. (2017a) for FULL\_Ty. The Ty method estimates a *constant* monthly background respiration rate fitted to match net ecosystem exchange fluxes of CO<sub>2</sub> from measurements assuming a linear or saturating dependence of GPP on PPFD. Calibration and evaluation of FULL\_DT, FULL\_NTsub, and FULL\_Ty are done only for sites and dates where observational data is available for all three datasets (DT, NT, and Ty), hence the distinction between FULL\_NTsub and FULL.

### 220 3.3 Model calibration

Calibration was performed only for the model parameters determining the quantum efficiency of photosynthesis ( $\widehat{\varphi}_0$  or  $\widehat{c}_L$ , respectively) and the dependence of the sensitivity of the soil moisture stress function on average aridity (parameters  $\widehat{a}_\theta$  and  $\widehat{b}_\theta$ ). Simulated GPP was calibrated to minimise the root mean square error (RMSE) compared to observed daily GPP (Sect. 3.5). We used Generalised Simulated Annealing from the *GenSA* R package (Yang Xiang et al., 2013) to optimise model parameters. This algorithm is particularly suited to find global minima of non-linear objective functions in situations where there can be a large number of local minima.



**Table 1.** Model setups. The standard fAPAR data is MODIS FPAR MCD15A3H, where the original data, given at 4-day intervals, is splined to daily values. Alternative greenness forcing data are based on MODIS EVI MOD13Q1, splined (spl.) from 8-day intervals to daily, and MODIS FPAR MCD15A3H, linearly interpolated (itpl.) from 4-day intervals to daily. Standard observational GPP data, used for model calibration and evaluation, are from FLUXNET 2015, based on the nighttime flux decomposition method (NT in the table, variable GPP\_NT\_VUT\_REF in FLUXNET 2015). Alternative GPP data used based on the daytime flux decomposition method (DT in the table, variable GPP\_DT\_VUT\_REF), and based on an alternative method (Wang et al., 2017a) (Ty in the table). For setups ORG, BRC, FULL, FULL\_FPARitp, and FULL\_EVI, data used for the model calibration is from all dates where NT data are available. For setups FULL\_DT, FULL\_Ty, and FULL\_NTsub, calibration data are from all dates where data is available for all three methods DT, NT, and Ty. Column  $\varphi_0(T)$  specifies whether the temperature dependence of intrinsic quantum yield is included. Column  $\beta(\theta)$  specifies whether soil moisture stress is included. Columns  $\widehat{\varphi}_0$ ,  $\widehat{c}_L$ ,  $\widehat{a}_\theta$  and  $\widehat{b}_\theta$  provide the calibrated parameter values in each simulation set.

Setup name	fAPAR data	GPP	Calibration set	$\varphi_0(T)$	$\beta(\theta)$	$\widehat{\varphi}_0$	$\widehat{c}_L$	$\widehat{a}_\theta$	$\widehat{b}_\theta$
ORG	FPAR MCD15A3H, spl.	NT	NT data	no	no	0.0492	–	–	–
BRC	FPAR MCD15A3H, spl.	NT	NT data	yes	no	–	0.0817	–	–
FULL	FPAR MCD15A3H, spl.	NT	NT data	yes	yes	–	0.0870	0	0.685
NULL	FPAR MCD15A3H, spl.	NT	NT data	no	no	0.2481*	–	–	–
FULL_FPARitp	FPAR MCD15A3H, itpl.	NT	NT data	yes	yes	–	0.0846	0	0.700
FULL_EVI	EVI MOD13Q1, spl.	NT	NT data	yes	yes	–	0.1293	0	0.766
FULL_DT	FPAR MCD15A3H, spl.	DT	NT, DT, Ty	yes	yes	–	0.0891	0	0.690
FULL_Ty	FPAR MCD15A3H, spl.	Ty	NT, DT, Ty	yes	yes	–	0.0868	0	0.721
FULL_NTsub	FPAR MCD15A3H, spl.	NT	NT, DT, Ty	yes	yes	–	0.0899	0	0.690

The value represents the fitted LUE, corresponding to  $(\varphi_0 m' M_C)$  in Eq. 19.

### 3.4 Forcing data

Unstressed light use efficiency,  $m'$  in Eq. 19, is simulated using monthly mean values for  $T$  and  $D$ ; temporally constant site-specific elevation (used to calculate atmospheric pressure, scaled from sea-level standard pressure of 101325 Pa); and annually varying observed atmospheric  $\text{CO}_2$  (MacFarling Meure et al., 2006), identical across sites. The choice of aggregating to monthly mean values is motivated by the time scale of Rubisco turnover, which limits the rate at which photosynthetic parameters can acclimate to changing environmental conditions (McNevin et al., 2006).

Predicted monthly LUE ( $m'$ ) is multiplied by daily varying  $I_{\text{abs}}$ , and response functions  $\varphi_0(T)$  and  $\beta(\theta)$ , driven by daily varying temperature and soil moisture. This choice is motivated by the known rapid response in stomatal conductance to drying soils (represented by  $\beta(\theta)$ ), and the instantaneous temperature response of the quantum yield efficiency ( $\varphi_0(T)$ ). Simulating GPP as the product of LUE and daily varying PPFD would not be consistent with the non-linear instantaneous response of  $A$  to light (Eq. 10) given the acclimation time scale of photosynthesis ((Suzuki et al., 2001; Maire et al., 2012). We therefore



evaluate simulated GPP averaged over 8-day periods. The choice of appropriate model prediction and evaluation time scales is further discussed in Sect. 5.

### 240 3.4.1 fAPAR

Three alternative datasets were used as model forcing for fAPAR (MODIS FPAR splined, MODIS FPAR linearly interpolated, and MODIS EVI, see Tab. 1). MODIS FPAR data are from the MCD15A3H, Collection 6 dataset (Myneni et al., 2015), given at a resolution of 500 m and 4 days. The data were filtered to remove data points where clouds were present, values equal to 1.00, and outliers (more than three times the inter-quartile range). Filtered values were replaced by the mean value for the  
245 respective day-of-year. To obtain daily varying  $I_{\text{abs}}$  (Eq. 18), two alternatives were explored. For the first, daily fAPAR values were derived using a cubic smoothing spline (function `smooth.spline()` with parameter `spar=0.01` in R (R Core Team, 2016)). For the second, values were linearly interpolated to each day. MODIS EVI data is from the MOD13Q1, collection 6 dataset (Didan, 2015), given at a resolution of 250 m and 8 days. This data were filtered based on the summary quality control flag, removing “cloudy” pixels. Gaps were filled and data was splined to daily values. All fAPAR data were downloaded from  
250 Google Earth Engine using the `google_earth_engine_subsets` library (Hufkens, 2017).

### 3.4.2 Meteorological data

The meteorological forcing data are derived from the FLUXNET 2015 Tier 1 dataset (daily means), which provides data from measurements taken and processed along with the CO<sub>2</sub> flux measurements. The photosynthetic photon flux density PPFD ( $\text{mol m}^{-2} \text{d}^{-1}$ ) is derived from shortwave downwelling radiation as  $\text{PPFD} = 60 \cdot 60 \cdot 24 \cdot 10^{-6} k_{\text{EC}} R_{\text{SW}}$ , where  $k_{\text{EC}} = 2.04 \mu\text{mol J}^{-1}$   
255 (Meek et al., 1984), and  $R_{\text{SW}}$  is incoming shortwave radiation from daily FLUXNET 2015 data (variable name `SW_IN_F`, given in  $\text{W m}^{-2}$ ). The factor  $k_{\text{EC}}$  accounts for the energy content of  $R_{\text{SW}}$  and the fraction of photosynthetically active radiation in total short-wave radiation. Vapour pressure deficit (VPD, or  $D$  in Sect. 2) is taken from daily FLUXNET 2015 data (variable name `VPD_F`) and represents means over half-hourly periods. We use daily air temperature from the FLUXNET 2015 dataset (variable name `T_F`), defined as the mean over half-hourly data. This is a simplification, as we are not using leaf temperature  
260 or VPD at the leaf surface, which are more directly relevant for photosynthesis.

## 3.5 Calibration and evaluation data

### 3.5.1 Site selection

We used data from 70 sites for model calibration and 131 sites for evaluation (Fig. 1, and Tab. A1). The number of valid daily GPP data points used for the calibration set was 160,061 and 260,284 for the evaluation set. The calibration sites were selected  
265 based on the apparent reliability of relationships between CO<sub>2</sub> fluxes, co-located greenness data, measured soil moisture, and meteorological variables, emerging from a previous analysis (Stocker et al., 2018). For the evaluation, we used all sites except those in cropland and seven sites where C<sub>4</sub> vegetation dominates (AU-How, DE-Kli, FR-Gri, IT-BCi, US-Ne1, US-Ne2, and US-Ne3).

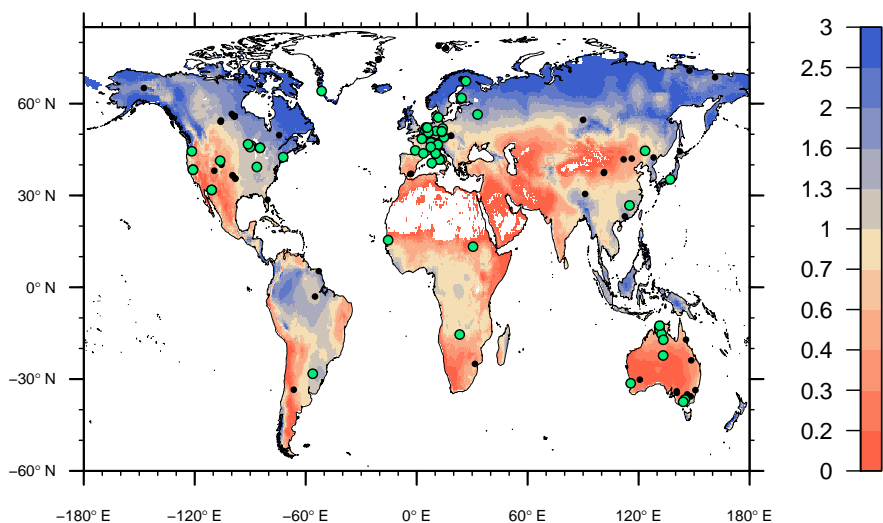


**Figure 1.** Overview of sites selected for model calibration (green dots) and evaluation (green and black dots). All sites and additional information are listed in Tab. A1. The color key represents aridity, quantified as the ratio of precipitation over potential evapotranspiration from Greve et al. (2014).

### 3.5.2 Data filtering

270 GPP predictions by the P-model are compared to GPP estimates from the FLUXNET 2015 Tier 1 data set (downloaded on 13  
November, 2016). We used GPP based on the nighttime partitioning method (Reichstein et al., 2005) (GPP\_NT\_VUT\_REF)  
and filtered out negative daily GPP values, data for which more than 50% of the half-hourly data are gap-filled and for which the  
daytime and nighttime partitioning methods (GPP\_DT\_VUT\_REF and GPP\_NT\_VUT\_REF, respectively) are inconsistent,  
i.e., the upper and lower 2.5% quantiles of the difference between GPP values quantified by each method. For additional  
275 simulation sets, model calibration and evaluation was performed using GPP data based on the daytime partitioning method  
(GPP\_DT\_VUT\_REF) (Lasslop et al., 2010) with analogous filtering steps, and GPP data based on an alternative method  
that fits a constant ecosystem respiration rate as the net ecosystem exchange under conditions where PPFD tends to zero  
(FULL\_Ty, Wang et al. (2017a)). For all calibration and evaluation, we removed data points before the “MODIS era” (before  
18th of February, 2000).

### 280 3.6 Evaluation methods

We evaluated both simulated LUE and GPP. The P-model (Sect. 2) predicts variations in LUE across sites (space) and months  
(monthly  $LUE = m'$ ), while simulated GPP is affected by the PPFD and fAPAR data used as model forcing (Eq. 19 and Sect.  
3.4). Conversely, “observed” LUE is calculated as  $LUE_{obs} = GPP_{obs}/(fAPAR \cdot PPFD)$  and the evaluation is thus also affected by  
the PPFD and fAPAR data. The evaluation of LUE tests the added explanatory power of the P-model compared to models that



**Table 2.** Description of Koeppen-Geiger climate zones (based on Falge et al. (2017)) and number of sites for which data is available per climate zone and hemisphere. Only zones with data from more than three sites are shown.

Code	<i>N</i> north	<i>N</i> south	Description
Aw	–	5	Tropical savannah with dry winter
BSk	5	–	Arid steppe cold
Cfa	11	–	Warm temperate fully humid with hot summer
Cfb	19	5	Warm temperate fully humid with warm summer
Csa	12	–	Warm temperate with dry and hot summer
Csb	4	–	Warm temperate with dry and warm summer
Dfb	17	–	Cold fully humid warm summer
Dfc	22	–	Cold fully humid cold summer

285 rely on fixed prescribed LUE values. Evaluating GPP facilitates the comparison of the model performance to similar models of terrestrial GPP. Model performance for GPP is benchmarked against a null model (NULL), which assumes a temporally constant and spatially uniform LUE. The LUE for the NULL model is fitted to observed GPP using splined MODIS FPAR and GPP data from the NT method, see Tab. 1. Thus, while LUE is constant, the NULL model preserves the spatial and temporal patterns in APAR (= fAPAR · PPFD).

### 290 3.6.1 Components of variability

For LUE, we separately analysed spatial (mean annual values by site) and monthly means only for the FULL setup. For GPP, we analyzed spatial, annual, seasonal (mean by day-of-year), 8-daily, and the variability in daily anomalies from the mean seasonal cycle for all setups. The seasonal variability was determined for different Koeppen-Geiger climatic zones (see Tab. 2). Information about the association of sites with climatic zones was extracted from Falge et al. (2017). Evaluations were made only for climatic zones with at least five sites. For each component of variability, we calculated the adjusted coefficient of determination ( $R_{adj}^2$ , thereafter referred to as  $R^2$ ), and the root mean square error (RMSE). Figures showing correlations between simulated and observed values additionally present the mean bias, the slope of the linear regression model, and the number of data points ( $N$ ).

### 3.6.2 Drought response

300 The bias in GPP (modelled minus observed) was calculated for 20 days before and 80 days after the onset of a drought event as identified by Stocker et al. (2018) for 36 sites. Drought events (fLUE droughts) are periods of consecutive days where soil moisture, separated from other drivers using neural networks, reduces LUE below a given threshold. The data specifying the timing and duration of drought events was downloaded from Zenodo (Stocker, 2018). We then re-arranged the data to align all



**Table 3.**  $R^2$  of simulated and observed GPP based on different model setups and for different components of variability.

Setup	8-daily	Spatial	Annual	Seasonal	var(daily)	var(annual)
FULL	0.75	0.70	0.70	0.74	0.28	0.09
BRC	0.72	0.66	0.62	0.73	0.26	0.06
ORG	0.69	0.62	0.57	0.69	0.25	0.06
NULL	0.69	0.64	0.58	0.71	0.25	0.04
FULL_FPARitp	0.73	0.70	0.70	0.74	0.25	0.09
FULL_EVI	0.70	0.56	0.47	0.72	0.29	0.14
FULL_DT	0.65	0.69	0.70	0.65	0.30	0.08
FULL_NTsub	0.67	0.70	0.70	0.68	0.30	0.09
FULL_Ty	0.69			0.69	0.49	

drought events at all sites, normalised data to their median value during the ten days before the onset of droughts (normalisation  
305 by subtracting median), and computed quantiles per day, where ‘day’ is defined with respect to the onset of each drought event.

## 4 Evaluation results

### 4.1 GPP variability across scales

Tables 3 and 4 provide an overview of model performance ( $R^2$  and RMSE) in simulating GPP at different scales. The ORG  
310 setup captures 69% of the variance in observed GPP with data aggregated to 8-day means (60’450 data points). Model per-  
formance both with respect to explained variance ( $R^2$ ) and the RMSE is improved by including the effects of temperature on  
quantum yield efficiency in the BRC model setup ( $R^2 = 72\%$ ), and by including the effects of soil moisture stress in the FULL  
model setup ( $R^2 = 75\%$ , Fig. 2). Both the BRC and FULL model setup outperform the NULL model.

The  $R^2$  for simulated GPP, aggregated to annual totals, ranges from 0.57 (ORG) to 0.70 (FULL). The NULL model achieves  
an  $R^2$  of 0.58. Most of the explanatory power of the different models for predicting annual total GPP stems from their power in  
315 predicting between-site (“spatial”) variations (Fig. 3). The  $R^2$  for spatial variations ranges from 0.62 (ORG) to 0.70 (FULL),  
and 0.64 for the NULL model. In contrast, inter-annual variations at a site are poorly simulated ( $R^2$ : 0.06-0.09 for P-model  
setups, and 0.04 for the NULL model). Inter-annual variations are generally much smaller than between site variations. Thus,  
capturing them is challenging. Inter-annual GPP variations are generally better simulated at sites where the variability is high  
and in particular at dry sites.



**Table 4.** Root mean square error (RMSE) of simulated and observed GPP based on different model setups and for different components of variability.

Setup	8-daily	Spatial	Annual	Seasonal	var(daily)	var(annual)
FULL	1.91	421.49	396.48	1.74	1.61	149.90
BRC	2.01	455.58	444.06	1.80	1.61	151.65
ORG	2.13	485.62	474.46	1.92	1.60	152.91
NULL	2.10	468.14	478.02	1.85	1.56	153.26
FULL_FPARitp	1.98	427.46	402.94	1.77	1.71	148.96
FULL_EVI	2.10	523.04	535.66	1.85	1.56	143.11
FULL_DT	2.08	390.45	363.55	1.94	1.73	155.03
FULL_NTsub	2.05	418.65	392.20	1.90	1.73	150.76
FULL_Ty	1.86			1.75	1.37	

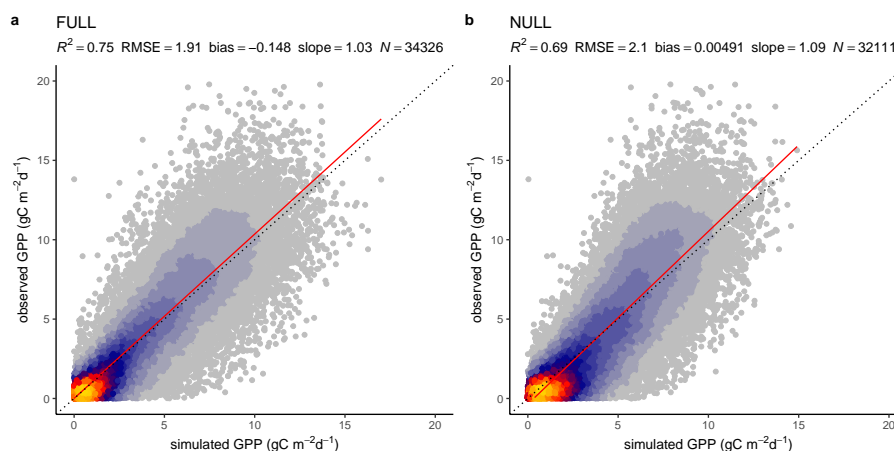


**Figure 2.** Correlation of observed and modelled GPP values of all sites pooled, mean over 8-day periods, for the model setup FULL (a) and NULL (b).

#### 320 4.1.1 Seasonal variations

Seasonal variations are generally reliably simulated ( $R^2$ : 0.69-0.74 for P-model setups, and  $R^2$ : 0.71 for the NULL model, Fig. 4). Also the NULL model captures most of the seasonal variability, especially in climate zones Dfb and Dfc, and Cfb and Cfa. This indicates that seasonal GPP variations are largely driven by seasonal changes in insolation (PPFD) and vegetation greenness (fAPAR). Accounting for temperature effects on the quantum yield efficiency reduces the overestimation of GPP in  
 325 spring, except in the case of climate zone Dfb. Observed GPP increases are lagged compared to vegetation greenness, with a



delay of up to 2 months at some sites (e.g., US-Los). This lag is clearly visible at almost all sites in Dfb. The early season high bias is largely absent for sites in climate zone Cfb, where observed GPP starts increasing early and the simulations match the observations except at sites CZ-wet, DE-Hai, and FR-Fon, where the simulated start of season is simulated too early.

330 GPP is overestimated during the dry season in climate zones with a marked dry season (Aw, BSk, Csa, and Csb) in model setups that do not account for soil moisture stress (ORG, BRC, NULL). The NULL model has the largest bias. High VPD during dry periods reduces simulated LUE and leads to lower GPP values and a smaller bias in all the P-model setups (ORG, BRC, FULL). The empirical soil moisture stress function applied in setup FULL eliminates the dryness-related bias in zones Aw, Csa, and Csb and substantially reduces this bias for sites in zone BSk. Observations suggest that GPP declines to values around zero during dry periods at sites in zone BSk (mostly savannah vegetation and grasslands, see Table A1). The remaining  
335 bias in the FULL model, which includes the soil moisture stress function, is related to the fact that fAPAR remains relatively high and that the soil moisture stress function does not decline to zero.

The ORG and BRC models tend to underestimate peak season GPP more strongly compared to the FULL model. This is a direct consequence of the calibration which balances errors across all data points. Across-site average peak-season maximum GPP is accurately captured by the FULL model in all zones (Fig. 4), except for an underestimation of GPP in zones Aw and Cfb,  
340 and an overestimation in zone Csa. Site-level evaluations suggests no clear relationship between peak-season underestimation and vegetation type in zone Cfb. The overestimation of peak-season GPP in zone Csa is caused by a high bias at sites with evergreen broadleaved vegetation (FR-Pue, IT-Cp2, IT-Cpz); sites with other vegetation types show no consistent peak season bias.

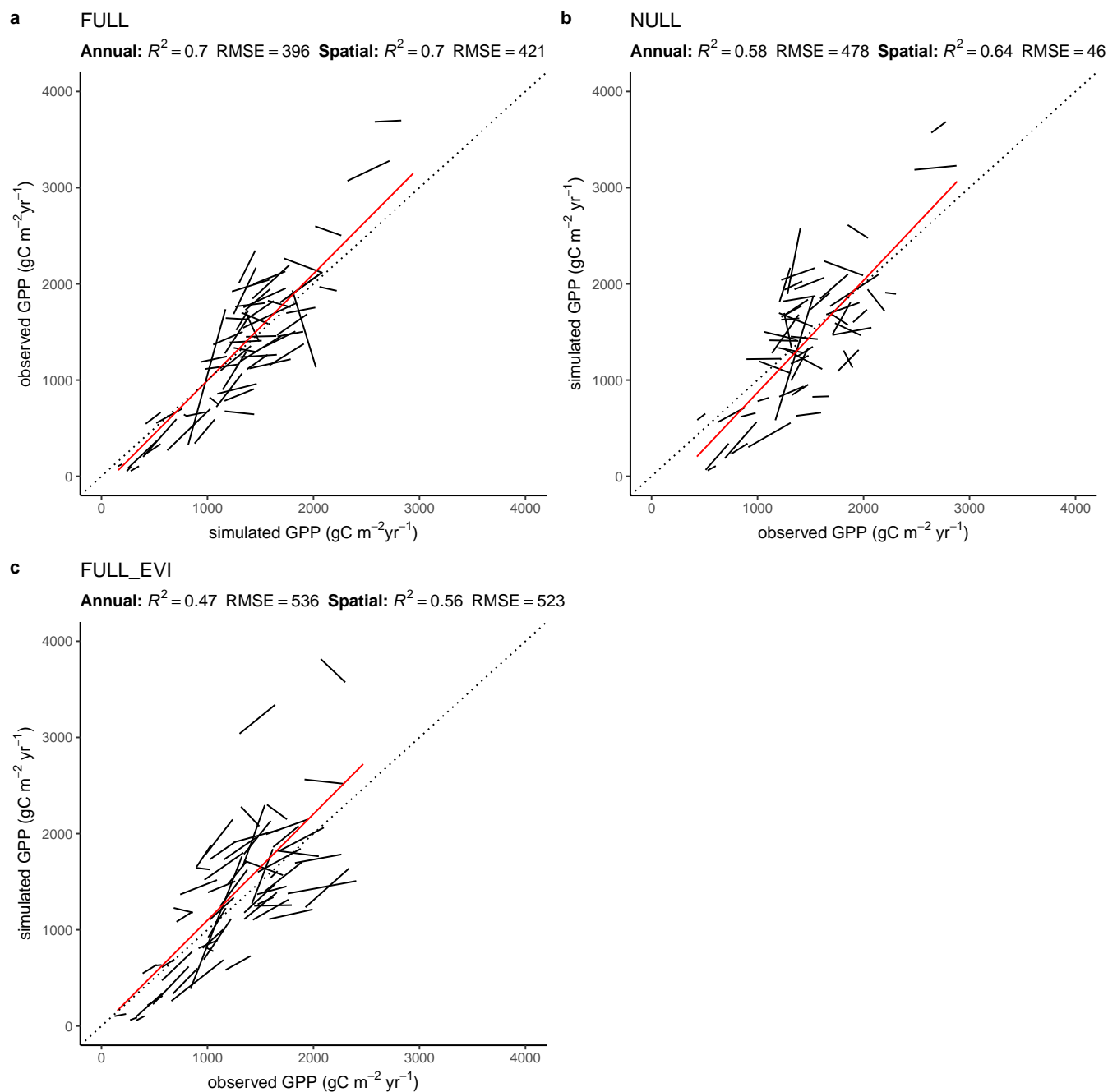


**Figure 3.** Correlation of modelled and observed annual GPP in simulations FULL (a), NULL (b) and FULL\_EVI (c). The red line and text are based on means across years by site and represents spatial (across-site) variations. Black lines and text are based on annual values, one line for each site. Lines represent linear regressions.  $R^2$  and RMSE statistics for annual values (black text) are based on pooled data from all sites. For a perfect fit between modelled and observed annual GPP values, all black lines (representing the linear regression model of annual values for a single site) would lie on the 1:1 line and have a slope of 1. Slopes that deviate substantially from 1, or even are negative, for some sites shows poor model performance in capturing inter-annual variability.

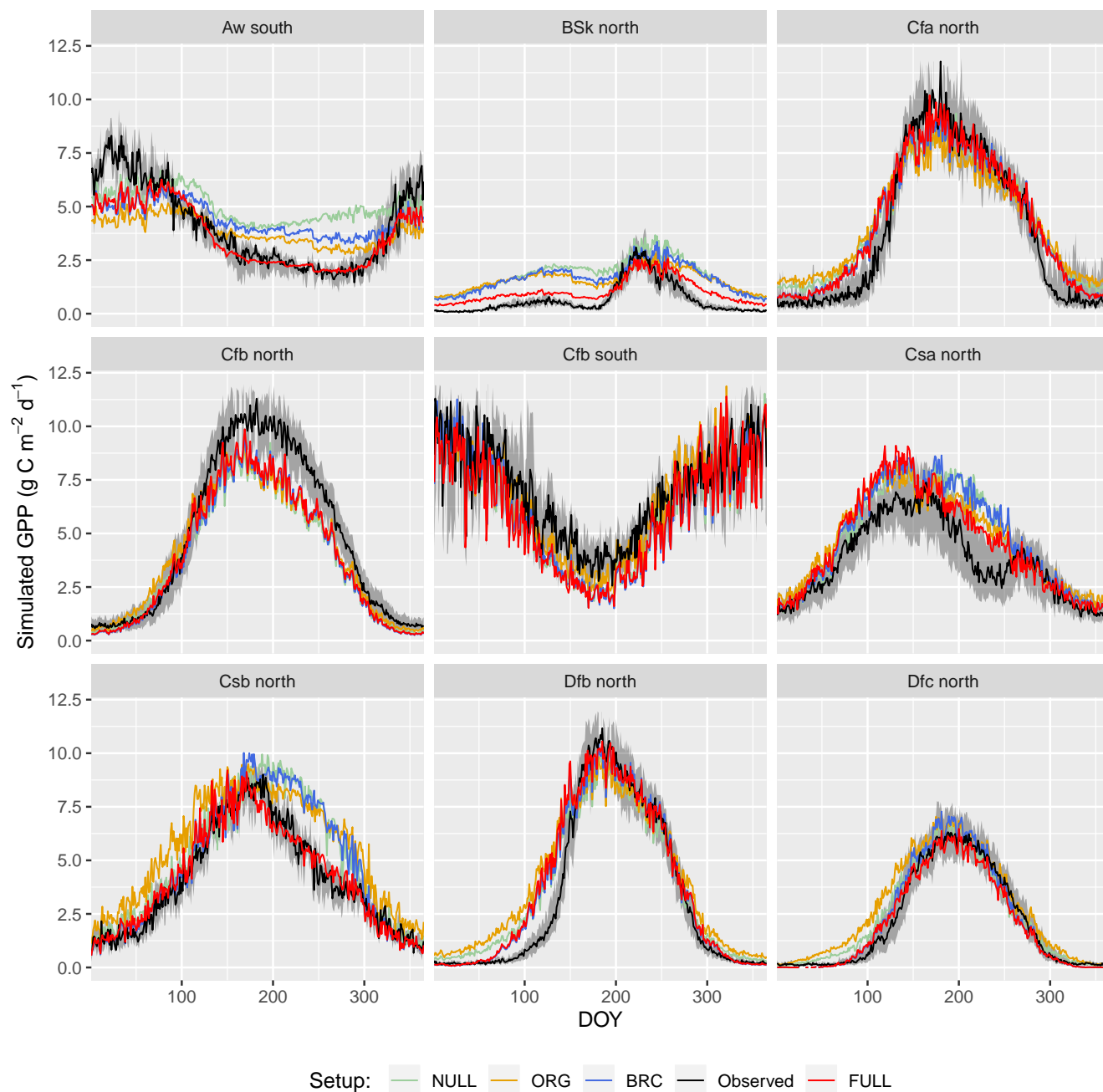


**Figure 4.** Mean seasonal cycle. Observations are given by the black line and grey band, representing the median and 33/66 % quantiles of all data (multiple sites and years) pooled by climate zone. Coloured lines represent different model setups. The annotation above each plot specifies the climate zone (see Tab. 2). Only climate zones are shown here for which data from at least five sites was available.



## 4.2 GPP target data

345 The different flux decomposition methods make fundamentally different assumptions regarding the sensitivity of ecosystem respiration to diurnal changes in temperature. This should lead to systematic differences in derived observational GPP values and should affect model-data disagreement.

Model predictions compare better to GPP data based on the flux decomposition method Ty (Wang et al., 2017a) than for GPP data based on the DT and NT methods. For GPP 8-day means, the model achieves an  $R^2$  of 0.70 when compared to GPP Ty (model setup FULL\_Ty), as opposed to 0.65 and 0.67 compared to the DT and NT methods, respectively (FULL\_DT and FULL\_NTsub, Tab. 3, Fig. 7). Variations in daily anomalies are much better captured by the model when evaluating to GPP Ty ( $R^2$ : 0.49), as compared to evaluations against DT or NT ( $R^2$ : 0.30). Spatial and annual correlations are not evaluated for GPP Ty due to missing data. Correlations at the 8-day, seasonal and daily time scales rely on dates for which neither the NT, DT, nor Ty method has missing values and thus contain an equal number of data points. Therefore NT evaluations, repeated  
355 here, are not identical to the ones above and are referred to as ‘NTsub’ in Tables 3 and 4.

We found a systematic low bias of simulated GPP in the peak-season in the climatic zone Cfb (warm temperate, fully humid, warm summer). However, as shown in Fig. 7, this bias does not seem to be affected by the choice of GPP evaluation data.

## 4.3 Drought response

The P-model setups that do not include the soil moisture stress function (ORG and BRC) systematically overestimate GPP during droughts (Fig. 5). This bias increases sharply at the onset of drought events and continues to increase throughout the drought period. The bias is strongly reduced by applying the empirical soil moisture stress function (Eq. 21) in the FULL model. A small bias remains also in the FULL model. This stems from overestimated values at a few sites (in particular AUDaP, US-Cop, US-SRG, US-SRM, US-Var, US-Whs, US-Wkg), mostly grasslands and sites in seasonally dry climate zones (Aw, BSk, and Csa, see Fig. 4), where flux measurements indicate an almost complete shut-down of photosynthetic activity during  
365 the dry season. In contrast, the fAPAR data (MODIS FPAR) suggest values substantially greater than zero at these sites during these periods. This suggests either contributions to PAR absorption by photosynthetically inactive tissue, underestimation of LUE sensitivity to dry soils at these sites, or an overestimation of the rooting zone moisture availability by SPLASH.

## 4.4 Uncertainty from fAPAR input data

Tests of the sensitivity of model performance to alternative fAPAR forcing datasets show that the difference between splined  
370 and linearly-interpolated MODIS FPAR is negligible. However, model performance is generally better using MODIS FPAR compared to simulations using MODIS EVI. Spatial variations are well captured using MODIS FPAR (Fig. 3,  $R^2$ : 0.70) compared to MODIS EVI ( $R^2$ : 0.56). However, the  $R^2$  of inter-annual variations is 0.14 for MODIS EVI and 0.09 for MODIS FPAR. In terms of biases in climate zones, the overestimation of GPP during the dry period in zone BSk is larger when using MODIS EVI than when using MODIS FPAR (Fig. 6, right). The positive spring bias in simulated GPP in zone Dfb is present  
375 irrespective of the source of the fAPAR forcing (Fig. 6, left), as is the peak-season bias of GPP in zones BSk, Cfb, and Csb.

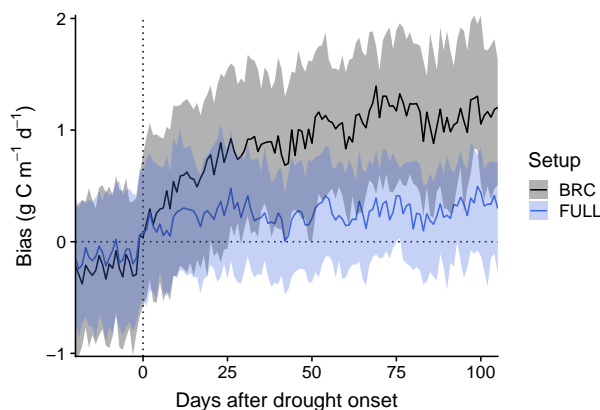


**Figure 5.** Bias in simulated GPP during the course of drought events. Simulated GPP is from a simulation with (FULL) and without (BRC) accounting for soil moisture stress. The timing of drought events is taken from Stocker et al. (2018) and is identified by an apparent soil moisture-related reduction of observed light use efficiency at 36 FLUXNET sites. The bias is calculated as simulated minus observed GPP. Data from multiple drought events and sites are aligned by the date of drought onset and aggregated across all sites and events (lines for medians, shaded ranges from the 33% and 66% quantiles).

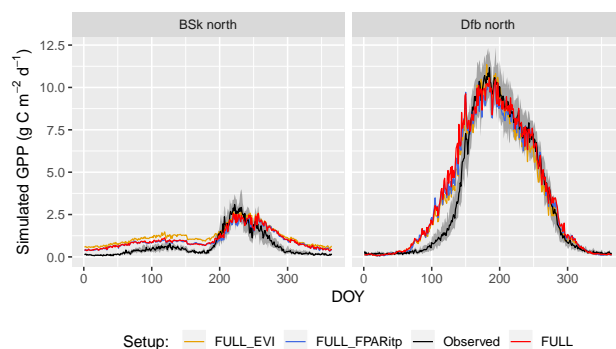


**Figure 6.** Mean seasonal cycle for model setups with different greenness forcing data for two climate zones (BSk and Dfb, both northern hemisphere). Observations are given by the black line and grey band, representing the median and 33/66 % quantiles by day-of-year (DOY) of all data (multiple sites and years) pooled by climate zone. Coloured lines represent model setups, forced with different greenness data. The annotation above each plot specifies the climate zone (see Tab. 2). Climate zones shown here are illustrative examples.

Differences between the EVI and FPAR-forced simulations depend on vegetation type. The EVI-forced simulation tends to be low biased in evergreen needle-leaved vegetation, and has generally lower values in all evergreen vegetation types compared to the FPAR-forced simulation. However, there is no general difference in model bias between simulations made with the two forcings in other vegetation types.

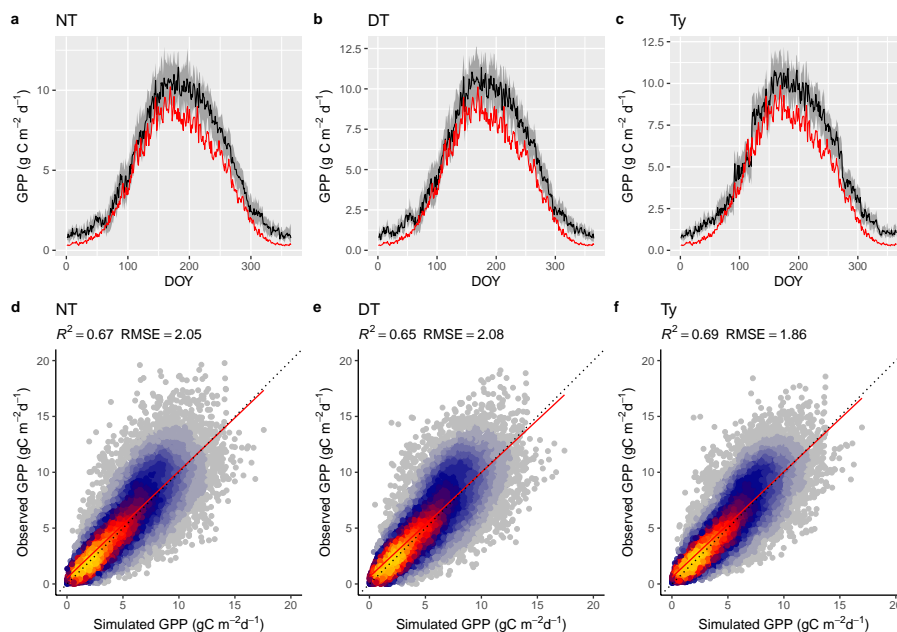


**Figure 7.** Model performance subject to comparison with different flux decomposition methods for GPP. (a-c): Mean seasonal cycle of simulated (red) and observed GPP (black) based on different flux decomposition methods. The grey band represents the 33/66 % quantiles of observed GPP by day-of-year (DOY). (d-f): Correlation of observed and simulated GPP values of all sites pooled, mean over 8-day periods. ‘Observed GPP’ refers to the different flux decomposition methods: DT for the daytime method (setup FULL\_DT), NT for the nighttime method (setup FULL\_NTsub) and Ty (setup FULL\_Ty) for the method applied for data used in Wang et al. (2017b). Dotted lines in (d-f) represent the 1:1 relationship, red lines represent the fitted linear regressions.

#### 380 4.5 Uncertainty from GPP target data

Model predictions compare better to GPP data based on the Ty than either the DT or NT methods. For GPP, 8-day means, the model achieves an  $R^2$  of 0.69 when compared to GPP Ty (model setup FULL\_Ty), compared to 0.65 and 0.67 for the DT and NT methods, respectively (FULL\_DT and FULL\_NTsub, Tab. 3, Fig. 7). Variations in daily GPP anomalies are much better captured in evaluations with Ty ( $R^2$ : 0.49) than DT or NT ( $R^2$ : 0.30). Spatial and annual correlations were not evaluated for  
385 Ty because of missing data. The systematic low bias of simulated peak-season GPP in climatic zone Cfb is not affected by the choice of GPP evaluation data (Fig. 7).

The systematic differences in the level of model-data agreement depending on the target GPP dataset (Fig. 7) reflect the fact that these datasets are derived using decomposition methods with different sensitivity to diurnal changes in temperature.

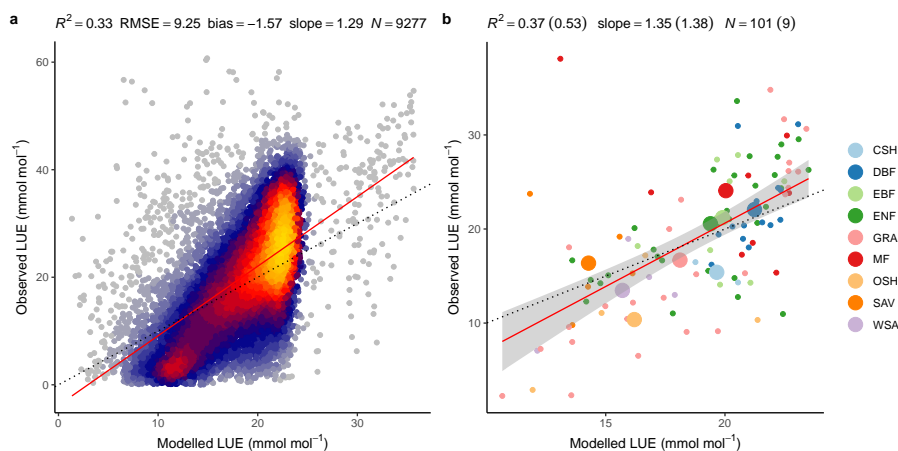


**Figure 8.** Modelled (simulations FULL) versus observed LUE. (a) Mean monthly LUE with data pooled from all sites and available years. (b) Mean annual LUE by site (small dots and color) and vegetation type (large dots and color). Model performance metrics are given at the top with numbers in brackets referring to the regression of data aggregated by vegetation types and non-bracketed numbers for data aggregated by sites. Dotted lines represent the 1:1 relationship, red lines represent the fitted linear regression to all data in (a) and to mean annual LUE by site in (b). The grey band in (b) represents the 95 % confidence interval of the linear regression. Vegetation types are: closed shrubland (CSH); deciduous broadleaf forest (DBF); evergreen broadleaf forest (EBF); evergreen needleleaf forest (ENF); grassland (GRA); mixed deciduous and evergreen needleleaf forest (MF); open shrubland (OSH); savanna ecosystem (SAV); woody savanna (WSA).

#### 4.6 LUE

390 The FULL version of the P-model captures 37% of the variability in mean annual LUE across all sites and across the full range  
of observed mean annual LUE values and vegetation types (Fig. 8). 53 % of the observed LUE variation within vegetation types  
is captured by the model through the relationships with climate, without the need to specify parameters for specific vegetation  
types.

395 33% of the variability in monthly mean LUE is captured by the model, with data from all sites and years pooled (Fig. 8). The  
model overestimates monthly LUE values and underestimates LUE at the lowest and highest end of the LUE range respectively.  
The low-end overestimation is reflected by the overestimation of GPP in the spring at winter-cold sites (Sect. 4.1.1) and during  
soil moisture droughts (Sect. 4.3). The underestimation of high monthly values is not clearly linked to any particular vegetation  
type.

#### 5 Discussion

400 The performance of the P-model can be compared to results obtained from other remote-sensing driven GPP models (RS-  
models). In its FULL setup, the P-model achieves an  $R^2$  of 0.75 and a RMSE of  $1.91 \text{ g C m}^{-2} \text{ d}^{-1}$ , in simulating 8-day mean  
GPP and evaluated against GPP data (NT method) from 131 sites. This can be compared to predictions from the VPM model



( $R^2$ : 0.74, RMSE: 2.08 g C m<sup>-2</sup> d<sup>-1</sup>, 113 sites, 8-daily, Zhang et al. (2017)), or BESS ( $R^2$ : 0.67, RMSE: 2.58 g C m<sup>-2</sup> d<sup>-1</sup>, 113 sites, 8-daily, Jiang and Ryu (2016)). The performance of the P-model in simulating *annual* GPP across all 131 sites ( $R^2$ : 0.70) can be compared to results from MODIS GPP (MOD17A2,  $R^2$ = 0.73, 12 sites, Heinsch et al. (2006), and for the updated version MOD17A2H:  $R^2$ = 0.62, 18 sites, Wang et al. (2017b)).

The coefficients of determination ( $R^2$ ) of simulated versus observed values are lower for LUE (0.37 for the spatial correlation in the FULL setup, Fig. 8b) than for GPP (0.70 for the spatial correlation in the FULL setup). This is because GPP variations are strongly driven by variations in absorbed light (PPFD·fAPAR), which are observed and used for modelling. In contrast, variations in LUE cannot be observed directly. Using remotely-sensed information for estimating LUE variations, e.g., based on sun-induced fluorescence (Frankenberg et al., 2018; Li et al., 2018; Ryu et al., 2019) or alternative reflectance indices (Gamon et al., 1992, 2016; Badgley et al., 2017), is an active field of research and the separation of remotely sensed signals into contributions by LUE and absorbed light remains challenging (Porcar-Castell et al., 2014; Ryu et al., 2019). Other remote sensing-based GPP models rely on vegetation type-specific model parameters for LUE (Zhang et al., 2017; Running et al., 2004; Jiang and Ryu, 2016). The P-model in its FULL setup explains 53% of the variations in LUE across sites aggregated to vegetation types without relying on vegetation or biome-type specific parametrisations. In its ORG setup, it explains 21% of the variations (not shown), and 51% of the variations when excluding sites classified as ‘open shrublands’, which tend to have a substantially lower LUE than simulated by the P-model (not shown). In spite of this substantial portion of explained variability, the NULL model with its temporally constant and spatially uniform LUE achieves higher  $R^2$  values for GPP than the ORG P-model setup at the spatial, annual, and seasonal scales (Tab. 3). This indicates that the spatial and temporal variations in absorbed light are the main drivers of GPP in LUE-type models and underlines the importance of evaluation against a NULL model benchmark. Taken together, these findings demonstrate that the P-model offers a simple but powerful method for simulating terrestrial GPP using readily available input datasets and a very small number of free (calibratable) parameters. Here, three parameters are calibrated (for the FULL setup). Other model parameters are derived from independent field and laboratory measurements.

Accounting for the temperature-dependence of the quantum yield efficiency ( $\varphi_0$ ) clearly improves model predictions. The parameter  $\varphi_0$  is commonly treated as a constant in global vegetation models (Rogers et al., 2017). Our results indicate potential for improving DVM photosynthesis routines by accounting for the temperature-dependence of  $\varphi_0$ .

$\varphi_0$  appears as a linear scalar in the LUE model. However, the magnitude of this scalar is uncertain and depends on whether incomplete light absorption by the leaf is included in the definition of  $\varphi_0$  or in fAPAR data. We have used MODIS FPAR and MODIS EVI data to define fAPAR in different model setups. While the two are well correlated, their absolute values differ. Hence, we have calibrated an *apparent* quantum yield efficiency ( $\widehat{\varphi}_0$ ) to GPP data separately for different fAPAR datasets, thereby implicitly distinguishing what components of light absorption factors are contained in the fAPAR data. The leaf absorbance  $a_L$ , which is typically taken to be around 0.8 in global vegetation models (Rogers et al., 2017) is similar to the ratio of fitted  $\widehat{\varphi}_0$  values for simulation FULL and FULL\_EVI, here calculated as 0.67 (Tab. 1).

An improvement in model performance is obtained by accounting for soil moisture stress using an empirical function. However, the use of an empirical function masks underlying processes. Furthermore, the use of an empirical function is not



consistent with the optimality approach that underlies the P-model. The reduced bias using an empirical soil moisture stress function implies something is missing in the theoretical approach which rests on an assumed constancy of the unit costs of transpiration ( $a$  in Eq. 3). Prentice et al. (2014) provide a definition of  $a$  that is explicit in terms of plant hydraulic traits and physical properties that determine water transport along the plant-soil-atmosphere continuum. In particular,  $a \propto (\Delta\Psi k_s)^{-1}$ , where  $\Delta\Psi$  is the maximum daytime difference in leaf-to-soil water potential and  $k_s$  is the sapwood area-specific permeability. However, large variations in stomatal conductance are known to occur in response to relatively fast soil dry-downs (time scale of days) (Keenan et al., 2010; Egea et al., 2011; Stocker et al., 2018). This suggests the potential to improve the P-model by allowing the unit cost of transpiration to be a function of rooting-zone moisture availability, and by coupling stomatal conductance with the soil water balance.

Observational uncertainty could affect both parameter calibration and model evaluation. Keenan et al. (2019) found a systematic bias in GPP estimates based on the nighttime partitioning method due to inhibition of leaf respiration in the light (Kok, 1949; Wehr et al., 2016), which affects fluxes unevenly throughout the season and across vegetation types. However, we found no clear difference in model-data agreement, nor in fitted parameters, in comparisons of three alternative GPP datasets that use different approaches to decompose net CO<sub>2</sub> exchange fluxes from eddy covariance measurements into ecosystem respiration and GPP terms.

We have found a consistent early-season high-bias in simulated GPP for numerous sites in regions with deciduous broadleaved vegetation in temperate and cold climates (in particular US-MMS, IT-Col, US-WCr, US-UMd, US-UMB, and US-Ha1), and also in mixed and needle-leaved stands (in particular US-Syv, US-NR1, FI-Hyy, CA-Qfo, and CA-Man). Additional analyses (not shown) suggested that this bias is not related to soil temperatures or the difference between soil and air temperatures in spring. The P-model, as applied here, uses daily air temperature for simulating acclimation. Hence, a bias is to be expected in view of the known delay in the resumption of photosynthesis after a cold dormant period (Huner et al., 1993; Oquist and Huner, 2003; Adams et al., 2004; Verhoeven, 2014; Bowling et al., 2018). Such delays are mediated by a biochemical down-regulation of photosynthesis, not included in the P-model, i.e. using xanthophyll carotenoids for photoprotection (Adams et al., 2004) to balance photochemical and biochemical processes – the former being less steeply temperature-dependent (Oquist and Huner, 2003). Cold-acclimation is a strategy to cope with frozen sap transport vessels during periods when air temperature is already high (Bowling et al., 2018), or for protecting against frost damage during early season cold spells (Vitasse et al., 2014). Approaches accounting for a delayed resumption of photosynthesis after cold periods (Pelkonen and Hari, 1980; Bergh et al., 1998; Mäkelä et al., 2004) offer scope for further improvement of the P-model.

There is a positive bias in simulated GPP during the dry season at a number of sites where the vegetation phenology is influenced by drought. The positive bias is related to the combination of using prescribed fAPAR data, which shows substantial absorption by non-green vegetation, and insufficient sensitivity of simulated LUE to soil drying. However, GPP is accurately simulated at other sites affected by seasonally recurring water stress. The modelled sensitivity to dry soils is determined by the soil moisture stress function, which depends on the mean aridity of the site as estimated using a fixed depth soil moisture "bucket". Accounting for variability in rooting zone depth, which may also be influenced by local topographical factors and access to groundwater (Fan et al., 2013, 2017) may help to minimise model biases in drought-prone areas.

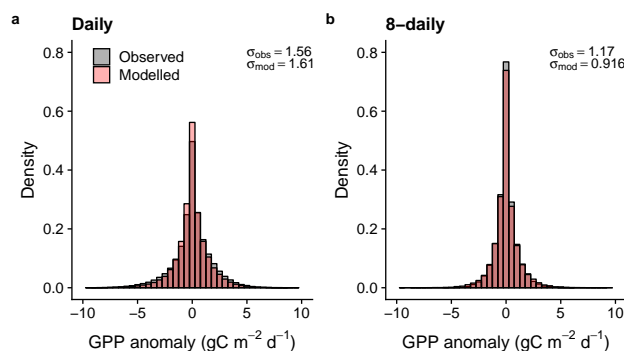


**Figure 9.** Distribution of anomalies from the mean seasonal cycle, evaluated for daily values (a) and 8-day means (b).

The current implementation of the P-model involves some simplifications in terms of climate drivers by using average daily meteorological conditions, measured above the canopy, as input. Optimality in balancing carbon and water costs for average  
475 daily conditions is not necessarily equivalent to optimality in balancing integrated water and carbon costs over the diurnal cycle. Large variations in ambient conditions over a diurnal cycle, combined with a non-linear dependence of costs on these conditions suggest that the approach of taking average daily conditions may be an over-simplification. Nevertheless, prior evaluations have shown robust and accurate predictions of optimal  $\chi$  across a range conditions (Wang et al., 2017a). Using above-canopy VPD values instead of VPD at the leaf surface for scaling water losses implicitly assumes a perfectly coupled  
480 atmospheric boundary layer. Using above-canopy air temperature instead of leaf temperatures introduces a bias when the two become decoupled (Michaletz et al., 2015). The impact of these simplifications may be minor but should be evaluated.

A further simplification is that investment in electron transport capacity (expressed by  $J_{\max}$ ) and investments in the carboxylation capacity (expressed by  $V_{\text{cmax}}$ ) are coordinated so that for conditions with which the model is forced (here, monthly means of daily averages), photosynthesis operates at the co-limitation point of the light- and Rubisco-limited assimilation rates and an  
485 effective linear relationship between absorbed light and mean assimilation emerges. This assumption follows from the *coordination hypothesis* (Chen et al., 1993; Haxeltine and Prentice, 1996), which itself can be understood as an optimality principle (Haxeltine and Prentice, 1996), and is well supported by observations (Maire et al., 2012). However, this coordination is contingent on the time scale at which photosynthetic acclimation occurs, which is not known precisely (Smith and Dukes, 2013; Way and Yamori, 2014). By simulating  $\chi$  using monthly mean meteorological variables, we assume a monthly time scale of  
490 acclimation. This is probably a conservative estimate (Smith and Dukes, 2017; Veres and Williams, 1984). Considering the concave relationship of assimilation rates and absorbed light that follows from the FvCB model for a given  $J_{\max}$ , linearly scaling a given monthly LUE term with daily varying absorbed light levels should lead to an overestimation of assimilation rates at high light levels. This overestimation should disappear as the time scale over which light levels are averaged is increased. However, our results do not confirm these expectations. The fact that the model did not exhibit a systematic error in simulating  
495 GPP variations when applied at the daily time scale suggests that the day-to-day variability in light levels is relatively small compared to the within-day variability.



## 6 Conclusions

The P-model provides a simple, parameter-sparse but powerful method to predict photosynthetic capacity and light use efficiency across a wide range of climatic conditions and vegetation types. It provides a basis for a terrestrial light use efficiency model driven by remotely sensed vegetation greenness. Using optimality principles for the formulation of the P-model reduces its dependence on uncertain or vegetation type-specific parameters and enables robust predictions of GPP and its variations through the seasons, between years, and across space. Further work is required to develop a distinct treatment of C<sub>4</sub> vegetation for global applications and additional evaluations are needed to examine the P-model's sensitivity to increasing CO<sub>2</sub>. We have shown that accounting for the effects of low soil moisture and the reduction in the quantum yield efficiency under low temperatures improves model performance. There is potential to include below-ground water limitation effects in the mechanistic optimality framework of the P-model.

*Code and data availability.* The P-model is implemented as an R package (*rpmodel*) and available through <https://stineb.github.io/rpmodel/>. The R package will be made available through CRAN. Code for all evaluations presented here is available through [https://github.com/stineb/eval\\_pmodel](https://github.com/stineb/eval_pmodel). Model outputs are available on *Zenodo* <http://doi.org/10.5281/zenodo.3247930>.

## 510 Appendix A: Site information

Table A1 provides meta information and references for each site from the FLUXNET2015 Tier 1 dataset, used for model calibration and evaluation in the present study.

## Appendix B: Temperature and pressure dependence of photosynthesis parameters

### B1 Photorespiratory Compensation Point $\Gamma^*$

515 The temperature and pressure-dependent photorespiratory compensation point in absence of dark respiration  $\Gamma^*(T, p)$  is calculated from its value at standard temperature ( $T_0 = 25^\circ\text{C}$ ) and atmospheric pressure ( $p_0 = 101325 \text{ Pa}$ ), referred to as  $\Gamma_{25, p_0}^*$ . It is modified by temperature following an Arrhenius-type temperature response function  $f_{\text{Arrh}}(T_K, \Delta H_{\Gamma^*})$  with activation energy  $\Delta H_{\Gamma^*}$ , and is corrected for atmospheric pressure  $p(z)$  at elevation  $z$ .

$$\Gamma^*(T_K, z) = \Gamma_{25, p_0}^* f_{\text{Arrh}}(T_K, \Delta H_{\Gamma^*}) \frac{p(z)}{p_0} \quad (\text{B1})$$

520 Values of  $\Delta H_{\Gamma^*}$  and  $\Gamma_{25, p_0}^*$  are taken from Bernacchi et al. (2001). The latter is converted to Pa and standardised to  $p_0$  simply by multiplication with  $p_0$  ( $\Gamma_{25, p_0}^* = 42.75 \mu\text{mol mol}^{-1} \cdot 10^{-6} \cdot 101325 \text{ Pa} = 4.332 \text{ Pa}$ ).  $\Delta H_{\Gamma^*}$  is  $37830 \text{ J mol}^{-1}$ . All parameter values are summarised in Tab. A7. The function  $p(z)$  is defined in Sec B4. Note that  $T_K$  indicates that the respective temperature value is given in Kelvin and  $T_{K,0} = 298.15 \text{ K}$ .



To correct for effects by temperature following the Arrhenius Equation with its form  $x(T_K) = \exp(c - \Delta H_a / (T_K R))$ , the  
 525 temperature-correction function  $f_{\text{Arrh}}(T_K, \Delta H_a)$ , used in Eq. B1 and further equations below, is given by:

$$f_{\text{Arrh}}(T_K) = x(T_K) / x(T_{K,0}) = \exp\left(\frac{\Delta H(T_K - T_{K,0})}{T_{K,0} R T_K}\right) \quad (\text{B2})$$

where  $\Delta H$  is the respective activation energy (e.g.,  $\Delta H_{\Gamma^*}$  in Eq. B1), and  $R$  is the universal gas constant ( $8.3145 \text{ J mol}^{-1} \text{ K}^{-1}$ ).

## B2 Deriving $\Gamma^*$

530 The temperature and pressure dependency of  $\Gamma^*$  follows from the temperature dependencies of  $K_c$ ,  $K_o$ ,  $V_{c,\text{max}}$ , and  $V_{o,\text{max}}$  and the pressure dependency of  $pO_2(p)$ :

$$\Gamma^*(T_K, p) = \frac{pO_2(p) K_c(T_K) V_{\text{omax}}(T_K)}{2 K_o(T_K) V_{c\text{max}}(T_K)} \quad (\text{B3})$$

$pO_2(p)$  is the partial pressure of atmospheric oxygen (Pa) and scales linearly with  $p(z)$ .  $K_c$  is the Michaelis-Menten constant for carboxylation (Pa);  $K_o$  is the Michaelis-Menten constant for oxygenation (Pa);  $V_{c\text{max}}$  is maximum rate of carboxylation  
 535 ( $\mu\text{mol m}^{-2} \text{ s}^{-1}$ ); and  $V_{o\text{max}}$  is the maximum rate of oxygenation ( $\mu\text{mol m}^{-2} \text{ s}^{-1}$ ). The temperature-dependency equations for these four terms are given in Table 1 of Bernacchi et al. (2001) with respective scaling constants  $c$  and activation energies  $\Delta H_a$  as :

$$K_c(T_K) = \exp(38.05 - 79.43 / (T_K R)) \quad (\text{B4a})$$

$$K_o(T_K) = 1000 \cdot \exp(20.30 - 36.38 / (T_K R)) \quad (\text{B4b})$$

$$540 V_{o,\text{max}}(T_K) = \exp(22.98 - 60.11 / (T_K R)) \quad (\text{B4c})$$

$$V_{c,\text{max}}(T_K) = \exp(26.35 - 65.33 / (T_K R)) \quad (\text{B4d})$$

By substituting the temperature-dependency equations for each term in Eq. B3 and rearranging terms,  $\Gamma^*$  can be written as

$$\Gamma^*(T_K, z) = pO_2(z) \exp(6.779 - 37.83 / (T_K R)) . \quad (\text{B5})$$

With  $pO_2(p)$  at standard atmospheric pressure (101325 Pa) taken to be 21000 Pa, and assuming a constant mixing ratio across  
 545 the troposphere, its pressure dependence can be expressed as

$$pO_2(p) = 0.2095 \cdot p(z) \quad (\text{B6})$$

hence

$$\Gamma^*(T_K, p) = p(z) \exp(5.205 - 37.83 / (T_K R)) \quad (\text{B7})$$

We can use this to calculate  $\Gamma^*$  at standard temperature ( $T_K = 298.15 \text{ K}$ ) and pressure ( $p(z) = 101325 \text{ Pa}$ ) as  $\Gamma_{25,p_0}^* = 4.332$   
 550 Pa.



Note that to convert Eq. B5 to the form corresponding to the one given by Bernacchi et al. (2001), the partial pressure of oxygen ( $pO_2$ ) has to be assumed at standard conditions.  $pO_2$  is approximately 21000 Pa and with the standard atmospheric pressure of 101325 Pa,  $pO_2$  can be converted from Pascals to parts-per-million (ppm) as  $21000/101325 \times 10^6 = 207254$  ppm =  $\exp(12.24)$  ppm. This can be combined with the exponent in Eq. B5 to  $\exp(12.24) \cdot \exp(6.779) = \exp(19.02)$ . This corresponds to the parameter values determining the temperature dependence of  $\Gamma^*$  given by Bernacchi et al. (2001) as  $\Gamma^* = \exp(19.02 - 37.83/(T_K R))$ .

### B3 Michaelis-Menten Coefficient of Photosynthesis

The effective Michaelis-Menten coefficient  $K$  (Pa) of Rubisco-limited photosynthesis (Eq. 6) is determined by the Michaelis-Menten constants for the carboxylation and oxygenation reactions (Farquhar et al., 1980):

$$560 \quad K(T_K, p) = K_c(T_K) \left( 1 + \frac{pO_2(p)}{K_o(T_K)} \right), \quad (\text{B8})$$

where  $K_c$  is the Michaelis-Menten constant for  $CO_2$  (Pa),  $K_o$  is the Michaelis-Menten constant for the carboxylation and oxygenation reaction, respectively, and  $pO_2$  is the partial pressure of oxygen (Pa).  $K_c$  and  $K_o$  follow a temperature dependence, given by the Arrhenius equation analogously to the temperature dependence of  $\Gamma^*$  (Eq. B1):

$$K_c(T_K) = K_{c25} f_{\text{Arrh}}(T_K, \Delta H_{K_c}) \quad (\text{B9a})$$

$$565 \quad K_o(T_K) = K_{o25} f_{\text{Arrh}}(T_K, \Delta H_{K_o}) \quad (\text{B9b})$$

Values  $\Delta H_{K_c} = 79430 \text{ J mol}^{-1}$ ,  $\Delta H_{K_o} = 36380 \text{ J mol}^{-1}$ ,  $K_{c25} = 39.97 \text{ Pa}$ , and  $K_{o25} = 27480 \text{ Pa}$  are taken from Bernacchi et al. (2001) and (see also Tab. A7). The latter two have been converted from  $\mu\text{mol mol}^{-1}$  in Bernacchi et al. (2001) to units of Pa by multiplication with the standard atmosphere (101325 Pa). Note that  $K_{c25}$  and  $K_{o25}$  are rate constants and are independent of atmospheric pressure. Pressure-dependence of  $K$  is solely in  $pO_2(p)$  (see Eq. B6).

### 570 B4 Atmospheric pressure

The elevation-dependence of atmospheric pressure is computed by assuming a linear decrease in temperature with elevation and a mean adiabatic lapse rate (Berberan-Santos et al., 1997):

$$p(z) = p_0 \left( 1 - \frac{Lz}{T_{K,0}} \right)^{gM_a(RL)^{-1}}, \quad (\text{B10})$$

where  $z$  is the elevation above mean sea level (m),  $g$  is the gravitational constant ( $9.80665 \text{ m s}^{-2}$ ),  $p_0$  is the standard atmospheric pressure at 0 m a.s.l. (101325 Pa),  $L$  is the mean adiabatic lapse rate ( $0.0065 \text{ K m}^{-2}$ ),  $M_a$  is the molecular weight for dry air ( $0.028963 \text{ kg mol}^{-1}$ ), and  $R$  is the universal gas constant ( $8.3145 \text{ J mol}^{-1} \text{ K}^{-1}$ ). All parameter values that are held fixed in the model (not calibrated) are summarised in Tab. A7.



## Appendix C: Corollary of the $\chi$ prediction

### C1 Stomatal conductance

580 Stomatal conductance  $g_s$  (mol C Pa<sup>-1</sup>) follows from the prediction of  $\chi$  given by Eq. 8 and  $g_s = A/(c_a(1 - \chi))$  (from Eq. 5).  
 Stomatal conductance can thus be written as

$$g_s = \left(1 + \frac{\xi}{\sqrt{D}}\right) \frac{A}{c_a - \Gamma^*}. \quad (C1)$$

This has a similar form as the solution for  $g_s$  derived from a different optimality principle by Medlyn et al. (2011) (their Eq. 11). Differences are that an additional term  $g_0$  is missing here and that  $\Gamma^*$  does not appear in Medlyn et al. (2011). The theory  
 585 presented by Prentice et al. (2014) provides a theoretical interpretation for the parameter  $g_1$  in Medlyn et al. (2011): It is given by  $\xi$  (Eq. 9) and can thus be predicted from the environment. However, it is notable that the underlying optimality criterion used by Medlyn et al. (2011), as proposed by Cowan and Farquhar (1977), is one that maintains a constant marginal water cost of carbon gain  $\lambda = \partial E/\partial A$ . It thus describes an instantaneous  $g_s$  adjustment, e.g., to diurnal variations in  $D$  and has been adopted into DVMs and ESMs for respective predictions (with a given  $V_{\text{cmax}}$ ). In contrast, the theory presented here and underlying the  
 590 P-model predicts  $\chi$  which is jointly controlled by  $g_s$  and  $V_{\text{cmax}}$ . In other words, it predicts a  $g_s$  that is coordinated with  $V_{\text{cmax}}$  and thus acclimates at a similar time scale (which is on the order of days to weeks). This  $\chi$  can be understood as a “set-point” for an average  $\chi$  with actual  $\chi$  varying around it at a daily to sub-daily time scale.

### C2 Intrinsic water use efficiency

The intrinsic water use efficiency (iWUE, in Pa) has been defined as the ratio of assimilation over stomatal conductance (to  
 595 water) (Beer et al., 2009) as  $\text{iWUE} = A/(1.6g_s)$ . The factor 1.6 accounts for the difference in diffusivity between CO<sub>2</sub> and H<sub>2</sub>O. Using Fick’s Law (Eq. 5), this is simply

$$\text{iWUE} = \frac{c_a(1 - \chi)}{1.6}, \quad (C2)$$

or, using the prediction of optimal  $\chi$  given by Eq. 8, this can be expressed as

$$\text{iWUE} = \frac{1}{1.6 \left(1 + \frac{\xi}{\sqrt{D}}\right)} (c_a - \Gamma^*) \quad (C3)$$

### 600 C3 Maximum carboxylation capacity

$V_{\text{cmax}}$  With  $A_J = A_C$ ,  $V_{\text{cmax}}$  can directly be derived as

$$V_{\text{cmax}} = \varphi_0 I_{\text{abs}} \frac{c_i + K}{c_i + 2\Gamma^*} = \varphi_0 I_{\text{abs}} \frac{m}{m_C}, \quad (C4)$$

$c_i$  is given by  $c_a\chi$ . The second part of the equation follows from the definitions of  $m$  (Eq. 11) and  $m_C$  (Eq. 7). Normalising  $V_{\text{cmax}}$  to standard temperature (25°C) following a modified Arrhenius function based on Kattge and Knorr (2007) gives  $V_{\text{cmax}25}$



605 as

$$V_{\text{cmax}25} = V_{\text{cmax}}/f_V(T_K, T_{K,0}) \quad (\text{C5})$$

$$f_V(T_K, T_{K,0}) = f_{\text{Arrh}}(T_K, \Delta H_V) \cdot \frac{1 + \exp((T_{K,0}\Delta S - H_d)/(T_{K,0}R))}{1 + \exp((T_K\Delta S - H_d)/(T_K R))} \quad (\text{C6})$$

with  $H_V$  being the activation energy (71513 J mol<sup>-1</sup>),  $H_d$  is the deactivation energy (200000 J mol<sup>-1</sup>), and  $\Delta S$  is an entropy term (J mol<sup>-1</sup> K<sup>-1</sup>) calculated using a linear relationship with  $T$  from Kattge and Knorr (2007), with a slope of  $b_S = 1.07$  J mol<sup>-1</sup> K<sup>-2</sup> and intercept of  $a_S = 668.39$  J mol<sup>-1</sup> K<sup>-1</sup>:

$$\Delta S = a_S - b_S T \quad (\text{C7})$$

Note that  $T$  is in units of °C in above equation. Equation C6 describes the *instantaneous* response to temperature and is not the same as the optimality-driven *acclimation* to temperature predicted by the P-model.

#### C4 Dark respiration $R_d$

615 Dark respiration at standard temperature  $R_{d25}$  is calculated as being proportional to  $V_{\text{cmax}25}$ :

$$R_{d25} = b_0 V_{\text{cmax}25} \quad (\text{C8})$$

where  $b_0 = 0.015$  (Atkin et al., 2015). Dark respiration follows a slightly different instantaneous temperature sensitivity than  $V_{\text{cmax}}$  following Heskell et al. (2016):

$$R_d = R_{d25} f_R \quad (\text{C9})$$

$$620 \quad f_R = \exp(0.1012(T_{K,0} - T_K) - 0.0005(T_{K,0}^2 - T_K^2)) \quad (\text{C10})$$

By combining Eqs. C6, C8, and C9,  $R_d$  at growth temperature  $T$  can directly be calculated from  $V_{\text{cmax}}$  as

$$R_d = b_0 \frac{f_R}{f_V} V_{\text{cmax}} \quad (\text{C11})$$

#### Appendix D: Soil water holding capacity

The soil water balance is solved following the SPLASH model. Precipitation in the form of rain ( $P_{\text{rain}}$ ) and snow ( $P_{\text{snow}}$ ) are taken from WATCH-WFDEI (Weedon et al., 2014) and are summed and converted from kg m<sup>-2</sup> s<sup>-1</sup> to mm d<sup>-1</sup> by multiplication with (60 · 60 · 24) s d<sup>-1</sup>. To obtain the total soil water holding capacity (WHC, in mm), we use soil depth-to-bedrock and texture data from SoilGrids (Hengl et al., 2014), extracted around the FLUXNET sites. We assumed that the plant-available WHC is determined by the WHC down to a maximum depth of 2 m and limited by the depth-to-bedrock. The water holding capacity ( $w_{\text{WHC}}$ , in mm) was defined as the difference in volumetric soil water storage at field capacity ( $W_{\text{FC}}$ , in m<sup>3</sup> m<sup>-3</sup>) and the permanent wilting point ( $W_{\text{PWP}}$ , in m<sup>3</sup> m<sup>-3</sup>):

$$630 \quad \theta_{\text{WHC}} = (W_{\text{FC}} - W_{\text{PWP}}) (1 - f_{\text{gravel}}) \cdot \min(z_{\text{bedrock}}, z_{\text{max}}) \quad (\text{D1})$$



$f_{\text{grave}}$  is the gravel fraction,  $z_{\text{bedrock}}$  is the depth to bedrock (in m), and  $z_{\text{max}}$  is 2 m. The volumetric soil water storage at field capacity and wilting point were obtained from texture and organic matter content data through pedotransfer functions, as described by Saxton and Rawls (2006). The volumetric soil water storage ( $\text{m}^3 \text{m}^{-3}$ ) at field capacity is calculated as:

$$635 \quad W_{\text{FC}} = k_{\text{FC}} + (1.283 \cdot k_{\text{FC}}^2 - 0.374 \cdot k_{\text{FC}} - 0.015), \quad (\text{D2})$$

where

$$k_{\text{FC}} = -0.251 \cdot f_{\text{sand}} + 0.195 \cdot f_{\text{clay}} + 0.011 \cdot f_{\text{OM}} \quad (\text{D3})$$

$$+ 0.006 \cdot (f_{\text{sand}} f_{\text{OM}}) \quad (\text{D4})$$

$$- 0.027 \cdot (f_{\text{clay}} f_{\text{OM}}) \quad (\text{D5})$$

$$640 \quad + 0.452 \cdot (f_{\text{sand}} f_{\text{clay}}) \quad (\text{D6})$$

$$+ 0.299 \quad (\text{D7})$$

$f_{\text{sand}}$ ,  $f_{\text{clay}}$ ,  $f_{\text{OM}}$  are the sand, clay and organic matter contents in percent by weight. The volumetric soil water storage ( $\text{m}^3 \text{m}^{-3}$ ) at the permanent wilting point is calculated as:

$$W_{\text{PWP}} = k_{\text{PWP}} + (0.14 \cdot k_{\text{PWP}} - 0.02), \quad (\text{D8})$$

645 where

$$k_{\text{PWP}} = -0.024 \cdot f_{\text{sand}} + 0.487 \cdot f_{\text{clay}} + 0.006 \cdot f_{\text{OM}} \quad (\text{D9})$$

$$+ 0.005 \cdot (f_{\text{sand}} f_{\text{OM}}) \quad (\text{D10})$$

$$- 0.013 \cdot (f_{\text{clay}} f_{\text{OM}}) \quad (\text{D11})$$

$$+ 0.068 \cdot (f_{\text{sand}} f_{\text{clay}}) \quad (\text{D12})$$

$$650 \quad + 0.031 \quad (\text{D13})$$

## Appendix E: Extended theory

### E1 Deriving $\chi$

Using Eqs. 4 and 5, the term on the left-hand side of Eq. 3 can thus be written as

$$\frac{\partial(E/A)}{\partial\chi} = \frac{1.6 D}{c_a (1 - \chi)^2}. \quad (\text{E1})$$

655 Using Equation 6 and the simplification  $\Gamma^* = 0$ , the derivative term on the right-hand-side of Eq.3 can be written as

$$\frac{\partial(V_{\text{cmax}}/A)}{\partial\chi} = -\frac{K}{c_a \chi^2}. \quad (\text{E2})$$



Eq. 3 can thus be written as

$$a \frac{1.6 D}{c_a (1 - \chi)^2} = b \frac{K}{c_a \chi^2} \quad (\text{E3})$$

and solved for  $\chi$ :

$$660 \quad \chi = \frac{\xi}{\xi + \sqrt{D}} \quad (\text{E4})$$

$$\xi = \sqrt{\frac{\beta K}{1.6 \eta^*}} \quad (\text{E5})$$

Where  $b/a = \beta/\eta^*$ . The exact solution, without the simplification  $\Gamma^* = 0$ , and following analogous steps, is

$$\chi = \frac{\Gamma^*}{c_a} + \left(1 - \frac{\Gamma^*}{c_a}\right) \frac{\xi}{\xi + \sqrt{D}} \quad (\text{E6})$$

$$\xi = \sqrt{\frac{b(K + \Gamma^*)}{1.6 a}} \quad (\text{E7})$$

665 This can also be written as

$$c_i = \frac{\Gamma^* \sqrt{D} + \xi c_a}{\xi + \sqrt{D}}. \quad (\text{E8})$$

## E2 Deriving the $J_{\max}$ limitation factor

By taking the derivative of  $A_J$  with respect to  $J_{\max}$ , Eq. 14 can be expressed as

$$c = \frac{m(\varphi_0 J_{\text{abs}})^3}{4 \sqrt{[(\varphi_0 J_{\text{abs}})^2 + (\frac{J_{\max}}{4})^2]^3}} \quad (\text{E9})$$

670 This can be re-arranged to

$$\left(\frac{4c}{m}\right)^{2/3} = \frac{1}{1 + \left(\frac{J_{\max}}{4\varphi_0 J_{\text{abs}}}\right)^2} \quad (\text{E10})$$

For simplification, we can substitute

$$k = \frac{4\varphi_0 J_{\text{abs}}}{J_{\max}} \quad (\text{E11})$$

and

$$675 \quad u = \left(\frac{4c}{m}\right)^{2/3} \quad (\text{E12})$$

With this, we can write

$$\frac{1}{1 + k^{-2}} = u. \quad (\text{E13})$$

This can be re-arranged to

$$(1 - u)^{1/2} = \frac{1}{\sqrt{1 + k^2}} \quad (\text{E14})$$

680 The right-hand term now corresponds to the  $J_{\max}$  limitation factor  $L$  in Eq. 13, and we get Eq. 15.



### E3 An alternative method for introducing the $J_{\max}$ limitation

Sect. 2.2 introduced the effect of a finite  $J_{\max}$  leading to a saturating relationship between absorbed light and the light-limited assimilation rate  $A_J$ . An alternative method was presented by Smith et al. (2019) and is implemented in *rpmode* as an optional method (argument `method_jmaxlim = "smith19"`). Following their approach, the light-limited assimilation rate  
 685 is described as

$$A_J = \left(\frac{J}{4}\right) m. \quad (\text{E15})$$

$m$  is the  $\text{CO}_2$  limitation factor (Eq. 11), and  $J$  is a saturating function of absorbed light, approaching  $J_{\max}$  for high light levels, following Farquhar et al. (1980):

$$\theta J^2 - (\varphi_0 I_{\text{abs}} + J_{\max}) J + \varphi_0 I_{\text{abs}} J_{\max} = 0. \quad (\text{E16})$$

690  $\theta$  is a unitless parameter determining the curvature of the response of  $J$  to  $I_{\text{abs}}$ , here taken as 0.85, based on Smith et al. (2019) and references therein. Eq. E16 can be substituted into Eq. E15 to yield

$$A_J = \left(\frac{m}{4}\right) \frac{\varphi_0 I_{\text{abs}} + J_{\max} \pm \sqrt{(\varphi_0 I_{\text{abs}} + J_{\max})^2 - 4\theta \varphi_0 I_{\text{abs}} J_{\max}}}{2\theta}, \quad (\text{E17})$$

from which the smaller root is used to derive  $A_J$ . Similar as in the method used by Wang et al. (2017a) and outlined in Sect. 2.2, a proportionality between  $A_J$  and  $J_{\max}$  is assumed ( $\partial A/\partial J_{\max} = c$ ; Eq. 14). Taking the derivative of Eq. E17 with respect  
 695 to  $J_{\max}$  and setting equal to  $c$  leads to

$$J_{\max} = \varphi_0 I_{\text{abs}} \omega \quad (\text{E18})$$

with

$$\omega = -(1 - 2\theta) + \sqrt{(1 - \theta) \left( \frac{1}{\frac{4c}{m} (1 - \theta \frac{4c}{m})} - 4\theta \right)}. \quad (\text{E19})$$

Using this,  $A_J$  can be written analogously to Eq. 16, but with

$$700 \quad m' = m \frac{\omega^*}{8\theta}, \quad (\text{E20})$$

and

$$\omega^* = 1 + \omega - \sqrt{(1 + \omega)^2 - 4\theta\omega}. \quad (\text{E21})$$

The cost parameter  $c$  was assumed to be non-varying. Under standard conditions of 25 °C, 101325 Pa atmospheric pressure, 1000 Pa vapor pressure deficit, and 360 ppm  $\text{CO}_2$ , at which the ratio of  $J_{\max}$  to  $V_{\text{cmax}}$  was assumed to be 2.07 (Smith and  
 705 Dukes, 2017),  $c$  was derived as 0.053 (Smith et al., 2019).

Using the definition of  $V_{\text{cmax}}$  from Eq. C4,  $m$  can be replaced by  $m'$  from Eq. E20 to calculate an “intermediate rate of  $V_{\text{cmax}}$ ” (Smith et al., 2019) as

$$V_{\text{cmax}} = \varphi_0 I_{\text{abs}} \frac{m'}{m_C} \quad (\text{E22})$$



#### **Appendix F: The `rpmode1()` function of the *rpmode1* R package**

710 The *rpmode1* R package provides an implementation of the P-model as described here. The main function is `rpmode1()` which returns a list of variables that are mutually consistent within the theory of the P-model (Sect. 2) and based on calculations defined in this paper. References for the returned list of variables are given in Tab. A8



**Table A1.** Sites used for evaluation. Lon. is longitude, negative values indicate west longitude; Lat. is latitude, positive values indicate north latitude; Veg. is vegetation type: deciduous broadleaf forest (DBF); evergreen broadleaf forest (EBF); evergreen needleleaf forest (ENF); grassland (GRA); mixed deciduous and evergreen needleleaf forest (MF); savanna ecosystem (SAV); shrub ecosystem (SHR); wetland (WET).

Site	Lon.	Lat.	Period	Veg.	Clim.	N	Calib.	Reference
AR-SLu	-66.46	-33.46	2009-2011	MF	Bwk	446		Ulke et al. (2015)
AR-Vir	-56.19	-28.24	2009-2012	ENF	Csb	749	Y	Posse et al. (2016)
AT-Neu	11.32	47.12	2002-2012	GRA	Dfc	3243		Wohlfahrt et al. (2008)
AU-Ade	131.12	-13.08	2007-2009	WSA	Aw	532	Y	Beringer et al. (2011a)
AU-ASM	133.25	-22.28	2010-2013	ENF	BSh	1045	Y	Cleverly et al. (2013)
AU-Cpr	140.59	-34.00	2010-2014	SAV	BSk	1370		Meyer et al. (2015)
AU-Cum	150.72	-33.61	2012-2014	EBF	Cfa	744		Beringer et al. (2016a)
AU-DaP	131.32	-14.06	2007-2013	GRA	Aw	1402	Y	Beringer et al. (2011b)
AU-DaS	131.39	-14.16	2008-2014	SAV	Aw	2265	Y	Hutley et al. (2011)
AU-Dry	132.37	-15.26	2008-2014	SAV	Aw	1598	Y	Cernusak et al. (2011)
AU-Emr	148.47	-23.86	2011-2013	GRA	Bwk	755		Schroder et al. (2014)
AU-Fog	131.31	-12.55	2006-2008	WET	Aw	878	Y	Beringer et al. (2013)
AU-Gin	115.71	-31.38	2011-2014	WSA	Csa	942	Y	Beringer et al. (2016b)
AU-GWW	120.65	-30.19	2013-2014	SAV	Bwk	663		Prober et al. (2012)
AU-Lox	140.66	-34.47	2008-2009	DBF	Bsh	273		Stevens et al. (2011)
AU-RDF	132.48	-14.56	2011-2013	WSA	Bwh	431		Bristow et al. (2016)
AU-Rig	145.58	-36.65	2011-2014	GRA	Cfb	1130		Beringer et al. (2016c)
AU-Rob	145.63	-17.12	2014-2014	EBF	Csb	337		Beringer et al. (2016d)
AU-Stp	133.35	-17.15	2008-2014	GRA	BSh	1318	Y	Beringer et al. (2011c)
AU-TTE	133.64	-22.29	2012-2013	OSH	BWh	94		Cleverly et al. (2016)
AU-Tum	148.15	-35.66	2001-2014	EBF	Cfb	4335		Leuning et al. (2005)
AU-Wac	145.19	-37.43	2005-2008	EBF	Cfb	979		Kilinc et al. (2013)
AU-Whr	145.03	-36.67	2011-2014	EBF	Cfb	1065	Y	McHugh et al. (2017)
AU-Wom	144.09	-37.42	2010-2012	EBF	Cfb	934	Y	Hinko-Najera et al. (2017)
AU-Ync	146.29	-34.99	2012-2014	GRA	BSk	392		Yee et al. (2015)
BE-Bra	4.52	51.31	1996-2014	MF	Cfb	4208	Y	Carrara et al. (2004)
BE-Vie	6.00	50.31	1996-2014	MF	Cfb	4733	Y	Aubinet et al. (2001)
BR-Sa3	-54.97	-3.02	2000-2004	EBF	Am	1206		Wick et al. (2005)
CA-Man	-98.48	55.88	1994-2008	ENF	Dfc	1411		Dunn et al. (2007)
CA-NS1	-98.48	55.88	2001-2005	ENF	Dfc	771		Goulden et al. (2006a)
CA-NS2	-98.52	55.91	2001-2005	ENF	Dfc	873		Goulden et al. (2006b)



**Table A2.** Continued from Table A1

Site	Lon.	Lat.	Period	Veg.	Clim.	N	Calib.	Reference
CA-NS3	-98.38	55.91	2001-2005	ENF	Dfc	1069		Goulden et al. (2006c)
CA-NS4	-98.38	55.91	2002-2005	ENF	Dfc	610		Goulden et al. (2006d)
CA-NS5	-98.48	55.86	2001-2005	ENF	Dfc	912		Goulden et al. (2006e)
CA-NS6	-98.96	55.92	2001-2005	OSH	Dfc	913		Goulden et al. (2006f)
CA-NS7	-99.95	56.64	2002-2005	OSH	Dfc	709		Goulden et al. (2006g)
CA-Qfo	-74.34	49.69	2003-2010	ENF	Dfc	1812		Bergeron et al. (2007)
CA-SF1	-105.82	54.48	2003-2006	ENF	Dfc	525		Mkhabela et al. (2009a)
CA-SF2	-105.88	54.25	2001-2005	ENF	Dfc	675		Mkhabela et al. (2009b)
CA-SF3	-106.01	54.09	2001-2006	OSH	Dfc	651		Mkhabela et al. (2009c)
CH-Cha	8.41	47.21	2005-2014	GRA	Cfb	2885		Merbold et al. (2014)
CH-Dav	9.86	46.82	1997-2014	ENF	ET	4444		Zielis et al. (2014)
CH-Fru	8.54	47.12	2005-2014	GRA	Cfb	2566	Y	Imer et al. (2013)
CH-Lae	8.37	47.48	2004-2014	MF	Cfb	3204	Y	Etzold et al. (2011)
CH-Oe1	7.73	47.29	2002-2008	GRA	Cfb	2104	Y	Ammann et al. (2009)
CN-Cha	128.10	42.40	2003-2005	MF	Dwb	982		Guan et al. (2006)
CN-Cng	123.51	44.59	2007-2010	GRA	Bsh	1113	Y	?
CN-Dan	91.07	30.50	2004-2005	GRA	ET	647		Shi et al. (2006)
CN-Din	112.54	23.17	2003-2005	EBF	Cfa	917		Yan et al. (2013)
CN-Du2	116.28	42.05	2006-2008	GRA	Dwb	616		Chen et al. (2009)
CN-Ha2	101.33	37.61	2003-2005	WET	ET	1030		?
CN-HaM	101.18	37.37	2002-2004	GRA		688		Kato et al. (2006)
CN-Qia	115.06	26.74	2003-2005	ENF	Cfa	992	Y	Wen et al. (2010)
CN-Sw2	111.90	41.79	2010-2012	GRA	Bsh	237		Shao et al. (2017)
CZ-BK1	18.54	49.50	2004-2008	ENF	Dfb	1100		Acosta et al. (2013)
CZ-BK2	18.54	49.49	2004-2006	GRA	Dfb	161		?
CZ-wet	14.77	49.02	2006-2014	WET	Cfb	2605	Y	Dušek et al. (2012)
DE-Gri	13.51	50.95	2004-2014	GRA	Cfb	3387	Y	Prescher et al. (2010)
DE-Hai	10.45	51.08	2000-2012	DBF	Cfb	3435	Y	Knohl et al. (2003)
DE-Lkb	13.30	49.10	2009-2013	ENF	Cfb	1001		Lindauer et al. (2014)
DE-Obe	13.72	50.78	2008-2014	ENF	Cfb	2043	Y	?
DE-RuR	6.30	50.62	2011-2014	GRA	Cfb	1195	Y	Post et al. (2015)



**Table A3.** Continued from Table A1

Site	Lon.	Lat.	Period	Veg.	Clim.	N	Calib.	Reference
DE-SfN	11.33	47.81	2012-2014	WET	Cfb	750		Hommeltenberg et al. (2014)
DE-Spw	14.03	51.89	2010-2014	WET	Cfb	1339	Y	?
DE-Tha	13.57	50.96	1996-2014	ENF	Cfb	4887	Y	Grünwald and Bernhofer (2007)
DK-NuF	-51.39	64.13	2008-2014	WET	ET	882	Y	Westergaard-Nielsen et al. (2013)
DK-Sor	11.64	55.49	1996-2014	DBF	Cfb	4483	Y	Pilegaard et al. (2011)
DK-ZaF	-20.55	74.48	2008-2011	WET	ET	381		Stiegler et al. (2016)
DK-ZaH	-20.55	74.47	2000-2014	GRA	ET	1696		Lund et al. (2012)
ES-LgS	-2.97	37.10	2007-2009	OSH	Csa	794		Reverter et al. (2010)
ES-Ln2	-3.48	36.97	2009-2009	OSH	Csa	69		Serrano-Ortiz et al. (2011)
FI-Hyy	24.30	61.85	1996-2014	ENF	Dfc	4222	Y	Suni et al. (2003)
FI-Lom	24.21	68.00	2007-2009	WET	Dfc	575		Aurela et al. (2015)
FI-Sod	26.64	67.36	2001-2014	ENF	Dfc	2816	Y	Thum et al. (2007)
FR-Fon	2.78	48.48	2005-2014	DBF	Cfb	2827	Y	Delpierre et al. (2015)
FR-LBr	-0.77	44.72	1996-2008	ENF	Cfb	2800	Y	Berbigier et al. (2001)
FR-Pue	3.60	43.74	2000-2014	EBF	Csa	4723	Y	Rambal et al. (2004)
GF-Guy	-52.92	5.28	2004-2014	EBF	Af	3719		Bonal et al. (2008)
IT-CA1	12.03	42.38	2011-2014	DBF	Csa	1036		Sabbatini et al. (2016a)
IT-CA3	12.02	42.38	2011-2014	DBF	Csa	913		Sabbatini et al. (2016b)
IT-Col	13.59	41.85	1996-2014	DBF	Cfa	2822	Y	Valentini et al. (1996)
IT-Cp2	12.36	41.70	2012-2014	EBF	Csa	764	Y	Fares et al. (2014)
IT-Cpz	12.38	41.71	1997-2009	EBF	Csa	2601	Y	Garbulsky et al. (2008)
IT-Isp	8.63	45.81	2013-2014	DBF	Cfb	588	Y	Ferréa et al. (2012)
IT-Lav	11.28	45.96	2003-2014	ENF	Cfb	3919	Y	Marcolla et al. (2003)
IT-MBo	11.05	46.01	2003-2013	GRA	Dfb	3236	Y	Marcolla et al. (2011)
IT-Noe	8.15	40.61	2004-2014	CSH	Cwb	3083	Y	Papale et al. (2014)
IT-PT1	9.06	45.20	2002-2004	DBF	Cfa	828	Y	Migliavacca et al. (2009)
IT-Ren	11.43	46.59	1998-2013	ENF	Dfc	3043	Y	Montagnani et al. (2009)
IT-Ro2	11.92	42.39	2002-2012	DBF	Csa	2671		Tedeschi et al. (2006)
IT-SR2	10.29	43.73	2013-2014	ENF	Csa	668	Y	Hoshika et al. (2017)
IT-SRo	10.28	43.73	1999-2012	ENF	Csa	3791	Y	Chiesi et al. (2005)
IT-Tor	7.58	45.84	2008-2014	GRA	Dfc	1487	Y	Galvagno et al. (2013)



**Table A4.** Continued from Table A1

Site	Lon.	Lat.	Period	Veg.	Clim.	N	Calib.	Reference
JP-MBF	142.32	44.39	2003-2005	DBF	Dfb	471		Matsumoto et al. (2008a)
JP-SMF	137.08	35.26	2002-2006	MF	Cfa	1288	Y	Matsumoto et al. (2008b)
NL-Hor	5.07	52.24	2004-2011	GRA	Cfb	2131	Y	Jacobs et al. (2007)
NL-Loo	5.74	52.17	1996-2013	ENF	Cfb	4507	Y	Moors (2012)
NO-Adv	15.92	78.19	2011-2014	WET	ET	151		?
NO-Blv	11.83	78.92	2008-2009	SNO	ET	112		Lüers et al. (2014)
RU-Che	161.34	68.61	2002-2005	WET	Dfc	313		Merbold et al. (2009b)
RU-Cok	147.49	70.83	2003-2014	OSH	Dfc	985		van der Molen et al. (2007)
RU-Fyo	32.92	56.46	1998-2014	ENF	Dfb	4042	Y	Kurbatova et al. (2008)
RU-Ha1	90.00	54.73	2002-2004	GRA	Dfc	519		Marchesini et al. (2007)
SD-Dem	30.48	13.28	2005-2009	SAV	BWh	762	Y	Ardo et al. (2008)
SN-Dhr	-15.43	15.40	2010-2013	SAV	BWh	686	Y	Tagesson et al. (2014)
US-AR1	-99.42	36.43	2009-2012	GRA	Cfa	1011		Raz-Yaseef et al. (2015a)
US-AR2	-99.60	36.64	2009-2012	GRA	Cfa	882		Raz-Yaseef et al. (2015b)
US-ARb	-98.04	35.55	2005-2006	GRA	Cfa	414		Raz-Yaseef et al. (2015c)
US-ARc	-98.04	35.55	2005-2006	GRA	Cfa	488		Raz-Yaseef et al. (2015d)
US-Blo	-120.63	38.90	1997-2007	ENF	Csb	1827		Goldstein et al. (2000)
US-Cop	-109.39	38.09	2001-2007	GRA	BSk	1067		Bowling et al. (2010)
US-GBT	-106.24	41.37	1999-2006	ENF	Dfc	541		Zeller and Nikolov (2000)
US-GLE	-106.24	41.37	2004-2014	ENF	Dfb	2254	Y	Frank et al. (2014)
US-Ha1	-72.17	42.54	1991-2012	DBF	Dfb	3259	Y	Urbanski et al. (2007)
US-KS2	-80.67	28.61	2003-2006	CSH	Cfa	1263		Powell et al. (2006)
US-Los	-89.98	46.08	2000-2014	WET	Dfb	2071	Y	Sulman et al. (2009)
US-Me1	-121.50	44.58	2004-2005	ENF	Csb	287		Irvine et al. (2007)
US-Me2	-121.56	44.45	2002-2014	ENF	Csb	3525	Y	Irvine et al. (2008)
US-Me6	-121.61	44.32	2010-2014	ENF	Csb	1283		Ruehr et al. (2012)
US-MMS	-86.41	39.32	1999-2014	DBF	Cfa	3524	Y	Dragoni et al. (2011)
US-Myb	-121.77	38.05	2010-2014	WET	Csb	1153		Matthes et al. (2014)
US-NR1	-105.55	40.03	1998-2014	ENF	Dfc	4084		Monson et al. (2002)
US-PFa	-90.27	45.95	1995-2014	MF	Dfb	3679		Desai et al. (2015)
US-Prr	-147.49	65.12	2010-2013	ENF	Dfc	546		Nakai et al. (2013)



**Table A5.** Continued from Table A1

Site	Lon.	Lat.	Period	Veg.	Clim.	N	Calib.	Reference
US-SRG	-110.83	31.79	2008-2014	GRA	BSk	2146	Y	Scott et al. (2015a)
US-SRM	-110.87	31.82	2004-2014	WSA	BSk	3093	Y	Scott et al. (2009)
US-Syv	-89.35	46.24	2001-2014	MF	Dfb	2045	Y	Desai et al. (2005)
US-Ton	-120.97	38.43	2001-2014	WSA	Csa	4321	Y	Baldocchi et al. (2010)
US-Tw1	-121.65	38.11	2012-2014	WET	Csa	688		Oikawa et al. (2017)
US-Tw4	-121.64	38.10	2013-2014	WET	Csa	325		Baldocchi (2016)
US-UMB	-84.71	45.56	2000-2014	DBF	Dfb	4015	Y	Gough et al. (2013a)
US-UMd	-84.70	45.56	2007-2014	DBF	Dfb	2050	Y	Gough et al. (2013b)
US-Var	-120.95	38.41	2000-2014	GRA	Csa	2981	Y	Ma et al. (2007)
US-WCr	-90.08	45.81	1999-2014	DBF	Dfb	2333	Y	Cook et al. (2004)
US-Whs	-110.05	31.74	2007-2014	OSH	BSk	1561		Scott et al. (2015b)
US-Wi0	-91.08	46.62	2002-2002	ENF	Dfb	228		Noormets et al. (2007a)
US-Wi3	-91.10	46.63	2002-2004	DBF	Dfb	415		Noormets et al. (2007b)
US-Wi4	-91.17	46.74	2002-2005	ENF	Dfb	712	Y	Noormets et al. (2007c)
US-Wi6	-91.30	46.62	2002-2003	OSH	Dfb	351		Noormets et al. (2007d)
US-Wi9	-91.08	46.62	2004-2005	ENF	Dfb	302		Noormets et al. (2007e)
US-Wkg	-109.94	31.74	2004-2014	GRA	BSk	2676		Scott et al. (2010)
ZA-Kru	31.50	-25.02	2000-2010	SAV	BSh	2124		Archibald et al. (2009)
ZM-Mon	23.25	-15.44	2000-2009	DBF	Aw	641	Y	Merbold et al. (2009a)



**Table A6.** Fixed parameters. 'SC' stands for 'at standard conditions' (25 °C, 101325 Pa). 'MM coef.' refers to 'Michaelis Menten coefficient'.

Symbol	Value	Units	Description	Reference
$\beta$	146.0	1	Unit cost ratio, Eq. 3	This study
$\Gamma_{25,p_0}^*$	4.332	Pa	Photorespiratory compensation point, SC	Bernacchi et al. (2001)
$K_{c25}$	39.97	Pa	MM coef. for CO <sub>2</sub> , SC	Bernacchi et al. (2001)
$K_{o25}$	27480	Pa	MM coef. for O <sub>2</sub> , SC	Bernacchi et al. (2001)
$\Delta H_{\Gamma^*}$	37830	J mol <sup>-1</sup>	Activation energy for $\Gamma^*$	Bernacchi et al. (2001)
$\Delta H_{K_c}$	79430	J mol <sup>-1</sup>	Activation energy for $K_c$	Bernacchi et al. (2001)
$\Delta H_{K_o}$	36380	J mol <sup>-1</sup>	Activation energy for $K_o$	Bernacchi et al. (2001)
$H_V$	71513	J mol <sup>-1</sup>	Activation energy for $V_{cmax}$	Kattge and Knorr (2007)
$H_d$	200000	J mol <sup>-1</sup>	Deactivation energy for $V_{cmax}$	Kattge and Knorr (2007)
$p_0$	101325	Pa	Standard atmosphere	–
$g$	9.80665	m s <sup>-2</sup>	Gravitation constant	–
$L$	0.0065	K m <sup>-2</sup>	Adiabatic lapse rate	–
$R$	8.3145	J mol <sup>-1</sup> K <sup>-1</sup>	Universal gas constant	–
$M_a$	28.963	g mol <sup>-1</sup>	Molecular mass of dry air	–
$M_C$	12.0107	g mol <sup>-1</sup>	Molecular mass of carbon	–
$a_S$	668.39	J mol <sup>-1</sup> K <sup>-1</sup>	Intercept for entropy term in Eq. C6	Kattge and Knorr (2007)
$b_S$	1.07	J mol <sup>-1</sup> K <sup>-2</sup>	Slope for entropy term in Eq. C6	Kattge and Knorr (2007)

**Table A7.** Fixed parameters. 'SC' stands for 'at standard conditions' (25 °C, 101325 Pa). 'MM coef.' refers to 'Michaelis Menten coefficient'.



**Table A8.** Variables returned by the function `rpmmodel()`. Variable names correspond to the named elements of the list returned by the `rpmmodel()` function call. Symbols correspond to their use in this paper.

Variable name	Symbol	Description	Units	Reference
<code>ca</code>	$c_a$	Ambient CO <sub>2</sub> partial pressure	Pa	Sect. 2.1
<code>gammastar</code>	$\Gamma^*$	Photorespiratory compensation point	Pa	Sect. B1
<code>kmm</code>	$K$	Michaelis-Menten coefficient for photosynthesis	Pa	Sect. B3
<code>ns_star</code>	$\eta^*$	Change in the viscosity of water, relative to its value at 25 °C	unitless	Huber et al. (2009)
<code>chi</code>	$\chi$	Ratio of leaf internal-to-ambient CO <sub>2</sub>	unitless	Sect. 2.1
<code>ci</code>	$c_i$	Leaf internal CO <sub>2</sub> partial pressure	Pa	Eq. E8
<code>lue</code>	LUE	Light use efficiency	$\text{g C mol}^{-1}$	Eq. 19
<code>mj</code>	$m$	CO <sub>2</sub> limitation factor for light-limited assimilation	unitless	Eq. 11
<code>mc</code>	$m_C$	CO <sub>2</sub> limitation factor for Rubisco-limited assimilation	unitless	Eq. 7
<code>gpp</code>	GPP	Gross primary production	$\text{g C m}^{-2} \text{d}^{-1}$	Eqs. 2 and 19
<code>iwue</code>	iWUE	Intrinsic water use efficiency	Pa	Eq. C2
<code>gs</code>	$g_s$	Stomatal conductance	$\text{mol C m}^{-2} \text{d}^{-1} \text{Pa}^{-1}$	Sect. C1
<code>vcmax</code>	$V_{\text{cmax}}$	Maximum rate of carboxylation	$\text{mol C m}^{-2} \text{d}^{-1}$	Eq. C4
<code>vcmax25</code>	$V_{\text{cmax}25}$	Maximum rate of carboxylation, normalised to 25 °C	$\text{mol C m}^{-2} \text{d}^{-1}$	Eq. C5
<code>rd</code>	$R_d$	Dark respiration	$\text{mol C m}^{-2} \text{d}^{-1}$	Eq. C11



*Author contributions.* B.D.S. designed the study, wrote the model code, conducted the analysis, and wrote the paper. H. W. developed the model and wrote the an initial version of the model description. N.G.S. developed the model and implemented model code. S.P.H. contributed to designing the study and writing the manuscript. T.K. contributed to study design, model implementation and manuscript writing. D.S. implemented the water holding capacity model. T.D. wrote an initial version of the model code and model documentation. I.C.P. developed the model and contributed to designing the study.

*Competing interests.* The authors have no competing interests.

*Acknowledgements.* B.D.S. was funded by ERC H2020-MSCA-IF-2015, grant number 701329. N.G.S. acknowledges support from Texas Tech University. T.F.K. acknowledges support from the Laboratory Directed Research and Development (LDRD) fund under the auspices of DOE, BER Office of Science at Lawrence Berkeley National Laboratory, and the NASA Terrestrial Ecology Program IDS Award NNH17AE86I. S.P.H. acknowledges support from the ERC-funded project GC 2.0 (Global Change 2.0: Unlocking the past for a clearer future, grant number 694481). I.C.P. acknowledges support from the ERC under the European Union's Horizon 2020 research and innovation programme (grant agreement no: 787203 REALM).



## 725 References

- Acosta, M., Pavelka, M., Montagnani, L., Kutsch, W., Lindroth, A., Juszczak, R., and Janouš, D.: Soil surface CO<sub>2</sub> efflux measurements in Norway spruce forests: Comparison between four different sites across Europe — from boreal to alpine forest, *Geoderma*, 192, 295–303, <https://doi.org/10.1016/j.geoderma.2012.08.027>, <https://doi.org/10.1016%2Fj.geoderma.2012.08.027>, 2013.
- Adams, W. W., Zarter, C. R., Ebbert, V., and Demmig-Adams, B.: Photoprotective Strategies of Overwintering Evergreens, *Bioscience*, 54, 41–49, 2004.
- 730 Ammann, C., Spirig, C., Leifeld, J., and Neftel, A.: Assessment of the nitrogen and carbon budget of two managed temperate grassland fields, *Agriculture, Ecosystems & Environment*, 133, 150–162, <https://doi.org/10.1016/j.agee.2009.05.006>, <https://doi.org/10.1016%2Fj.agee.2009.05.006>, 2009.
- Archibald, S. A., Kirton, A., van der Merwe, M. R., Scholes, R. J., Williams, C. A., and Hanan, N.: Drivers of inter-annual variability in Net Ecosystem Exchange in a semi-arid savanna ecosystem, South Africa, *Biogeosciences*, 6, 251–266, <https://doi.org/10.5194/bg-6-251-2009>, <https://doi.org/10.5194%2Fbg-6-251-2009>, 2009.
- 735 Ardo, J., Molder, M., El-Tahir, B. A., and Elkhidir, H. A. M.: Seasonal variation of carbon fluxes in a sparse savanna in semi arid Sudan, *Carbon Balance and Management*, 3, 7, <https://doi.org/10.1186/1750-0680-3-7>, <https://doi.org/10.1186%2F1750-0680-3-7>, 2008.
- Atkin, O. K., Bloomfield, K. J., Reich, P. B., Tjoelker, M. G., Asner, G. P., Bonal, D., Bönisch, G., Bradford, M. G., Cernusak, L. A., Cosio, E. G., Creek, D., Crous, K. Y., Domingues, T. F., Dukes, J. S., Egerton, J. J. G., Evans, J. R., Farquhar, G. D., Fyllas, N. M., Gauthier, P. P. G., Gloor, E., Gimeno, T. E., Griffin, K. L., Guerrieri, R., Heskell, M. A., Huntingford, C., Ishida, F. Y., Kattge, J., Lambers, H., Liddell, M. J., Lloyd, J., Lusk, C. H., Martin, R. E., Maksimov, A. P., Maximov, T. C., Malhi, Y., Medlyn, B. E., Meir, P., Mercado, L. M., Mirotnick, N., Ng, D., Niinemets, U., O'Sullivan, O. S., Phillips, O. L., Poorter, L., Poot, P., Prentice, I. C., Salinas, N., Rowland, L. M., Ryan, M. G., Sitch, S., Slot, M., Smith, N. G., Turnbull, M. H., VanderWel, M. C., Valladares, F., Veneklaas, E. J., Weerasinghe, L. K., Wirth, C., Wright, I. J., Wythers, K. R., Xiang, J., Xiang, S., and Zaragoza-Castells, J.: Global variability in leaf respiration in relation to climate, plant functional types and leaf traits, *New Phytologist*, 206, 614–636, <https://doi.org/10.1111/nph.13253>, <https://nph.onlinelibrary.wiley.com/doi/abs/10.1111/nph.13253>, 2015.
- 740 Aubinet, M., Chermanne, B., Vandenhaute, M., Longdoz, B., Yernaux, M., and Laitat, E.: Long term carbon dioxide exchange above a mixed forest in the Belgian Ardennes, *Agricultural and Forest Meteorology*, 108, 293–315, [https://doi.org/10.1016/s0168-1923\(01\)00244-1](https://doi.org/10.1016/s0168-1923(01)00244-1), <https://doi.org/10.1016%2Fs0168-1923%2801%2900244-1>, 2001.
- 750 Aurela, M., Lohila, A., Tuovinen, J. P., Hatakka, J., Penttilä, T., and Laurila, T.: Carbon dioxide and energy flux measurements in four northern-boreal ecosystems at Pallas, *Boreal Environment Research*, 20, 455–473, 2015.
- Badgley, G., Field, C. B., and Berry, J. A.: Canopy near-infrared reflectance and terrestrial photosynthesis, *Sci Adv*, 3, e1602244, 2017.
- Baldocchi, D.: AmeriFlux US-Tw4 Twitchell East End Wetland from 2013-Present, <https://doi.org/10.17190/AMF/1246151>, <https://doi.org/10.17190/AMF/1246151>, 2016.
- 755 Baldocchi, D., Chen, Q., Chen, X., Ma, S., Miller, G., Ryu, Y., Xiao, J., Wenk, R., and Battles, J.: The Dynamics of Energy, Water, and Carbon Fluxes in a Blue Oak (*Quercus douglasii*) Savanna in California, in: *Ecosystem Function in Savannas*, pp. 135–151, CRC Press, <https://doi.org/10.1201/b10275-10>, <https://doi.org/10.1201%2Fb10275-10>, 2010.
- Ball, J. T., Timothy Ball, J., Woodrow, I. E., and Berry, J. A.: A Model Predicting Stomatal Conductance and its Contribution to the Control of Photosynthesis under Different Environmental Conditions, in: *Progress in Photosynthesis Research*, pp. 221–224, 1987.
- 760



- Beer, C., Ciais, P., Reichstein, M., Baldocchi, D., Law, B. E., Papale, D., Soussana, J.-F., Ammann, C., Buchmann, N., Frank, D., Gianelle, D., Janssens, I. A., Knohl, A., Köstner, B., Moors, E., Rouspard, O., Verbeeck, H., Vesala, T., Williams, C. A., and Wohlfahrt, G.: Temporal and among-site variability of inherent water use efficiency at the ecosystem level, *Global Biogeochemical Cycles*, 23, <https://doi.org/10.1029/2008GB003233>, <https://agupubs.onlinelibrary.wiley.com/doi/abs/10.1029/2008GB003233>, 2009.
- 765 Berberan-Santos, M. N., Bodunov, E. N., and Pogliani, L.: On the barometric formula, *American Journal of Physics*, 65, 404–412, 1997.
- Berbigier, P., Bonnefond, J.-M., and Mellmann, P.: CO<sub>2</sub> and water vapour fluxes for 2 years above Euroflux forest site, *Agricultural and Forest Meteorology*, 108, 183–197, [https://doi.org/10.1016/s0168-1923\(01\)00240-4](https://doi.org/10.1016/s0168-1923(01)00240-4), <https://doi.org/10.1016%2Fs0168-1923%2801%2900240-4>, 2001.
- Bergeron, O., Margolis, H. A., Black, T. A., Coursolle, C., Dunn, A. L., Barr, A. G., and Wofsy, S. C.: Comparison of carbon dioxide fluxes  
770 over three boreal black spruce forests in Canada, *Global Change Biology*, 13, 89–107, <https://doi.org/10.1111/j.1365-2486.2006.01281.x>, <https://doi.org/10.1111%2Fj.1365-2486.2006.01281.x>, 2007.
- Bergh, J., McMurtrie, R. E., and Linder, S.: Climatic factors controlling the productivity of Norway spruce: A model-based analysis, *For. Ecol. Manage.*, 110, 127–139, 1998.
- Beringer, J., Hacker, J., Hutley, L. B., Leuning, R., Arndt, S. K., Amiri, R., Bannehr, L., Cernusak, L. A., Grover, S., Hensley, C., Hocking, D., Isaac, P., Jamali, H., Kanniah, K., Livesley, S., Neining, B., U, K. T. P., Sea, W., Straten, D., Tapper, N., Weinmann, R., Wood, S., and Zegelin, S.: SPECIAL—Savanna Patterns of Energy and Carbon Integrated across the Landscape, *Bulletin of the American Meteorological Society*, 92, 1467–1485, <https://doi.org/10.1175/2011bams2948.1>, <https://doi.org/10.1175%2F2011bams2948.1>, 2011a.
- Beringer, J., Hutley, L. B., Hacker, J. M., Neining, B., and U, K. T. P.: Patterns and processes of carbon, water and energy cycles across northern Australian landscapes: From point to region, *Agricultural and Forest Meteorology*, 151, 1409–1416,  
780 <https://doi.org/10.1016/j.agrformet.2011.05.003>, <https://doi.org/10.1016%2Fj.agrformet.2011.05.003>, 2011b.
- Beringer, J., Hutley, L. B., Hacker, J. M., Neining, B., and U, K. T. P.: Patterns and processes of carbon, water and energy cycles across northern Australian landscapes: From point to region, *Agricultural and Forest Meteorology*, 151, 1409–1416, <https://doi.org/10.1016/j.agrformet.2011.05.003>, <https://doi.org/10.1016%2Fj.agrformet.2011.05.003>, 2011c.
- Beringer, J., Livesley, S. J., Randle, J., and Hutley, L. B.: Carbon dioxide fluxes dominate the greenhouse gas exchanges of  
785 a seasonal wetland in the wet–dry tropics of northern Australia, *Agricultural and Forest Meteorology*, 182–183, 239–247, <https://doi.org/10.1016/j.agrformet.2013.06.008>, <https://doi.org/10.1016%2Fj.agrformet.2013.06.008>, 2013.
- Beringer, J., Hutley, L. B., McHugh, I., Arndt, S. K., Campbell, D., Cleugh, H. A., Cleverly, J., de Dios, V. R., Eamus, D., Evans, B., Ewenz, C., Grace, P., Griebel, A., Haverd, V., Hinko-Najera, N., Huete, A., Isaac, P., Kanniah, K., Leuning, R., Liddell, M. J., Macfarlane, C., Meyer, W., Moore, C., Pendall, E., Phillips, A., Phillips, R. L., Prober, S. M., Restrepo-Coupe, N., Rutledge, S., Schroder, I., Silberstein,  
790 R., Southall, P., Yee, M. S., Tapper, N. J., van Gorsel, E., Vote, C., Walker, J., and Wardlaw, T.: An introduction to the Australian and New Zealand flux tower network – OzFlux, *Biogeosciences*, 13, 5895–5916, <https://doi.org/10.5194/bg-13-5895-2016>, <https://doi.org/10.5194%2Fbg-13-5895-2016>, 2016a.
- Beringer, J., Hutley, L. B., McHugh, I., Arndt, S. K., Campbell, D., Cleugh, H. A., Cleverly, J., De Dios, V. R., Eamus, D., Evans, B., Ewenz, C., Grace, P., Griebel, A., Haverd, V., Hinko-Najera, N., Huete, A., Isaac, P., Kanniah, K., Leuning, R., Liddell, M. J., MacFarlane, C., Meyer, W., Moore, C., Pendall, E., Phillips, A., Phillips, R. L., Prober, S. M., Restrepo-Coupe, N., Rutledge, S., Schroder, I., Silberstein,  
795 R., Southall, P., Sun Yee, M., Tapper, N. J., Van Gorsel, E., Vote, C., Walker, J., and Wardlaw, T.: An introduction to the Australian and New Zealand flux tower network - OzFlux, *Biogeosciences*, 13, 5895–5916, <https://doi.org/10.5194/bg-13-5895-2016>, <http://www.biogeosciences.net/13/5895/2016/> <https://doi.org/10.5194https://doi.org/10.5194%2Fbg-13-5895-2016>, 2016b.



- 800 Beringer, J., Hutley, L. B., McHugh, I., Arndt, S. K., Campbell, D., Cleugh, H. A., Cleverly, J., de Dios, V. R., Eamus, D., Evans, B., Ewenz, C., Grace, P., Griebel, A., Haverd, V., Hinko-Najera, N., Huete, A., Isaac, P., Kanniah, K., Leuning, R., Liddell, M. J., Macfarlane, C., Meyer, W., Moore, C., Pendall, E., Phillips, A., Phillips, R. L., Prober, S. M., Restrepo-Coupe, N., Rutledge, S., Schroder, I., Silberstein, R., Southall, P., Yee, M. S., Tapper, N. J., van Gorsel, E., Vote, C., Walker, J., and Wardlaw, T.: An introduction to the Australian and New Zealand flux tower network – OzFlux, *Biogeosciences*, 13, 5895–5916, <https://doi.org/10.5194/bg-13-5895-2016>, <https://doi.org/10.5194%2Fbg-13-5895-2016>, 2016c.
- 805 Beringer, J., Hutley, L. B., McHugh, I., Arndt, S. K., Campbell, D., Cleugh, H. A., Cleverly, J., de Dios, V. R., Eamus, D., Evans, B., Ewenz, C., Grace, P., Griebel, A., Haverd, V., Hinko-Najera, N., Huete, A., Isaac, P., Kanniah, K., Leuning, R., Liddell, M. J., Macfarlane, C., Meyer, W., Moore, C., Pendall, E., Phillips, A., Phillips, R. L., Prober, S. M., Restrepo-Coupe, N., Rutledge, S., Schroder, I., Silberstein, R., Southall, P., Yee, M. S., Tapper, N. J., van Gorsel, E., Vote, C., Walker, J., and Wardlaw, T.: An introduction to the Australian and New Zealand flux tower network – OzFlux, *Biogeosciences*, 13, 5895–5916, <https://doi.org/10.5194/bg-13-5895-2016>, <https://doi.org/10.5194%2Fbg-13-5895-2016>, 2016d.
- 810 Bernacchi, C. J., Singaas, E. L., Pimentel, C., Portis, A. R. J., and Long, S. P.: Improved temperature response functions for models of Rubisco-limited photosynthesis, *Plant, Cell and Environment*, 24, 253–259, 2001.
- Bernacchi, C. J., Pimentel, C., and Long, S. P.: In vivo temperature response functions of parameters required to model RuBP-limited photosynthesis, *Plant Cell Environ.*, 26, 1419–1430, 2003.
- 815 Bonal, D., Bosc, A., Ponton, S., Goret, J.-Y., Burban, B., Gross, P., Bonnefond, J.-M., Elbers, J., Longdoz, B., Epron, D., Guehl, J.-M., and Granier, A.: Impact of severe dry season on net ecosystem exchange in the Neotropical rainforest of French Guiana, *Global Change Biology*, 14, 1917–1933, <https://doi.org/10.1111/j.1365-2486.2008.01610.x>, <https://doi.org/10.1111%2Fj.1365-2486.2008.01610.x>, 2008.
- Bowling, D. R., Bethers-Marchetti, S., Lunch, C. K., Grote, E. E., and Belnap, J.: Carbon, water, and energy fluxes in a semiarid cold desert grassland during and following multiyear drought, *Journal of Geophysical Research*, 115, <https://doi.org/10.1029/2010jg001322>, <https://doi.org/10.1029%2F2010jg001322>, 2010.
- 820 Bowling, D. R., Logan, B. A., Hufkens, K., Aubrecht, D. M., Richardson, A. D., Burns, S. P., Anderegg, W. R. L., Blanken, P. D., and Eiriksson, D. P.: Limitations to winter and spring photosynthesis of a Rocky Mountain subalpine forest, *Agric. For. Meteorol.*, 252, 241–255, 2018.
- Bristow, M., Hutley, L. B., Beringer, J., Livesley, S. J., Edwards, A. C., and Arndt, S. K.: Quantifying the relative importance of greenhouse gas emissions from current and future savanna land use change across northern Australia, *Biogeosciences Discussions*, pp. 1–47, <https://doi.org/10.5194/bg-2016-191>, <https://doi.org/10.5194%2Fbg-2016-191>, 2016.
- 825 Carrara, A., Janssens, I. A., Yuste, J. C., and Ceulemans, R.: Seasonal changes in photosynthesis, respiration and NEE of a mixed temperate forest, *Agricultural and Forest Meteorology*, 126, 15–31, <https://doi.org/10.1016/j.agrformet.2004.05.002>, <https://doi.org/10.1016%2Fj.agrformet.2004.05.002>, 2004.
- 830 Cernusak, L. A., Hutley, L. B., Beringer, J., Holtum, J. A., and Turner, B. L.: Photosynthetic physiology of eucalypts along a sub-continental rainfall gradient in northern Australia, *Agricultural and Forest Meteorology*, 151, 1462–1470, <https://doi.org/10.1016/j.agrformet.2011.01.006>, <https://doi.org/10.1016%2Fj.agrformet.2011.01.006>, 2011.
- Chen, J.-L., Reynolds, J. F., Harley, P. C., and Tenhunen, J. D.: Coordination theory of leaf nitrogen distribution in a canopy, *Oecologia*, 93, 63–69, 1993.



- 835 Chen, S., Chen, J., Lin, G., Zhang, W., Miao, H., Wei, L., Huang, J., and Han, X.: Energy balance and partition in Inner Mongolia steppe ecosystems with different land use types, *Agricultural and Forest Meteorology*, 149, 1800–1809, <https://doi.org/10.1016/j.agrformet.2009.06.009>, <https://doi.org/10.1016%2Fj.agrformet.2009.06.009>, 2009.
- Chiesi, M., Maselli, F., Bindi, M., Fibbi, L., Cherubini, P., Arlotta, E., Tirone, G., Matteucci, G., and Seufert, G.: Modelling carbon budget of Mediterranean forests using ground and remote sensing measurements, *Agricultural and Forest Meteorology*, 135, 22–34, <https://doi.org/10.1016/j.agrformet.2005.09.011>, <https://doi.org/10.1016%2Fj.agrformet.2005.09.011>, 2005.
- 840 Cleverly, J., Boulain, N., Villalobos-Vega, R., Grant, N., Faux, R., Wood, C., Cook, P. G., Yu, Q., Leigh, A., and Eamus, D.: Dynamics of component carbon fluxes in a semi-arid Acacia woodland, central Australia, *Journal of Geophysical Research: Biogeosciences*, 118, 1168–1185, <https://doi.org/10.1002/jgrg.20101>, <https://doi.org/10.1002%2Fjgrg.20101>, 2013.
- Cleverly, J., Eamus, D., Van Gorsel, E., Chen, C., Rumman, R., Luo, Q., Coupe, N. R., Li, L., Kljun, N., Faux, R., Yu, Q., and Huete, A.: Productivity and evapotranspiration of two contrasting semiarid ecosystems following the 2011 global carbon land sink anomaly, *Agricultural and Forest Meteorology*, 220, 151–159, <https://doi.org/10.1016/j.agrformet.2016.01.086>, <http://linkinghub.elsevier.com/retrieve/pii/S0168192316300971>, 2016.
- Cook, B. D., Davis, K. J., Wang, W., Desai, A., Berger, B. W., Teclaw, R. M., Martin, J. G., Bolstad, P. V., Bakwin, P. S., Yi, C., and Heilman, W.: Carbon exchange and venting anomalies in an upland deciduous forest in northern Wisconsin, USA, *Agricultural and Forest*
- 850 *Meteorology*, 126, 271–295, <https://doi.org/10.1016/j.agrformet.2004.06.008>, <https://doi.org/10.1016%2Fj.agrformet.2004.06.008>, 2004.
- Cowan, I. R. and Farquhar, G. D.: Stomatal function in relation to leaf metabolism and environment, *Symp. Soc. Exp. Biol.*, 31, 471–505, 1977.
- Davis, T. W., Prentice, I. C., Stocker, B. D., Thomas, R. T., Whitley, R. J., Wang, H., Evans, B. J., Gallego-Sala, A. V., Sykes, M. T., and Cramer, W.: Simple process-led algorithms for simulating habitats (SPLASH v.1.0): robust indices of radiation, evapotranspiration
- 855 and plant-available moisture, *Geoscientific Model Development*, 10, 689–708, <https://doi.org/10.5194/gmd-10-689-2017>, <http://www.geosci-model-dev.net/10/689/2017/>, 2017.
- Delpierre, N., Berveiller, D., Granda, E., and Dufrière, E.: Wood phenology, not carbon input, controls the interannual variability of wood growth in a temperate oak forest, *New Phytologist*, 210, 459–470, <https://doi.org/10.1111/nph.13771>, <https://doi.org/10.1111%2Fnph.13771>, 2015.
- 860 Desai, A. R., Bolstad, P. V., Cook, B. D., Davis, K. J., and Carey, E. V.: Comparing net ecosystem exchange of carbon dioxide between an old-growth and mature forest in the upper Midwest, USA, *Agricultural and Forest Meteorology*, 128, 33–55, <https://doi.org/10.1016/j.agrformet.2004.09.005>, <https://doi.org/10.1016%2Fj.agrformet.2004.09.005>, 2005.
- Desai, A. R., Xu, K., Tian, H., Weishampel, P., Thom, J., Baumann, D., Andrews, A. E., Cook, B. D., King, J. Y., and Kolka, R.: Landscape-level terrestrial methane flux observed from a very tall tower, *Agricultural and Forest Meteorology*, 201, 61–75, <https://doi.org/10.1016/j.agrformet.2014.10.017>, <https://doi.org/10.1016%2Fj.agrformet.2014.10.017>, 2015.
- 865 Didan, K.: MOD13Q1 MODIS/Terra Vegetation Indices 16-Day L3 Global 250m SIN Grid V006, <https://doi.org/10.5067/MODIS/MOD13Q1.006>, <https://doi.org/doi.org/10.5067/MODIS/MOD13Q1.006>, 2015.
- Dragoni, D., Schmid, H. P., Wayson, C. A., Potter, H., Grimmond, C. S. B., and Randolph, J. C.: Evidence of increased net ecosystem productivity associated with a longer vegetated season in a deciduous forest in south-central Indiana, USA, *Global Change Biology*, 17, 886–897, <https://doi.org/10.1111/j.1365-2486.2010.02281.x>, <https://doi.org/10.1111%2Fj.1365-2486.2010.02281.x>, 2011.
- 870



- Dunn, A. L., Barford, C. C., Wofsy, S. C., Goulden, M. L., and Daube, B. C.: A long-term record of carbon exchange in a boreal black spruce forest: means, responses to interannual variability, and decadal trends, *Global Change Biology*, 13, 577–590, <https://doi.org/10.1111/j.1365-2486.2006.01221.x>, <https://doi.org/10.1111%2Fj.1365-2486.2006.01221.x>, 2007.
- 875 Dušek, J., Čížková, H., Stellner, S., Czerný, R., and Květ, J.: Fluctuating water table affects gross ecosystem production and gross radiation use efficiency in a sedge-grass marsh, *Hydrobiologia*, 692, 57–66, <https://doi.org/10.1007/s10750-012-0998-z>, <https://doi.org/10.1007%2Fs10750-012-0998-z>, 2012.
- Egea, G., Verhoef, A., and Vidale, P. L.: Towards an improved and more flexible representation of water stress in coupled photosynthesis–stomatal conductance models, *Agric. For. Meteorol.*, 151, 1370–1384, 2011.
- 880 Etzold, S., Ruehr, N. K., Zweifel, R., Dobbertin, M., Zingg, A., Pluess, P., Häsler, R., Eugster, W., and Buchmann, N.: The Carbon Balance of Two Contrasting Mountain Forest Ecosystems in Switzerland: Similar Annual Trends, but Seasonal Differences, *Ecosystems*, 14, 1289–1309, <https://doi.org/10.1007/s10021-011-9481-3>, <https://doi.org/10.1007%2Fs10021-011-9481-3>, 2011.
- Falge, E., Aubinet, M., Bakwin, P. S., Baldocchi, D., Berbigier, P., Bernhofer, C., Black, T. A., Ceulemans, R., Davis, K. J., Dolman, A. J., Goldstein, A., Goulden, M. L., Granier, A., Hollinger, D. Y., Jarvis, P. G., Jensen, N., Pilegaard, K., Katul, G., Kyaw Tha Paw, P., Law, B. E., Lindroth, A., Loustau, D., Mahli, Y., Monson, R., Moncrieff, P., Moors, E., Munger, J. W., Meyers, T., Oechel, W., 885 Schulze, E. d., Thorgeirsson, H., Tenhunen, J., Valentini, R., Verma, S. B., Vesala, T., and Wofsy, S. C.: FLUXNET Research Network Site Characteristics, Investigators, and Bibliography, 2016, <https://doi.org/10.3334/ornl/daac/1530>, [https://daac.ornl.gov/cgi-bin/dsviewer.pl?ds\\_id=1530](https://daac.ornl.gov/cgi-bin/dsviewer.pl?ds_id=1530), 2017.
- Fan, Y., Li, H., and Miguez-Macho, G.: Global Patterns of Groundwater Table Depth, *Science*, 339, 940–943, <https://doi.org/10.1126/science.1229881>, <http://science.sciencemag.org/content/339/6122/940>, 2013.
- 890 Fan, Y., Miguez-Macho, G., Jobbágy, E. G., Jackson, R. B., and Otero-Casal, C.: Hydrologic regulation of plant rooting depth, *Proceedings of the National Academy of Sciences*, 114, 10572–10577, <https://doi.org/10.1073/pnas.1712381114>, <https://www.pnas.org/content/114/40/10572>, 2017.
- Fares, S., Savi, F., Muller, J., Matteucci, G., and Paoletti, E.: Simultaneous measurements of above and below canopy ozone fluxes help partitioning ozone deposition between its various sinks in a Mediterranean Oak Forest, *Agricultural and Forest Meteorology*, 198–199, 895 181–191, <https://doi.org/10.1016/j.agrformet.2014.08.014>, <https://doi.org/10.1016%2Fj.agrformet.2014.08.014>, 2014.
- Farquhar, G. D. and Wong, S. C.: An Empirical Model of Stomatal Conductance, *Functional Plant Biology*, 11, 191–210, <https://doi.org/10.1071/PP9840191>, 1984.
- Farquhar, G. D., von Caemmerer, S., and Berry, J. A.: A biochemical model of photosynthetic CO<sub>2</sub> assimilation in leaves of C<sub>3</sub> species, *Planta*, 149, 78–90, 1980.
- 900 Ferréa, C., Zenone, T., Comolli, R., and Seufert, G.: Estimating heterotrophic and autotrophic soil respiration in a semi-natural forest of Lombardy, Italy, *Pedobiologia*, 55, 285–294, <https://doi.org/10.1016/j.pedobi.2012.05.001>, <https://doi.org/10.1016%2Fj.pedobi.2012.05.001>, 2012.
- Fick, A.: Ueber Diffusion, *Annalen der Physik*, 170, 59–86, <https://doi.org/10.1002/andp.18551700105>, <https://onlinelibrary.wiley.com/doi/abs/10.1002/andp.18551700105>, 1855.
- 905 Field, C. B., Randerson, J. T., and Malmström, C. M.: Global net primary production: Combining ecology and remote sensing, *Remote Sensing of Environment*, 51, 74 – 88, [https://doi.org/http://dx.doi.org/10.1016/0034-4257\(94\)00066-V](https://doi.org/http://dx.doi.org/10.1016/0034-4257(94)00066-V), <http://www.sciencedirect.com/science/article/pii/003442579400066V>, 1995.



- Frank, J. M., Massman, W. J., Ewers, B. E., Huckaby, L. S., and Negrón, J. F.: Ecosystem CO<sub>2</sub>/H<sub>2</sub>O fluxes are explained by hydraulically limited gas exchange during tree mortality from spruce bark beetles, *Journal of Geophysical Research: Biogeosciences*, 119, 1195–1215, 910 <https://doi.org/10.1002/2013jg002597>, <https://doi.org/10.1002%2F2013jg002597>, 2014.
- Frankenberg, C., Köhler, P., Magney, T. S., Geier, S., Lawson, P., Schwochert, M., McDuffie, J., Drewry, D. T., Pavlick, R., and Kuhnert, A.: The Chlorophyll Fluorescence Imaging Spectrometer (CFIS), mapping far red fluorescence from aircraft, *Remote Sens. Environ.*, 217, 523–536, 2018.
- Galvagno, M., Wohlfahrt, G., Cremonese, E., Rossini, M., Colombo, R., Filippa, G., Julitta, T., Manca, G., Siniscalco, C., di Cella, U. M., 915 and Migliavacca, M.: Phenology and carbon dioxide source/sink strength of a subalpine grassland in response to an exceptionally short snow season, *Environmental Research Letters*, 8, 025 008, <https://doi.org/10.1088/1748-9326/8/2/025008>, <https://doi.org/10.1088%2F1748-9326%2F8%2F2%2F025008>, 2013.
- Gamon, J., Peñuelas, J., and Field, C.: A narrow-waveband spectral index that tracks diurnal changes in photosynthetic efficiency, *Remote Sensing of Environment*, 41, 35 – 44, [https://doi.org/http://dx.doi.org/10.1016/0034-4257\(92\)90059-S](https://doi.org/http://dx.doi.org/10.1016/0034-4257(92)90059-S), <http://www.sciencedirect.com/science/article/pii/003442579290059S>, 1992. 920
- Gamon, J. A., Huemmrich, K. F., Wong, C. Y. S., Ensminger, I., Garrity, S., Hollinger, D. Y., Noormets, A., and Peñuelas, J.: A remotely sensed pigment index reveals photosynthetic phenology in evergreen conifers, *Proceedings of the National Academy of Sciences*, 113, 13 087–13 092, <https://doi.org/10.1073/pnas.1606162113>, <http://www.pnas.org/content/113/46/13087.abstract>, 2016.
- Garbulsky, M. F., Peñuelas, J., Papale, D., and Filella, I.: Remote estimation of carbon dioxide uptake by a Mediterranean forest, 925 *Global Change Biology*, 14, 2860–2867, <https://doi.org/10.1111/j.1365-2486.2008.01684.x>, <https://doi.org/10.1111%2Fj.1365-2486.2008.01684.x>, 2008.
- Goldstein, A., Hultman, N., Fracheboud, J., Bauer, M., Panek, J., Xu, M., Qi, Y., Guenther, A., and Baugh, W.: Effects of climate variability on the carbon dioxide, water, and sensible heat fluxes above a ponderosa pine plantation in the Sierra Nevada (CA), *Agricultural and Forest Meteorology*, 101, 113–129, [https://doi.org/10.1016/s0168-1923\(99\)00168-9](https://doi.org/10.1016/s0168-1923(99)00168-9), <https://doi.org/10.1016%2Fs0168-1923%2899%2900168-9>, 2000. 930
- Gough, C. M., Hardiman, B. S., Nave, L. E., Bohrer, G., Maurer, K. D., Vogel, C. S., Nadelhoffer, K. J., and Curtis, P. S.: Sustained carbon uptake and storage following moderate disturbance in a Great Lakes forest, *Ecological Applications*, 23, 1202–1215, <https://doi.org/10.1890/12-1554.1>, <https://doi.org/10.1890%2F12-1554.1>, 2013a.
- Gough, C. M., Hardiman, B. S., Nave, L. E., Bohrer, G., Maurer, K. D., Vogel, C. S., Nadelhoffer, K. J., and Curtis, P. S.: Sustained carbon uptake and storage following moderate disturbance in a Great Lakes forest, *Ecological Applications*, 23, 1202–1215, 935 <https://doi.org/10.1890/12-1554.1>, <https://doi.org/10.1890%2F12-1554.1>, 2013b.
- Goulden, M. L., Winston, G. C., McMillan, A. M. S., Litvak, M. E., Read, E. L., Rocha, A. V., and Elliot, J. R.: An eddy covariance mesonet to measure the effect of forest age on land?atmosphere exchange, *Global Change Biology*, 12, 2146–2162, <https://doi.org/10.1111/j.1365-2486.2006.01251.x>, <https://doi.org/10.1111%2Fj.1365-2486.2006.01251.x>, 2006a.
- Goulden, M. L., Winston, G. C., McMillan, A. M. S., Litvak, M. E., Read, E. L., Rocha, A. V., and Elliot, J. R.: An eddy covariance mesonet to measure the effect of forest age on land?atmosphere exchange, *Global Change Biology*, 12, 2146–2162, <https://doi.org/10.1111/j.1365-2486.2006.01251.x>, <https://doi.org/10.1111%2Fj.1365-2486.2006.01251.x>, 2006b. 940
- Goulden, M. L., Winston, G. C., McMillan, A. M. S., Litvak, M. E., Read, E. L., Rocha, A. V., and Elliot, J. R.: An eddy covariance mesonet to measure the effect of forest age on land?atmosphere exchange, *Global Change Biology*, 12, 2146–2162, <https://doi.org/10.1111/j.1365-2486.2006.01251.x>, <https://doi.org/10.1111%2Fj.1365-2486.2006.01251.x>, 2006c. 945



- Goulden, M. L., Winston, G. C., McMillan, A. M. S., Litvak, M. E., Read, E. L., Rocha, A. V., and Elliot, J. R.: An eddy covariance mesonet to measure the effect of forest age on land-atmosphere exchange, *Global Change Biology*, 12, 2146–2162, <https://doi.org/10.1111/j.1365-2486.2006.01251.x>, <https://doi.org/10.1111%2Fj.1365-2486.2006.01251.x>, 2006d.
- 950 Goulden, M. L., Winston, G. C., McMillan, A. M. S., Litvak, M. E., Read, E. L., Rocha, A. V., and Elliot, J. R.: An eddy covariance mesonet to measure the effect of forest age on land-atmosphere exchange, *Global Change Biology*, 12, 2146–2162, <https://doi.org/10.1111/j.1365-2486.2006.01251.x>, <https://doi.org/10.1111%2Fj.1365-2486.2006.01251.x>, 2006e.
- Goulden, M. L., Winston, G. C., McMillan, A. M. S., Litvak, M. E., Read, E. L., Rocha, A. V., and Elliot, J. R.: An eddy covariance mesonet to measure the effect of forest age on land-atmosphere exchange, *Global Change Biology*, 12, 2146–2162, <https://doi.org/10.1111/j.1365-2486.2006.01251.x>, <https://doi.org/10.1111%2Fj.1365-2486.2006.01251.x>, 2006f.
- 955 Goulden, M. L., Winston, G. C., McMillan, A. M. S., Litvak, M. E., Read, E. L., Rocha, A. V., and Elliot, J. R.: An eddy covariance mesonet to measure the effect of forest age on land-atmosphere exchange, *Global Change Biology*, 12, 2146–2162, <https://doi.org/10.1111/j.1365-2486.2006.01251.x>, <https://doi.org/10.1111%2Fj.1365-2486.2006.01251.x>, 2006g.
- Greve, P., Orlowsky, B., Mueller, B., Sheffield, J., Reichstein, M., and Seneviratne, S. I.: Global assessment of trends in wetting and drying over land, *Nature Geosci*, 7, 716–721, <http://dx.doi.org/10.1038/ngeo2247>, 2014.
- 960 Grünwald, T. and Bernhofer, C.: A decade of carbon, water and energy flux measurements of an old spruce forest at the Anchor Station Tharandt, *Tellus B*, 59, <https://doi.org/10.3402/tellusb.v59i3.17000>, <https://doi.org/10.3402%2Ftellusb.v59i3.17000>, 2007.
- Guan, D.-X., Wu, J.-B., Zhao, X.-S., Han, S.-J., Yu, G.-R., Sun, X.-M., and Jin, C.-J.: CO<sub>2</sub> fluxes over an old, temperate mixed forest in northeastern China, *Agricultural and Forest Meteorology*, 137, 138–149, <https://doi.org/10.1016/j.agrformet.2006.02.003>, <https://doi.org/10.1016%2Fj.agrformet.2006.02.003>, 2006.
- 965 Haxeltine, A. and Prentice, I. C.: A General Model for the Light-Use Efficiency of Primary Production, *Funct. Ecol.*, 10, 551, 1996.
- Heinsch, F. A., Running, S. W., Kimball, J. S., Nemani, R. R., Davis, K. J., Bolstad, P. V., Cook, B. D., Desai, A. R., Ricciuto, D. M., Law, B. E., Oechel, W. C., Wofsy, S. C., Dunn, A. L., Munger, J. W., Baldocchi, D. D., Hollinger, D. Y., Richardson, A. D., Stoy, P. C., Siqueira, M. B. S., Monson, R. K., Burns, S. P., and Flanagan, L. B.: Evaluation of remote sensing based terrestrial productivity from MODIS using regional tower eddy flux network observations, *IEEE Transactions on Geoscience and Remote Sensing*, 44, 1908–1925, <https://doi.org/10.1109/TGRS.2005.853936>, 2006.
- 970 Hengl, T., de Jesus, J. M., MacMillan, R. A., Batjes, N. H., Heuvelink, G. B. M., Ribeiro, E., Samuel-Rosa, A., Kempen, B., Leenaars, J. G. B., Walsh, M. G., and Gonzalez, M. R.: SoilGrids1km—global soil information based on automated mapping, *PLoS One*, 9, e105992, 2014.
- Heskel, M., O’Sullivan, O., Reich, P., Tjoelker, M., Weerasinghe, L., Penillard, A., Egerton, J., Creek, D., Bloomfield, K., Xiang, J., Sinca, F., Stangl, Z., Martinez-De La Torre, A., Griffin, K., Huntingford, C., Hurry, V., Meir, P., Turnbull, M., and Atkin, O.: Convergence in the temperature response of leaf respiration across biomes and plant functional types, *Proceedings of the National Academy of Sciences of the United States of America*, 113, 3832–3837, <https://doi.org/10.1073/pnas.1520282113>, 2016.
- 975 Hinko-Najera, N., Isaac, P., Beringer, J., van Gorsel, E., Ewenz, C., McHugh, I., Exbrayat, J.-F., Livesley, S. J., and Arndt, S. K.: Net ecosystem carbon exchange of a dry temperate eucalypt forest, *Biogeosciences*, 14, 3781–3800, <https://doi.org/10.5194/bg-14-3781-2017>, <https://www.biogeosciences.net/14/3781/2017/>, 2017.
- 980 Hommeltenberg, J., Schmid, H. P., Drösler, M., and Werle, P.: Can a bog drained for forestry be a stronger carbon sink than a natural bog forest?, *Biogeosciences*, 11, 3477–3493, <https://doi.org/10.5194/bg-11-3477-2014>, <https://doi.org/10.5194%2Fbg-11-3477-2014>, 2014.



- Hoshika, Y., Fares, S., Savi, F., Gruening, C., Goded, I., De Marco, A., Sicard, P., and Paoletti, E.: Stomatal conductance models for ozone risk assessment at canopy level in two Mediterranean evergreen forests, *Agricultural and Forest Meteorology*, 234–235, 212–221, <https://doi.org/10.1016/j.agrformet.2017.01.005>, 2017.
- 985
- Huber, M. L., Perkins, R. A., Laesecke, A., Friend, D. G., Sengers, J. V., Assael, M. J., Metaxa, I. N., Vogel, E., Mareš, R., and Miyagawa, K.: New international formulation for the viscosity of H<sub>2</sub>O, *Journal of Physical and Chemical Reference Data*, 38, 101–125, 2009.
- Hufkens, K.: khufkens/gee\_subset: Google Earth Engine subset script and library, <https://doi.org/10.5281/zenodo.833789>, 2017.
- Huner, N. P., Oquist, G., Hurry, V. M., Krol, M., Falk, S., and Griffith, M.: Photosynthesis, photoinhibition and low temperature acclimation in cold tolerant plants, *Photosynth. Res.*, 37, 19–39, 1993.
- 990
- Hutley, L. B., Beringer, J., Isaac, P. R., Hacker, J. M., and Cernusak, L. A.: A sub-continental scale living laboratory: Spatial patterns of savanna vegetation over a rainfall gradient in northern Australia, *Agricultural and Forest Meteorology*, 151, 1417–1428, <https://doi.org/10.1016/j.agrformet.2011.03.002>, <https://doi.org/10.1016%2Fj.agrformet.2011.03.002>, 2011.
- Imer, D., Merbold, L., Eugster, W., and Buchmann, N.: Temporal and spatial variations of soil CO<sub>2</sub>, CH<sub>4</sub> and N<sub>2</sub>O fluxes at three differently managed grasslands, *Biogeosciences*, 10, 5931–5945, <https://doi.org/10.5194/bg-10-5931-2013>, <https://doi.org/10.5194%2Fbg-10-5931-2013>, 2013.
- 995
- Irvine, J., Law, B. E., and Hibbard, K. A.: Postfire carbon pools and fluxes in semiarid ponderosa pine in Central Oregon, *Global Change Biology*, 13, 1748–1760, <https://doi.org/10.1111/j.1365-2486.2007.01368.x>, <https://doi.org/10.1111%2Fj.1365-2486.2007.01368.x>, 2007.
- Irvine, J., Law, B. E., Martin, J. G., and Vickers, D.: Interannual variation in soil CO<sub>2</sub> efflux and the response of root respiration to climate and canopy gas exchange in mature ponderosa pine, *Global Change Biology*, 14, 2848–2859, <https://doi.org/10.1111/j.1365-2486.2008.01682.x>, <https://doi.org/10.1111%2Fj.1365-2486.2008.01682.x>, 2008.
- 1000
- Jacobs, C. M. J., Jacobs, A. F. G., Bosveld, F. C., Hendriks, D. M. D., Hensen, A., Kroon, P. S., Moors, E. J., Nol, L., Schrier-Uijl, A., and Veenendaal, E. M.: Variability of annual CO<sub>2</sub> exchange from Dutch grasslands, *Biogeosciences*, 4, 803–816, <https://doi.org/10.5194/bg-4-803-2007>, <https://doi.org/10.5194%2Fbg-4-803-2007>, 2007.
- 1005
- Jiang, C. and Ryu, Y.: Multi-scale evaluation of global gross primary productivity and evapotranspiration products derived from Breathing Earth System Simulator (BESS), *Remote Sens. Environ.*, 186, 528–547, 2016.
- Jung, M., Reichstein, M., Margolis, H. A., Cescatti, A., Richardson, A. D., Arain, M. A., Arneth, A., Bernhofer, C., Bonal, D., Chen, J., Gianelle, D., Gobron, N., Kiely, G., Kutsch, W., Lasslop, G., Law, B. E., Lindroth, A., Merbold, L., Montagnani, L., Moors, E. J., Papale, D., Sottocornola, M., Vaccari, F., and Williams, C.: Global patterns of land-atmosphere fluxes of carbon dioxide, latent heat, and sensible heat derived from eddy covariance, satellite, and meteorological observations, *Journal of Geophysical Research: Biogeosciences*, 116, n/a–n/a, <https://doi.org/10.1029/2010JG001566>, <http://dx.doi.org/10.1029/2010JG001566>, g00J07, 2011.
- 1010
- Kato, T., Tang, Y., Gu, S., Hirota, M., Du, M., Li, Y., and Zhao, X.: Temperature and biomass influences on interannual changes in CO<sub>2</sub> exchange in an alpine meadow on the Qinghai-Tibetan Plateau, *Global Change Biology*, 12, 1285–1298, <https://doi.org/10.1111/j.1365-2486.2006.01153.x>, <https://doi.org/10.1111%2Fj.1365-2486.2006.01153.x>, 2006.
- 1015
- Kattge, J. and Knorr, W.: Temperature acclimation in a biochemical model of photosynthesis: a reanalysis of data from 36 species, *Plant, Cell and Environment*, 30, 1176–1190, 2007.
- Keenan, T., Sabate, S., and Gracia, C.: Soil water stress and coupled photosynthesis–conductance models: Bridging the gap between conflicting reports on the relative roles of stomatal, mesophyll conductance and biochemical limitations to photosynthesis, *Agric. For. Meteorol.*, 150, 443–453, 2010.



- 1020 Keenan, T. F., Colin Prentice, I., Canadell, J. G., Williams, C. A., Wang, H., Raupach, M., and James Collatz, G.: Corrigendum: Recent pause in the growth rate of atmospheric CO<sub>2</sub> due to enhanced terrestrial carbon uptake, *Nat. Commun.*, 8, 16 137, 2017.
- Keenan, T. F., Migliavacca, M., Papale, D., Baldocchi, D., Reichstein, M., Torn, M., and Wutzler, T.: Widespread inhibition of daytime ecosystem respiration, *Nature Ecology & Evolution*, <https://doi.org/10.1038/s41559-019-0809-2>, <https://doi.org/10.1038/s41559-019-0809-2>, 2019.
- 1025 Kilinc, M., Beringer, J., Hutley, L. B., Tapper, N. J., and McGuire, D. A.: Carbon and water exchange of the world's tallest angiosperm forest, *Agricultural and Forest Meteorology*, 182-183, 215–224, <https://doi.org/10.1016/j.agrformet.2013.07.003>, <https://doi.org/10.1016%2Fj.agrformet.2013.07.003>, 2013.
- Knohl, A., Schulze, E.-D., Kolle, O., and Buchmann, N.: Large carbon uptake by an unmanaged 250-year-old deciduous forest in Central Germany, *Agricultural and Forest Meteorology*, 118, 151–167, [https://doi.org/10.1016/s0168-1923\(03\)00115-1](https://doi.org/10.1016/s0168-1923(03)00115-1), <https://doi.org/10.1016%2Fs0168-1923%2803%2900115-1>, 2003.
- 1030 Kok, B.: On the interrelation of respiration and photosynthesis in green plants, *Biochimica et Biophysica Acta*, 3, 625 – 631, [https://doi.org/https://doi.org/10.1016/0006-3002\(49\)90136-5](https://doi.org/https://doi.org/10.1016/0006-3002(49)90136-5), <http://www.sciencedirect.com/science/article/pii/0006300249901365>, 1949.
- Kurbatova, J., Li, C., Varlagin, A., Xiao, X., and Vygodskaya, N.: Modeling carbon dynamics in two adjacent spruce forests with different soil conditions in Russia, *Biogeosciences*, 5, 969–980, <https://doi.org/10.5194/bg-5-969-2008>, <https://doi.org/10.5194%2Fbg-5-969-2008>, 2008.
- 1035 Landsberg, J. J. and Waring, R. H.: A generalised model of forest productivity using simplified concepts of radiation-use efficiency, carbon balance and partitioning, *For. Ecol. Manage.*, 95, 209–228, 1997.
- Lasslop, G., Reichstein, M., Papale, D., Richardson, A., Arneth, A., Barr, A., Stoy, P., and Wohlfahrt, G.: Separation of net ecosystem exchange into assimilation and respiration using a light response curve approach: critical issues and global evaluation, *Global Change Biology*, 16, 187–208, <https://doi.org/10.1111/j.1365-2486.2009.02041.x>, 2010.
- 1040 Leuning, R.: A critical appraisal of a combined stomatal-photosynthesis model for C<sub>3</sub> plants, *Plant Cell Environ.*, 18, 339–355, 1995.
- Leuning, R., Cleugh, H. A., Zegelin, S. J., and Hughes, D.: Carbon and water fluxes over a temperate Eucalyptus forest and a tropical wet/dry savanna in Australia: measurements and comparison with MODIS remote sensing estimates, *Agricultural and Forest Meteorology*, 129, 151–173, <https://doi.org/10.1016/j.agrformet.2004.12.004>, <https://doi.org/10.1016%2Fj.agrformet.2004.12.004>, 2005.
- 1045 Li, X., Xiao, J., He, B., Altaf Arain, M., Beringer, J., Desai, A. R., Emmel, C., Hollinger, D. Y., Krasnova, A., Mammarella, I., Noe, S. M., Ortiz, P. S., Rey-Sanchez, A. C., Rocha, A. V., and Varlagin, A.: Solar-induced chlorophyll fluorescence is strongly correlated with terrestrial photosynthesis for a wide variety of biomes: First global analysis based on OCO-2 and flux tower observations, *Glob. Chang. Biol.*, 2018.
- 1050 Lindauer, M., Schmid, H., Grote, R., Mauder, M., Steinbrecher, R., and Wolpert, B.: Net ecosystem exchange over a non-cleared wind-throw-disturbed upland spruce forest—Measurements and simulations, *Agricultural and Forest Meteorology*, 197, 219–234, <https://doi.org/10.1016/j.agrformet.2014.07.005>, <https://doi.org/10.1016%2Fj.agrformet.2014.07.005>, 2014.
- Lloyd, J. and Farquhar, G. D.: 13C discrimination during CO<sub>2</sub> assimilation by the terrestrial biosphere, *Oecologia*, 99, 201–215, <https://doi.org/10.1007/BF00627732>, <https://doi.org/10.1007/BF00627732>, 1994.
- 1055 Long, S. P., Postl, W. F., and Bolhár-Nordenkampf, H. R.: Quantum yields for uptake of carbon dioxide in C<sub>3</sub> vascular plants of contrasting habitats and taxonomic groupings, *Planta*, 189, 226–234, 1993.



- Lüers, J., Westermann, S., Piel, K., and Boike, J.: Annual CO<sub>2</sub> budget and seasonal CO<sub>2</sub> exchange signals at a high Arctic permafrost site on Spitsbergen, Svalbard archipelago, *Biogeosciences*, 11, 6307–6322, <https://doi.org/10.5194/bg-11-6307-2014>, <https://doi.org/10.5194/2Fbg-11-6307-2014>, 2014.
- 1060 Lund, M., Falk, J. M., Friborg, T., Mbufong, H. N., Sigsgaard, C., Soegaard, H., and Tamstorf, M. P.: Trends in CO<sub>2</sub> exchange in a high Arctic tundra heath, 2000–2010, *Journal of Geophysical Research: Biogeosciences*, 117, n/a–n/a, <https://doi.org/10.1029/2011jg001901>, <https://doi.org/10.1029/2F2011jg001901>, 2012.
- Ma, S., Baldocchi, D. D., Xu, L., and Hehn, T.: Inter-annual variability in carbon dioxide exchange of an oak/grass savanna and open grassland in California, *Agricultural and Forest Meteorology*, 147, 157–171, <https://doi.org/10.1016/j.agrformet.2007.07.008>, <https://doi.org/10.1016/2Fj.agrformet.2007.07.008>, 2007.
- 1065 MacFarling Meure, C., Etheridge, D., Trudinger, C., Steele, P., Langenfelds, R., van Ommen, T., Smith, A., and Elkins, J.: Law Dome CO<sub>2</sub>, CH<sub>4</sub> and N<sub>2</sub>O ice core records extended to 2000 years BP, *Geophys. Res. Lett.*, 33, <https://doi.org/10.1029/2006GL026152>, 2006.
- Maire, V., Martre, P., Kattge, J., Gastal, F., Esser, G., Fontaine, S., and Soussana, J.-F.: The coordination of leaf photosynthesis links C and N fluxes in C3 plant species, *PLoS One*, 7, e38345, 2012.
- 1070 Mäkelä, A., Hari, P., Berninger, F., Hänninen, H., and Nikinmaa, E.: Acclimation of photosynthetic capacity in Scots pine to the annual cycle of temperature, *Tree Physiol.*, 24, 369–376, 2004.
- Marchesini, L. B., Papale, D., Reichstein, M., Vuichard, N., Tchebakova, N., and Valentini, R.: Carbon balance assessment of a natural steppe of southern Siberia by multiple constraint approach, *Biogeosciences Discussions*, 4, 165–208, <https://doi.org/10.5194/bgd-4-165-2007>, <https://doi.org/10.5194/2Fbgd-4-165-2007>, 2007.
- 1075 Marcolla, B., Pitacco, A., and Cescatti, A.: Canopy Architecture and Turbulence Structure in a Coniferous Forest, *Boundary-Layer Meteorology*, 108, 39–59, <https://doi.org/10.1023/a:1023027709805>, <https://doi.org/10.1023/2Fa%3A1023027709805>, 2003.
- Marcolla, B., Cescatti, A., Manca, G., Zorer, R., Cavagna, M., Fiora, A., Gianelle, D., Rodeghiero, M., Sottocornola, M., and Zampedri, R.: Climatic controls and ecosystem responses drive the inter-annual variability of the net ecosystem exchange of an alpine meadow, *Agricultural and Forest Meteorology*, 151, 1233–1243, <https://doi.org/10.1016/j.agrformet.2011.04.015>, <https://doi.org/10.1016/2Fj.agrformet.2011.04.015>, 2011.
- 1080 Matsumoto, K., Ohta, T., Nakai, T., Kuwada, T., Daikoku, K., Iida, S., Yabuki, H., Kononov, A. V., van der Molen, M. K., Kodama, Y., Maximov, T. C., Dolman, A. J., and Hattori, S.: Energy consumption and evapotranspiration at several boreal and temperate forests in the Far East, *Agricultural and Forest Meteorology*, 148, 1978–1989, <https://doi.org/10.1016/j.agrformet.2008.09.008>, <https://doi.org/10.1016/2Fj.agrformet.2008.09.008>, 2008a.
- 1085 Matsumoto, K., Ohta, T., Nakai, T., Kuwada, T., Daikoku, K., Iida, S., Yabuki, H., Kononov, A. V., van der Molen, M. K., Kodama, Y., Maximov, T. C., Dolman, A. J., and Hattori, S.: Energy consumption and evapotranspiration at several boreal and temperate forests in the Far East, *Agricultural and Forest Meteorology*, 148, 1978–1989, <https://doi.org/10.1016/j.agrformet.2008.09.008>, <https://doi.org/10.1016/2Fj.agrformet.2008.09.008>, 2008b.
- Matthes, J. H., Sturtevant, C., Verfaillie, J., Knox, S., and Baldocchi, D.: Parsing the variability in CH<sub>4</sub> flux at a spatially heterogeneous wetland: Integrating multiple eddy covariance towers with high-resolution flux footprint analysis, *Journal of Geophysical Research: Biogeosciences*, 119, 1322–1339, <https://doi.org/10.1002/2014jg002642>, <https://doi.org/10.1002/2F2014jg002642>, 2014.
- 1090 McHugh, I. D., Beringer, J., Cunningham, S. C., Baker, P. J., Cavagnaro, T. R., Nally, R. M., and Thompson, R. M.: Interactions between nocturnal turbulent flux, storage and advection at an “ideal” eucalypt woodland site, *Biogeosciences*, 14, 3027–3050, <https://doi.org/10.5194/bg-14-3027-2017>, <https://doi.org/10.5194/2Fbg-14-3027-2017>, 2017.



- 1095 McNevin, D., von Caemmerer, S., and Farquhar, G.: Determining RuBisCO activation kinetics and other rate and equilibrium constants by simultaneous multiple non-linear regression of a kinetic model, *J. Exp. Bot.*, 57, 3883–3900, 2006.
- Medlyn, B. E.: Physiological basis of the light use efficiency model, *Tree Physiol.*, 18, 167–176, 1998.
- Medlyn, B. E., Duursma, R. A., Eamus, D., Ellsworth, D. S., Colin Prentice, I., Barton, C. V. M., Crous, K. Y., de Angelis, P., Freeman, M., and Wingate, L.: Reconciling the optimal and empirical approaches to modelling stomatal conductance, *Glob. Chang. Biol.*, 17, 2134–2144, 2011.
- 1100 Meek, D. W., Hatfield, J. L., Howell, T. A., Idso, S. B., and Reginato, R. J.: A Generalized Relationship between Photosynthetically Active Radiation and Solar Radiation<sup>1</sup>, *Agron. J.*, 76, 939–945, 1984.
- Merbold, L., Ardö, J., Arneth, A., Scholes, R. J., Nouvellon, Y., de Grandcourt, A., Archibald, S., Bonnefond, J. M., Boulain, N., Brueggemann, N., Bruemmer, C., Cappelaere, B., Ceschia, E., El-Khidir, H. A. M., El-Tahir, B. A., Falk, U., Lloyd, J., Kergoat, L., Dantec, V. L., Mougou, E., Muchinda, M., Mukelabai, M. M., Ramier, D., Rouspard, O., Timouk, F., Veenendaal, E. M., and Kutsch, W. L.: Precipitation as driver of carbon fluxes in 11 African ecosystems, *Biogeosciences*, 6, 1027–1041, <https://doi.org/10.5194/bg-6-1027-2009>, <https://doi.org/10.5194%2Fbg-6-1027-2009>, 2009a.
- 1105 Merbold, L., Kutsch, W. L., Corradi, C., Kolle, O., Rebmann, C., Stoy, P. C., Zimov, S. A., and Schulze, E.-D.: Artificial drainage and associated carbon fluxes (CO<sub>2</sub>/CH<sub>4</sub>) in a tundra ecosystem, *Global Change Biology*, 15, 2599–2614, <https://doi.org/10.1111/j.1365-2486.2009.01962.x>, <https://doi.org/10.1111%2Fj.1365-2486.2009.01962.x>, 2009b.
- 1110 Merbold, L., Eugster, W., Stieger, J., Zahniser, M., Nelson, D., and Buchmann, N.: Greenhouse gas budget (CO<sub>2</sub>, CH<sub>4</sub> and N<sub>2</sub>O) of intensively managed grassland following restoration, *Global Change Biology*, 20, 1913–1928, <https://doi.org/10.1111/gcb.12518>, <https://doi.org/10.1111%2Fgcb.12518>, 2014.
- Meyer, W. S., Kondrlovà, E., and Koerber, G. R.: Evaporation of perennial semi-arid woodland in southeastern Australia is adapted for irregular but common dry periods, *Hydrological Processes*, 29, 3714–3726, <https://doi.org/10.1002/hyp.10467>, <https://doi.org/10.1002%2Fhyp.10467>, 2015.
- 1115 Michaletz, S. T., Weiser, M. D., Zhou, J., Kaspari, M., Helliker, B. R., and Enquist, B. J.: Plant Thermoregulation: Energetics, Trait-Environment Interactions, and Carbon Economics, *Trends Ecol. Evol.*, 30, 714–724, 2015.
- Migliavacca, M., Meroni, M., Busetto, L., Colombo, R., Zenone, T., Matteucci, G., Manca, G., and Seufert, G.: Modeling Gross Primary Production of Agro-Forestry Ecosystems by Assimilation of Satellite-Derived Information in a Process-Based Model, *Sensors*, 9, 922–942, <https://doi.org/10.3390/s90200922>, <https://doi.org/10.3390%2Fs90200922>, 2009.
- 1120 Mkhabela, M., Amiro, B., Barr, A., Black, T., Hawthorne, I., Kidston, J., McCaughey, J., Orchansky, A., Nesic, Z., Sass, A., Shashkov, A., and Zha, T.: Comparison of carbon dynamics and water use efficiency following fire and harvesting in Canadian boreal forests, *Agricultural and Forest Meteorology*, 149, 783–794, <https://doi.org/10.1016/j.agrformet.2008.10.025>, <https://doi.org/10.1016%2Fj.agrformet.2008.10.025>, 2009a.
- 1125 Mkhabela, M., Amiro, B., Barr, A., Black, T., Hawthorne, I., Kidston, J., McCaughey, J., Orchansky, A., Nesic, Z., Sass, A., Shashkov, A., and Zha, T.: Comparison of carbon dynamics and water use efficiency following fire and harvesting in Canadian boreal forests, *Agricultural and Forest Meteorology*, 149, 783–794, <https://doi.org/10.1016/j.agrformet.2008.10.025>, <https://doi.org/10.1016%2Fj.agrformet.2008.10.025>, 2009b.
- 1130 Mkhabela, M., Amiro, B., Barr, A., Black, T., Hawthorne, I., Kidston, J., McCaughey, J., Orchansky, A., Nesic, Z., Sass, A., Shashkov, A., and Zha, T.: Comparison of carbon dynamics and water use efficiency following fire and harvesting in Canadian boreal forests, *Agricultural and*



- Forest Meteorology, 149, 783–794, <https://doi.org/10.1016/j.agrformet.2008.10.025>, <https://doi.org/10.1016%2Fj.agrformet.2008.10.025>, 2009c.
- 1135 Monson, R. K., Turnipseed, A. A., Sparks, J. P., Harley, P. C., Scott-Denton, L. E., Sparks, K., and Huxman, T. E.: Carbon sequestration in a high-elevation, subalpine forest, *Global Change Biology*, 8, 459–478, <https://doi.org/10.1046/j.1365-2486.2002.00480.x>, <https://doi.org/10.1046%2Fj.1365-2486.2002.00480.x>, 2002.
- Montagnani, L., Manca, G., Canepa, E., Georgieva, E., Acosta, M., Feigenwinter, C., Janous, D., Kerschbaumer, G., Lindroth, A., Minach, L., Minerbi, S., Mölder, M., Pavelka, M., Seufert, G., Zeri, M., and Ziegler, W.: A new mass conservation approach to the study of CO<sub>2</sub> advection in an alpine forest, *Journal of Geophysical Research*, 114, <https://doi.org/10.1029/2008jd010650>, <https://doi.org/10.1029%2F2008jd010650>, 2009.
- 1140 Monteith, J. L.: Solar Radiation and Productivity in Tropical Ecosystems, *Journal of Applied Ecology*, 9, 747–766, <http://www.jstor.org/stable/2401901>, 1972.
- Moors, E.: Water Use of Forests in The Netherlands, Ph.D. thesis, Vrije Universiteit Amsterdam, 2012.
- Myneni, R., Knyazikhin, Y., and Park, T.: MOD15A3H MODIS/Combined Terra+Aqua Leaf Area Index/FPAR Daily L4 Global 500m SIN Grid, <http://doi.org/10.5067/MODIS/MOD15A3H.006>, <https://doi.org/10.5067/MODIS/MOD15A3H.006>, 2015.
- 1145 Nakai, T., Kim, Y., Busey, R. C., Suzuki, R., Nagai, S., Kobayashi, H., Park, H., Sugiura, K., and Ito, A.: Characteristics of evapotranspiration from a permafrost black spruce forest in interior Alaska, *Polar Science*, 7, 136–148, <https://doi.org/10.1016/j.polar.2013.03.003>, <https://doi.org/10.1016%2Fj.polar.2013.03.003>, 2013.
- Noormets, A., Chen, J., and Crow, T. R.: Age-Dependent Changes in Ecosystem Carbon Fluxes in Managed Forests in Northern Wisconsin, USA, *Ecosystems*, 10, 187–203, <https://doi.org/10.1007/s10021-007-9018-y>, <https://doi.org/10.1007%2Fs10021-007-9018-y>, 2007a.
- Noormets, A., Chen, J., and Crow, T. R.: Age-Dependent Changes in Ecosystem Carbon Fluxes in Managed Forests in Northern Wisconsin, USA, *Ecosystems*, 10, 187–203, <https://doi.org/10.1007/s10021-007-9018-y>, <https://doi.org/10.1007%2Fs10021-007-9018-y>, 2007b.
- Noormets, A., Chen, J., and Crow, T. R.: Age-Dependent Changes in Ecosystem Carbon Fluxes in Managed Forests in Northern Wisconsin, USA, *Ecosystems*, 10, 187–203, <https://doi.org/10.1007/s10021-007-9018-y>, <https://doi.org/10.1007%2Fs10021-007-9018-y>, 2007c.
- 1155 Noormets, A., Chen, J., and Crow, T. R.: Age-Dependent Changes in Ecosystem Carbon Fluxes in Managed Forests in Northern Wisconsin, USA, *Ecosystems*, 10, 187–203, <https://doi.org/10.1007/s10021-007-9018-y>, <https://doi.org/10.1007%2Fs10021-007-9018-y>, 2007d.
- Noormets, A., Chen, J., and Crow, T. R.: Age-Dependent Changes in Ecosystem Carbon Fluxes in Managed Forests in Northern Wisconsin, USA, *Ecosystems*, 10, 187–203, <https://doi.org/10.1007/s10021-007-9018-y>, <https://doi.org/10.1007%2Fs10021-007-9018-y>, 2007e.
- Oikawa, P. Y., Jenerette, G. D., Knox, S. H., Sturtevant, C., Verfaillie, J., Dronova, I., Poindexter, C. M., Eichelmann, E., and Baldocchi, D. D.: Evaluation of a hierarchy of models reveals importance of substrate limitation for predicting carbon dioxide and methane exchange in restored wetlands, *Journal of Geophysical Research: Biogeosciences*, 122, 145–167, <https://doi.org/10.1002/2016jg003438>, <https://doi.org/10.1002%2F2016jg003438>, 2017.
- 1160 Oquist, G. and Huner, N. P. A.: Photosynthesis of overwintering evergreen plants, *Annu. Rev. Plant Biol.*, 54, 329–355, 2003.
- Papale, D., Migliavacca, M., Cremonese, E., Cescatti, A., Alberti, G., Balzarolo, M., Marchesini, L. B., Canfora, E., Casa, R., Duce, P., Facini, O., Galvagno, M., Genesio, L., Gianelle, D., Magliulo, V., Matteucci, G., Montagnani, L., Petrella, F., Pitacco, A., Seufert, G., Spano, D., Stefani, P., Vaccari, F. P., and Valentini, R.: Carbon, Water and Energy Fluxes of Terrestrial Ecosystems in Italy, in: *The Greenhouse Gas Balance of Italy*, pp. 11–45, Springer Berlin Heidelberg, [https://doi.org/10.1007/978-3-642-32424-6\\_2](https://doi.org/10.1007/978-3-642-32424-6_2), [https://doi.org/10.1007%2F978-3-642-32424-6\\_2](https://doi.org/10.1007%2F978-3-642-32424-6_2), 2014.



- 1170 Pelkonen, P. and Hari, P.: The Dependence of the Springtime Recovery of CO<sub>2</sub> Uptake in Scots Pine on Temperature and Internal Factors, *Flora*, 169, 398–404, 1980.
- Pilegaard, K., Ibrom, A., Courtney, M. S., Hummelshøj, P., and Jensen, N. O.: Increasing net CO<sub>2</sub> uptake by a Danish beech forest during the period from 1996 to 2009, *Agricultural and Forest Meteorology*, 151, 934–946, <https://doi.org/10.1016/j.agrformet.2011.02.013>, <https://doi.org/10.1016%2Fj.agrformet.2011.02.013>, 2011.
- 1175 Porcar-Castell, A., Tyystjärvi, E., Atherton, J., van der Tol, C., Flexas, J., Pfündel, E. E., Moreno, J., Frankenberg, C., and Berry, J. A.: Linking chlorophyll a fluorescence to photosynthesis for remote sensing applications: mechanisms and challenges, *J. Exp. Bot.*, 65, 4065–4095, 2014.
- Posse, G., Lewczuk, N., Richter, K., and Cristiano, P.: Carbon and water vapor balance in a subtropical pine plantation, *iForest - Biogeosciences and Forestry*, 9, 736–742, <https://doi.org/10.3832/ifer1815-009>, <https://doi.org/10.3832%2Fifer1815-009>, 2016.
- 1180 Post, H., Franssen, H. J. H., Graf, A., Schmidt, M., and Vereecken, H.: Uncertainty analysis of eddy covariance CO<sub>2</sub> flux measurements for different EC tower distances using an extended two-tower approach, *Biogeosciences*, 12, 1205–1221, <https://doi.org/10.5194/bg-12-1205-2015>, <https://doi.org/10.5194%2Fbg-12-1205-2015>, 2015.
- Powell, T. L., Bracho, R., Li, J., Dore, S., Hinkle, C. R., and Drake, B. G.: Environmental controls over net ecosystem carbon exchange of scrub oak in central Florida, *Agricultural and Forest Meteorology*, 141, 19–34, <https://doi.org/10.1016/j.agrformet.2006.09.002>, <https://doi.org/10.1016%2Fj.agrformet.2006.09.002>, 2006.
- 1185 Prentice, I. C., Dong, N., Gleason, S. M., Maire, V., and Wright, I. J.: Balancing the costs of carbon gain and water transport: testing a new theoretical framework for plant functional ecology, *Ecology Letters*, 17, 82–91, <https://doi.org/10.1111/ele.12211>, <http://dx.doi.org/10.1111/ele.12211>, 2014.
- Prentice, I. C., Liang, X., Medlyn, B. E., and Wang, Y.-P.: Reliable, robust and realistic: the three R's of next-generation land-surface modelling, *Atmos. Chem. Phys.*, 15, 5987–6005, 2015.
- 1190 Prescher, A.-K., Grünwald, T., and Bernhofer, C.: Land use regulates carbon budgets in eastern Germany: From NEE to NBP, *Agricultural and Forest Meteorology*, 150, 1016–1025, <https://doi.org/10.1016/j.agrformet.2010.03.008>, <https://doi.org/10.1016%2Fj.agrformet.2010.03.008>, 2010.
- Priestley, C. H. B. and Taylor, R. J.: On the Assessment of Surface Heat Flux and Evaporation Using Large-Scale Parameters, *Mon. Weather Rev.*, 100, 81–92, 1972.
- 1195 Prober, S. M., Thiele, K. R., Rundel, P. W., Yates, C. J., Berry, S. L., Byrne, M., Christidis, L., Gosper, C. R., Grierson, P. F., Lemson, K., Lyons, T., Macfarlane, C., O'Connor, M. H., Scott, J. K., Standish, R. J., Stock, W. D., van Etten, E. J., Wardell-Johnson, G. W., and Watson, A.: Facilitating adaptation of biodiversity to climate change: A conceptual framework applied to the world's largest Mediterranean-climate woodland, *Climatic Change*, 110, 227–248, <https://doi.org/10.1007/s10584-011-0092-y>, <http://link.springer.com/10.1007/s10584-011-0092-y>, 2012.
- 1200 R Core Team: R: A Language and Environment for Statistical Computing, R Foundation for Statistical Computing, Vienna, Austria, <https://www.R-project.org/>, 2016.
- Rambal, S., Joffre, R., Ourcival, J. M., Cavender-Bares, J., and Rocheteau, A.: The growth respiration component in eddy CO<sub>2</sub> flux from a *Quercus ilex* mediterranean forest, *Global Change Biology*, 10, 1460–1469, <https://doi.org/10.1111/j.1365-2486.2004.00819.x>, <https://doi.org/10.1111%2Fj.1365-2486.2004.00819.x>, 2004.



- 1205 Raz-Yaseef, N., Billesbach, D. P., Fischer, M. L., Biraud, S. C., Gunter, S. A., Bradford, J. A., and Torn, M. S.: Vulnerability of crops and native grasses to summer drying in the U.S. Southern Great Plains, *Agriculture, Ecosystems & Environment*, 213, 209–218, <https://doi.org/10.1016/j.agee.2015.07.021>, <https://doi.org/10.1016%2Fj.agee.2015.07.021>, 2015a.
- Raz-Yaseef, N., Billesbach, D. P., Fischer, M. L., Biraud, S. C., Gunter, S. A., Bradford, J. A., and Torn, M. S.: Vulnerability of crops and native grasses to summer drying in the U.S. Southern Great Plains, *Agriculture, Ecosystems & Environment*, 213, 209–218, <https://doi.org/10.1016/j.agee.2015.07.021>, <https://doi.org/10.1016%2Fj.agee.2015.07.021>, 2015b.
- 1210 Raz-Yaseef, N., Billesbach, D. P., Fischer, M. L., Biraud, S. C., Gunter, S. A., Bradford, J. A., and Torn, M. S.: Vulnerability of crops and native grasses to summer drying in the U.S. Southern Great Plains, *Agriculture, Ecosystems & Environment*, 213, 209–218, <https://doi.org/10.1016/j.agee.2015.07.021>, <https://doi.org/10.1016%2Fj.agee.2015.07.021>, 2015c.
- Raz-Yaseef, N., Billesbach, D. P., Fischer, M. L., Biraud, S. C., Gunter, S. A., Bradford, J. A., and Torn, M. S.: Vulnerability of crops and native grasses to summer drying in the U.S. Southern Great Plains, *Agriculture, Ecosystems & Environment*, 213, 209–218, <https://doi.org/10.1016/j.agee.2015.07.021>, <https://doi.org/10.1016%2Fj.agee.2015.07.021>, 2015d.
- 1215 Reichstein, M., Falge, E., Baldocchi, D., Papale, D., Aubinet, M., Berbigier, P., Bernhofer, C., Buchmann, N., Gilmanov, T., Granier, A., Grunwald, T., Havrankova, K., Ilvesniemi, H., Janous, D., Knohl, A., Laurila, T., Lohila, A., Loustau, D., Matteucci, G., Meyers, T., Miglietta, F., Ourcival, J.-M., Pumpanen, J., Rambal, S., Rotenberg, E., Sanz, M., Tenhunen, J., Seufert, G., Vaccari, F., Vesala, T., Yakir, D., and Valentini, R.: On the separation of net ecosystem exchange into assimilation and ecosystem respiration: review and improved algorithm, *Glob. Chang. Biol.*, 11, 1424–1439, 2005.
- Reverter, B. R., Sánchez-Cañete, E. P., Resco, V., Serrano-Ortiz, P., Oyonarte, C., and Kowalski, A. S.: Analyzing the major drivers of NEE in a Mediterranean alpine shrubland, *Biogeosciences*, 7, 2601–2611, <https://doi.org/10.5194/bg-7-2601-2010>, <https://doi.org/10.5194%2Fbg-7-2601-2010>, 2010.
- 1225 Rogers, A.: The use and misuse of  $V_{c,max}$  in Earth System Models, *Photosynthesis Research*, 119, 15–29, <https://doi.org/10.1007/s11120-013-9818-1>, <https://doi.org/10.1007/s11120-013-9818-1>, 2014.
- Rogers, A., Medlyn, B. E., Dukes, J. S., Bonan, G., von Caemmerer, S., Dietze, M. C., Kattge, J., Leakey, A. D. B., Mercado, L. M., Niinemets, U., Prentice, I. C., Serbin, S. P., Sitch, S., Way, D. A., and Zaehle, S.: A roadmap for improving the representation of photosynthesis in Earth system models, *New Phytologist*, 213, 22–42, <https://doi.org/10.1111/nph.14283>, <http://dx.doi.org/10.1111/nph.14283>, 2016-22284, 2017.
- 1230 Ruehr, N. K., Martin, J. G., and Law, B. E.: Effects of water availability on carbon and water exchange in a young ponderosa pine forest: Above- and belowground responses, *Agricultural and Forest Meteorology*, 164, 136–148, <https://doi.org/10.1016/j.agrformet.2012.05.015>, <https://doi.org/10.1016%2Fj.agrformet.2012.05.015>, 2012.
- Running, S. W., Nemani, R. R., Heinsch, F. A., Zhao, M., Reeves, M., and Hashimoto, H.: A Continuous Satellite-Derived Measure of Global Terrestrial Primary Production, *BioScience*, 54, 547–560, [https://doi.org/10.1641/0006-3568\(2004\)054\[0547:ACSMOG\]2.0.CO;2](https://doi.org/10.1641/0006-3568(2004)054[0547:ACSMOG]2.0.CO;2), [https://doi.org/10.1641/0006-3568\(2004\)054\[0547:ACSMOG\]2.0.CO;2](https://doi.org/10.1641/0006-3568(2004)054[0547:ACSMOG]2.0.CO;2), 2004.
- 1235 Ryu, Y., Berry, J. A., and Baldocchi, D. D.: What is global photosynthesis? History, uncertainties and opportunities, *Remote Sens. Environ.*, 223, 95–114, 2019.
- Sabbatini, S., Arriga, N., Bertolini, T., Castaldi, S., Chiti, T., Consalvo, C., Djomo, S. N., Gioli, B., Matteucci, G., and Papale, D.: Greenhouse gas balance of cropland conversion to bioenergy poplar short-rotation coppice, *Biogeosciences*, 13, 95–113, <https://doi.org/10.5194/bg-13-95-2016>, <https://doi.org/10.5194%2Fbg-13-95-2016>, 2016a.
- 1240



- Sabbatini, S., Arriga, N., Bertolini, T., Castaldi, S., Chiti, T., Consalvo, C., Djomo, S. N., Gioli, B., Matteucci, G., and Papale, D.: Greenhouse gas balance of cropland conversion to bioenergy poplar short-rotation coppice, *Biogeosciences*, 13, 95–113, <https://doi.org/10.5194/bg-13-95-2016>, <https://doi.org/10.5194%2Fbg-13-95-2016>, 2016b.
- 1245 Saxton, K. E. and Rawls, W. J.: Soil Water Characteristic Estimates by Texture and Organic Matter for Hydrologic Solutions, *Soil Sci. Soc. Am. J.*, 70, 1569–1578, 2006.
- Schroder, I., Kuske, T., and Zegelin, S.: Eddy Covariance Dataset for Arcturus (2011-2013), Geoscience Australia, Canberra, Tech. rep., <https://doi.org/10.1001/14249>, 2014.
- Scott, R. L., Jenerette, G. D., Potts, D. L., and Huxman, T. E.: Effects of seasonal drought on net carbon dioxide exchange from a woody-plant-encroached semiarid grassland, *Journal of Geophysical Research*, 114, <https://doi.org/10.1029/2008jg000900>, <https://doi.org/10.1029%2F2008jg000900>, 2009.
- 1250 Scott, R. L., Hamerlynck, E. P., Jenerette, G. D., Moran, M. S., and Barron-Gafford, G. A.: Carbon dioxide exchange in a semidesert grassland through drought-induced vegetation change, *Journal of Geophysical Research*, 115, <https://doi.org/10.1029/2010jg001348>, <https://doi.org/10.1029%2F2010jg001348>, 2010.
- 1255 Scott, R. L., Biederman, J. A., Hamerlynck, E. P., and Barron-Gafford, G. A.: The carbon balance pivot point of southwestern U.S. semiarid ecosystems: Insights from the 21st century drought, *Journal of Geophysical Research: Biogeosciences*, 120, 2612–2624, <https://doi.org/10.1002/2015jg003181>, <https://doi.org/10.1002%2F2015jg003181>, 2015a.
- Scott, R. L., Biederman, J. A., Hamerlynck, E. P., and Barron-Gafford, G. A.: The carbon balance pivot point of southwestern U.S. semiarid ecosystems: Insights from the 21st century drought, *Journal of Geophysical Research: Biogeosciences*, 120, 2612–2624, <https://doi.org/10.1002/2015jg003181>, <https://doi.org/10.1002%2F2015jg003181>, 2015b.
- 1260 Serrano-Ortiz, P., Marañón-Jiménez, S., Reverter, B. R., Sánchez-Cañete, E. P., Castro, J., Zamora, R., and Kowalski, A. S.: Post-fire salvage logging reduces carbon sequestration in Mediterranean coniferous forest, *Forest Ecology and Management*, 262, 2287–2296, <https://doi.org/10.1016/j.foreco.2011.08.023>, <http://linkinghub.elsevier.com/retrieve/pii/S0378112711005159>, 2011.
- Shao, C., Chen, J., Li, L., Dong, G., Han, J., Abraha, M., and John, R.: Grazing effects on surface energy fluxes in a desert steppe on the Mongolian Plateau, *Ecological Applications*, 27, 485–502, <https://doi.org/10.1002/eap.1459>, 2017.
- 1265 Shi, P., Sun, X., Xu, L., Zhang, X., He, Y., Zhang, D., and Yu, G.: Net ecosystem CO<sub>2</sub> exchange and controlling factors in a steppe—Kobresia meadow on the Tibetan Plateau, *Science in China Series D: Earth Sciences*, 49, 207–218, <https://doi.org/10.1007/s11430-006-8207-4>, <https://doi.org/10.1007%2Fs11430-006-8207-4>, 2006.
- Singsaas, E. L., Ort, D. R., and DeLucia, E. H.: Variation in measured values of photosynthetic quantum yield in ecophysiological studies, *Oecologia*, 128, 15–23, <https://doi.org/10.1007/s004420000624>, <https://doi.org/10.1007/s004420000624>, 2001.
- 1270 Smith, E. L.: THE INFLUENCE OF LIGHT AND CARBON DIOXIDE ON PHOTOSYNTHESIS, *J. Gen. Physiol.*, 20, 807–830, 1937.
- Smith, N. G. and Dukes, J. S.: Plant respiration and photosynthesis in global-scale models: incorporating acclimation to temperature and CO<sub>2</sub>, *Glob. Chang. Biol.*, 19, 45–63, 2013.
- Smith, N. G. and Dukes, J. S.: Short-term acclimation to warmer temperatures accelerates leaf carbon exchange processes across plant types, *Glob. Chang. Biol.*, 23, 4840–4853, 2017.
- 1275 Smith, N. G., Keenan, T. F., Colin Prentice, I., Wang, H., Wright, I. J., Niinemets, U., Crous, K. Y., Domingues, T. F., Guerrieri, R., Yoko Ishida, F., Kattge, J., Kruger, E. L., Maire, V., Rogers, A., Serbin, S. P., Tarvainen, L., Togashi, H. F., Townsend, P. A., Wang, M., Weerasinghe, L. K., and Zhou, S.-X.: Global photosynthetic capacity is optimized to the environment, *Ecol. Lett.*, 2019.



- Stevens, R. M., Ewenz, C. M., Grigson, G., and Conner, S. M.: Water use by an irrigated almond orchard, *Irrigation Science*, 30, 189–200, <https://doi.org/10.1007/s00271-011-0270-8>, <https://doi.org/10.1007%2Fs00271-011-0270-8>, 2011.
- 1280 Stiegler, C., Lund, M., Christensen, T. R., Mastepanov, M., and Lindroth, A.: Two years with extreme and little snowfall: effects on energy partitioning and surface energy exchange in a high-Arctic tundra ecosystem, *The Cryosphere*, 10, 1395–1413, <https://doi.org/10.5194/tc-10-1395-2016>, <https://doi.org/10.5194%2Ftc-10-1395-2016>, 2016.
- Stocker, B.: fLUE, <https://doi.org/10.5281/zenodo.1158524>, <https://doi.org/10.5281/zenodo.1158524>, 2018.
- 1285 Stocker, B. D., Zscheischler, J., Keenan, T. F., Prentice, I. C., Peñuelas, J., and Seneviratne, S. I.: Quantifying soil moisture impacts on light use efficiency across biomes, *New Phytologist*, 218, 1430–1449, 2018.
- Sulman, B. N., Desai, A. R., Cook, B. D., Saliendra, N., and Mackay, D. S.: Contrasting carbon dioxide fluxes between a drying shrub wetland in Northern Wisconsin, USA, and nearby forests, *Biogeosciences*, 6, 1115–1126, <https://doi.org/10.5194/bg-6-1115-2009>, <https://doi.org/10.5194%2Fbg-6-1115-2009>, 2009.
- 1290 Suni, T., Rinne, J., Reissel, A., Altimir, N., Keronen, P., Rannik, Ü., Maso, M., Kulmala, M., and Vesala, T.: Long-term measurements of surface fluxes above a Scots pine forest in Hyytiälä, southern Finland, *Boreal Environ. Res.*, 4, 287–301, 2003.
- Suzuki, Y., Makino, A., and Mae, T.: Changes in the turnover of Rubisco and levels of mRNAs of *rbcL* and *rbcS* in rice leaves from emergence to senescence, *Plant Cell Environ.*, 24, 1353–1360, 2001.
- Tagesson, T., Fensholt, R., Guiro, I., Rasmussen, M. O., Huber, S., Mbow, C., Garcia, M., Horion, S., Sandholt, I., Holm-Rasmussen, B., 1295 Götsche, F. M., Ridler, M.-E., Olén, N., Olsen, J. L., Ehammer, A., Madsen, M., Olesen, F. S., and Ardö, J.: Ecosystem properties of semiarid savanna grassland in West Africa and its relationship with environmental variability, *Global Change Biology*, 21, 250–264, <https://doi.org/10.1111/gcb.12734>, <https://doi.org/10.1111%2Fgcb.12734>, 2014.
- Tedeschi, V., Rey, A., Manca, G., Valentini, R., Jarvis, P. G., and Borghetti, M.: Soil respiration in a Mediterranean oak forest at different developmental stages after coppicing, *Global Change Biology*, 12, 110–121, <https://doi.org/10.1111/j.1365-2486.2005.01081.x>, <https://doi.org/10.1111%2Fj.1365-2486.2005.01081.x>, 1300 //doi.org/10.1111%2Fj.1365-2486.2005.01081.x, 2006.
- Thum, T., Aalto, T., Laurila, T., Aurela, M., Kolari, P., and Hari, P.: Parametrization of two photosynthesis models at the canopy scale in a northern boreal Scots pine forest, *Tellus B*, 59, <https://doi.org/10.3402/tellusb.v59i5.17066>, <https://doi.org/10.3402%2Ftellusb.v59i5.17066>, 2007.
- Ulke, A. G., Gattinoni, N. N., and Posse, G.: Analysis and modelling of turbulent fluxes in two different ecosystems in Argentina, *International Journal of Environment and Pollution*, 58, 52, <https://doi.org/10.1504/ijep.2015.076583>, <https://doi.org/10.1504%2Fijep.2015.076583>, 2015.
- 1305 Urbanski, S., Barford, C., Wofsy, S., Kucharik, C., Pyle, E., Budney, J., McKain, K., Fitzjarrald, D., Czikowsky, M., and Munger, J. W.: Factors controlling CO<sub>2</sub> exchange on timescales from hourly to decadal at Harvard Forest, *Journal of Geophysical Research*, 112, <https://doi.org/10.1029/2006jg000293>, <https://doi.org/10.1029%2F2006jg000293>, 2007.
- 1310 Valentini, R., Angelis, P., Matteucci, G., Monaco, R., Dore, S., and Mucnozza, G. E. S.: Seasonal net carbon dioxide exchange of a beech forest with the atmosphere, *Global Change Biology*, 2, 199–207, <https://doi.org/10.1111/j.1365-2486.1996.tb00072.x>, <https://doi.org/10.1111%2Fj.1365-2486.1996.tb00072.x>, 1996.
- van der Molen, M. K., van Huissteden, J., Parmentier, F. J. W., Petrescu, A. M. R., Dolman, A. J., Maximov, T. C., Kononov, A. V., Karsanaev, S. V., and Suzdalov, D. A.: The growing season greenhouse gas balance of a continental tundra site in the Indigirka lowlands, NE Siberia, 1315 *Biogeosciences*, 4, 985–1003, <https://doi.org/10.5194/bg-4-985-2007>, <https://doi.org/10.5194%2Fbg-4-985-2007>, 2007.



- Veres, J. S. and Williams, III, G. J.: Time course of photosynthetic temperature acclimation in *Carex eleocharis* Bailey, *Plant Cell Environ.*, 7, 545–547, 1984.
- Verhoeven, A.: Sustained energy dissipation in winter evergreens, *New Phytol.*, 201, 57–65, 2014.
- Vitasse, Y., Lenz, A., and Körner, C.: The interaction between freezing tolerance and phenology in temperate deciduous trees, *Front. Plant Sci.*, 5, 541, 2014.
- 1320 von Caemmerer, S. and Farquhar, G. D.: Some relationships between the biochemistry of photosynthesis and the gas exchange of leaves, *Planta*, 153, 376–387, 1981.
- Wang, H., Prentice, I. C., Keenan, T. F., Davis, T. W., Wright, I. J., Cornwell, W. K., Evans, B. J., and Peng, C.: Towards a universal model for carbon dioxide uptake by plants, *Nat Plants*, 3, 734–741, 2017a.
- 1325 Wang, L., Zhu, H., Lin, A., Zou, L., Qin, W., and Du, Q.: Evaluation of the Latest MODIS GPP Products across Multiple Biomes Using Global Eddy Covariance Flux Data, *Remote Sensing*, 9, <https://doi.org/10.3390/rs9050418>, <http://www.mdpi.com/2072-4292/9/5/418>, 2017b.
- Way, D. A. and Yamori, W.: Thermal acclimation of photosynthesis: on the importance of adjusting our definitions and accounting for thermal acclimation of respiration, *Photosynth. Res.*, 119, 89–100, 2014.
- 1330 Weedon, G. P., Balsamo, G., Bellouin, N., Gomes, S., Best, M. J., and Viterbo, P.: The WFDEI meteorological forcing data set: WATCH Forcing Data methodology applied to ERA-Interim reanalysis data, *Water Resour. Res.*, 50, 7505–7514, 2014.
- Wehr, R., Munger, J. W., McManus, J. B., Nelson, D. D., Zahniser, M. S., Davidson, E. A., Wofsy, S. C., and Saleska, S. R.: Seasonality of temperate forest photosynthesis and daytime respiration, *Nature*, 534, 680 EP –, <https://doi.org/10.1038/nature17966>, 2016.
- Wen, X. F., Wang, H. M., Wang, J. L., Yu, G. R., and Sun, X. M.: Ecosystem carbon exchanges of a subtropical evergreen coniferous plantation subjected to seasonal drought, 2003–2007, *Biogeosciences*, 7, 357–369, <https://doi.org/10.5194/bg-7-357-2010>, 2010.
- 1335 Westergaard-Nielsen, A., Lund, M., Hansen, B. U., and Tamstorf, M. P.: Camera derived vegetation greenness index as proxy for gross primary production in a low Arctic wetland area, *ISPRS Journal of Photogrammetry and Remote Sensing*, 86, 89–99, <https://doi.org/10.1016/j.isprsjprs.2013.09.006>, <https://doi.org/10.1016%2Fj.isprsjprs.2013.09.006>, 2013.
- Wick, B., Veldkamp, E., de Mello, W. Z., Keller, M., and Crill, P.: Nitrous oxide fluxes and nitrogen cycling along a pasture chronosequence in Central Amazonia, Brazil, *Biogeosciences*, 2, 175–187, <https://doi.org/10.5194/bg-2-175-2005>, <https://doi.org/10.5194%2Fbg-2-175-2005>, 2005.
- 1340 Wohlfahrt, G., Hammerle, A., Haslwanter, A., Bahn, M., Tappeiner, U., and Cernusca, A.: Seasonal and inter-annual variability of the net ecosystem CO<sub>2</sub> exchange of a temperate mountain grassland: Effects of weather and management, *Journal of Geophysical Research*, 113, <https://doi.org/10.1029/2007jd009286>, <https://doi.org/10.1029%2F2007jd009286>, 2008.
- 1345 Yan, J., Zhang, Y., Yu, G., Zhou, G., Zhang, L., Li, K., Tan, Z., and Sha, L.: Seasonal and inter-annual variations in net ecosystem exchange of two old-growth forests in southern China, *Agricultural and Forest Meteorology*, 182–183, 257–265, <https://doi.org/10.1016/j.agrformet.2013.03.002>, <http://linkinghub.elsevier.com/retrieve/pii/S0168192313000567>, 2013.
- Yang Xiang, Gubian, S., Suomela, B., and Hoeng, J.: Generalized Simulated Annealing for Efficient Global Optimization: the GenSA Package for R., *The R Journal Volume 5/1*, June 2013, <http://journal.r-project.org/>, 2013.
- 1350 Yee, M. S., Pauwels, V. R., Daly, E., Beringer, J., Rüdiger, C., McCabe, M. F., and Walker, J. P.: A comparison of optical and microwave scintillometers with eddy covariance derived surface heat fluxes, *Agricultural and Forest Meteorology*, 213, 226–239, <https://doi.org/10.1016/j.agrformet.2015.07.004>, <https://doi.org/10.1016%2Fj.agrformet.2015.07.004>, 2015.



- Zeller, K. and Nikolov, N.: Quantifying simultaneous fluxes of ozone, carbon dioxide and water vapor above a subalpine forest ecosystem, *Environmental Pollution*, 107, 1–20, [https://doi.org/10.1016/s0269-7491\(99\)00156-6](https://doi.org/10.1016/s0269-7491(99)00156-6), <https://doi.org/10.1016%2Fs0269-7491%2899%2900156-6>, 2000.
- 1355
- Zhang, Y., Xiao, X., Wu, X., Zhou, S., Zhang, G., Qin, Y., and Dong, J.: A global moderate resolution dataset of gross primary production of vegetation for 2000–2016, *Scientific Data*, 4, 170 165, 2017.
- Zielis, S., Etzold, S., Zweifel, R., Eugster, W., Haeni, M., and Buchmann, N.: NEP of a Swiss subalpine forest is significantly driven not only by current but also by previous year’s weather, *Biogeosciences*, 11, 1627–1635, <https://doi.org/10.5194/bg-11-1627-2014>, <https://doi.org/10.5194%2Fbg-11-1627-2014>, 2014.
- 1360